THE TRACTIVE PERFORMANCE OF A FRICTION-BASED PROTOTYPE TRACK

TINGMIN YU

Submitted in partial fulfillment of the requirements for the

Degree of

Philosophiae Doctor

in

The Faculty of Engineering, Built Environment and Information Technology

University of Pretoria

Pretoria

October, 2005

SUMMARY

THE TRACTIVE PERFORMANCE OF A FRICTION-BASED PROTOTYPE TRACK

Supervisor: Professor H.L.M. du Plessis
Department: Civil and Biosystems Engineering
Degree: Philosophiae Doctor (Engineering)

In recent years, the interest in the design, construction and utilization of rubber tracks for agriculture and earth moving machinery has increased considerably. The development of such types of tracks was initiated by the efforts to invent a more environmentally friendly vehicle-terrain system. These tracks are also the result of the continuous effort to develop more cost-effective traction systems.

A rubber-surfaced and friction-based prototype track was developed and mounted on the patented modification of a new Allis Chalmers four wheel drive tractor. The track is propelled by smooth pneumatic tyres by means of rubber-rubber friction and the tractive effort of the track is mainly generated by soil-rubber friction between the rubber surface of the track elements and terrain.

The experimental track layer tractor, based on an Allis Chalmers 8070 tractor (141 kW) was tested on concrete and on cultivated sandy loam soil at 7.8%; 13% and 21% soil water content. The contact pressure and the tangential force on an instrumented track element, as well as the total torque input to one track, was simultaneously recorded during the drawbar pull-slip tests. Soil characteristics for pressure-sinkage and friction-displacement were obtained from the field tests by using an instrumented linear shear and soil sinkage device.

By applying the approach based on the classical bevameter technique, analytical methods were implemented for modelling the traction performance of the prototype track system. Different possible pressure distribution profiles under the tracks were considered and compared to the recorded data. Two possible traction models were proposed, one constant pressure model, for minimal inward track deflection and the other a flexible track model with inward deflection and a higher contact pressure at both the front free-wheeling and rear driving tyres. For both models, the traction force was mainly generated by rubber-soil friction and adhesion with limited influence by soil shear. For individual track elements, close agreement between the measured and predicted contact pressure and traction force was observed based on the flexible track model.

The recorded and calculated values of the coefficient of traction based on the summation of the traction force for the series of track elements were comparable to the values predicted from modelling. However, the measured values of drawbar pull coefficient were considerably lower than the predicted values, largely caused by internal track friction in addition to energy dissipated by soil compaction. The tractive efficiency for soft surface was also unacceptably low, probably due to the high internal track friction and the low travel speeds applied for the tests.

The research undertaken identified and confirmed a model to be used to predict contact pressure and tangential stresses for a single track element. It was capable of predicting the tractive performance for different possible contact pressure values.

Key terms: adhesion, contact pressure, rubber track, soil-rubber friction, traction, traction modelling, tractive performance.

ACKNOWLEDGEMENTS

I wish to express my appreciation to Professor H.L.M. du Plessis, my supervisor, for his instruction, advice, support and encouragement throughout my study and work.

Appreciation is also expressed to the following people for their valuable advice and help:

- Mr. C. du Toit, Agricultural Engineering Workshop Manager.
- Mr. J. Nkosi, Mr. D. Sithole and Mr. W. Morake, Technical Assistants in the Agricultural Engineering Workshop.
- Dr. R. Sinclair for reviewing the manuscript.

Finally, appreciation is expressed to my wife, my children and my parents for their love, support, encouragement and sacrifice.

TABLE OF CONTENTS

NOMENCLATURE

A	contact area, (m^2).
b	track contact width, (m).
b_o	width of octagonal ring transducer, (m).
b_t	tyre section width, (m).
b_w	width of wheel, (m).
C	constant to relate the entrance and the exit angles.
C_a	a constant to calculate the actual speed based on r_d and π.
C_{ct}	coefficient of traction.
C_t	a constant to calculate the theoretical speed based on r_d and π.
c	soil cohesion, (Pa).
c_a	soil-rubber adhesion, (Pa).
D	wheel diameter, (m).
d	tyre diameter, (m).
E	modulus of elasticity of octagonal ring transducer material, (Pa).
e	eccentric distance of centre of gravity in longitudinal direction, (m).
F	force, (N).
F_h	drawbar pull, (N).
F_{hi}	longitudinal force on i-th track segment, (N).
F_{hmax}	maximum drawbar pull, (N).
F_t	tractive force, (N).
F_{ti}	tractive force for i-th track segment, (N).
F_{tmax}	maximum tractive effort, (N).
F_x	force in horizontal direction, (N).
F_y	force in vertical direction, (N).
f_a	frequency recorded by ground speed sensor.
f_t	frequency recorded by theoretical speed sensor.
G	sand penetration resistance gradient, (Pa/m).
H	horizontal force, (N).
h	height, (m).
i	slip as decimal.

j	tangential displacement, (m).
K	tangential deformation modulus, (m).
K_1, K_2	empirical constants for soil shear.
K_r	ratio of the residual shear stress τ_r to the maximum shear stress τ_{max}.
K_ω	shear displacement where the maximum shear stress τ_{max} occurs, (m).
k_F	constant for measuring force F for extended octagonal ring transducer.
k_P	constant for measuring force P for extended octagonal ring transducer.
k_c	Bekker sinkage parameter related to cohesion, (kN/m^{n+1}).
k_ϕ	Bekker sinkage parameter related to internal soil friction, (kN/m^{n+2}).
k_c' and k_ϕ'	dimensionless constants related to pressure-sinkage tests.
L	track contact length, (m).
L_o	half distance between two circular centres of extended octagonal ring transducer, (m).
L_t	average travel distance, (m).
ℓ	length, (m).
ℓ_t	contact length, (m).
ℓ_i	track length represented by i-th track segment, (m).
N_{cs}	wheel numeric.
N_t	revolutions of drive wheel.
n	exponent of terrain deformation for Bekker sinkage equations
n_p	number of periods.
P	force, (N).
P_{in}	input power, (kW).
P_{out}	output power, (kW).
p	contact pressure, (Pa).
p_1	contact pressure at the front of the track, (Pa).
p_2	contact pressure at the rear of the track, (Pa).
p_c	pressure due to stiffness of the tyre carcass, (Pa).
p_i	contact pressure for i-th track segment, (Pa).
p_{ti}	tyre inflation pressure, (Pa).
$p(x)$	contact pressure on track at distance x (meter) from front, (Pa).
R	radius of deformed track between front and rear tires, (m).

R_c	motion resistance due to soil compaction, (N).
R_e	external track resistance, (N).
R_i	internal track resistance, (N).
R_r	total motion resistance, (N).
r	wheel radius, (m).
r_d	effective radius of the drum to measure ground speed, (m).
r_i	radius for i-th track segment, (m).
r_o	mean radius of octagonal ring, (m).
r_r	rolling radius of wheel, (m).
r_t	effective rolling radius of the track drive wheel, (m).
S_t	total slip of track as decimal.
T	torque, (N·m).
T_0	track pre-tension, (N).
t	time, (second).
t_o	thickness of octagonal ring transducer, (m).
V	forward velocity of tractor, (m/s).
V_a	absolute velocity, (m/s).
V_j	slip velocity, (m/s).
V_t	theoretical velocity, (m/s).
W	total vertical load, (N).
W_f	vertical load on front wheels, (N).
W_i	vertical load on i-th track segment, (N).
W_r	vertical load on rear wheels, (N).
X	projected distance in horizontal direction, (m).
x	distance, (m).
Z	vertical difference in height of contact circle between front and rear wheels, (m).
Z_r	depth of rut, (m).
z	sinkage, (m).
z_0	wheel sinkage, (m).
z_f	sinkage of track front, (m).
z_{f0}	initial sinkage of track front, (m).

z_r	sinkage of track rear, (m).
z_t	track sinkage, (m).
α	angle, (rad).
α_{1f}	entrance angle of front tire, (rad).
α_{2f}	exit angle of front tire, (rad).
α_{1r}	entrance angle of rear tire, (rad).
α_{2r}	exit angle of rear tire, (rad).
α_i	entrance angle of i-th track segment, (rad).
α_{i+1}	exit angle of i-th track segment, (rad).
β	tilt angle, (rad).
γ_s	unit weight of soil, (N/m^3).
δ	angle of rubber-soil friction, (degree).
$\varepsilon_{\phi P}$	strain caused by force P.
$\varepsilon_{\phi F}$	strain caused by force F.
η	tractive efficiency.
θ	angle, (rad).
θ_0	wheel entrance angle, (rad).
μ	traction coefficient.
μ_g	gross traction coefficient.
μ_φ	friction coefficient between contact surfaces.
π	wrap angle, (180°).
ρ	motion resistance ratio.
σ	contact pressure, (Pa).
τ	shear stress, (Pa).
τ_f	frictional stress, (Pa).
τ_{fi}	frictional stress for i-th segment of track, (Pa).
τ_{fmax}	maximum frictional stress, (Pa).
τ_{max}	maximum shear stress, (Pa).
τ_r	residual shear stress, (Pa).
ϕ	angle of soil internal shearing resistance, (degree).

ϕ_F	nodal angle for measuring force F on octagonal rings, (degree).
ϕ_P	nodal angle for measuring force P on octagonal rings, (degree).
ψ	tyre deflection, (m).
ω	angular velocity, (rad/s).
ω_d	angular speed of the drum for measuring ground speed, (rad/s).
ω_t	theoretical angular velocity, (rad/s).

CHAPTER I

INTRODUCTION

1.1 DEVELOPMENTS IN TERRAIN-VEHICLE MECHANICS

For a long period, one of the challenges in the design of an off-road vehicle was to equip it with a traction device that can develop high traction efficiently with the minimum soil degradation. The aim of terrain-vehicle mechanics is to provide guiding principles to obtain a better understanding of the interaction of the soil-vehicle system. The studies of terrain-vehicle mechanics are generally directed toward the problems most frequently encountered in the categories of (Yong, 1984):

- excessive soil compaction induced by vehicle traffic;
- excessive wheel or track sinkage due to the imposed ground pressure and physical characteristics of both the soil and the vehicle; and
- excessive wheel or track slippage and insufficient traction caused by internal soil shear or surface friction failure.

Generally, terrain-vehicle mechanics can be divided into three highly interdependent areas as shown in Figure 1.1. Traffic ability and terrain characterization is concerned with the ability of the terrain surface to support vehicle traffic and the environmental consequences of damage to the terrain. Performance prediction and evaluation for a vehicle is the core issue when one considers the vehicle and the environment as an integral system to be optimized. The vehicle design considerations are relevant to the design parameters and specifications of the vehicle.

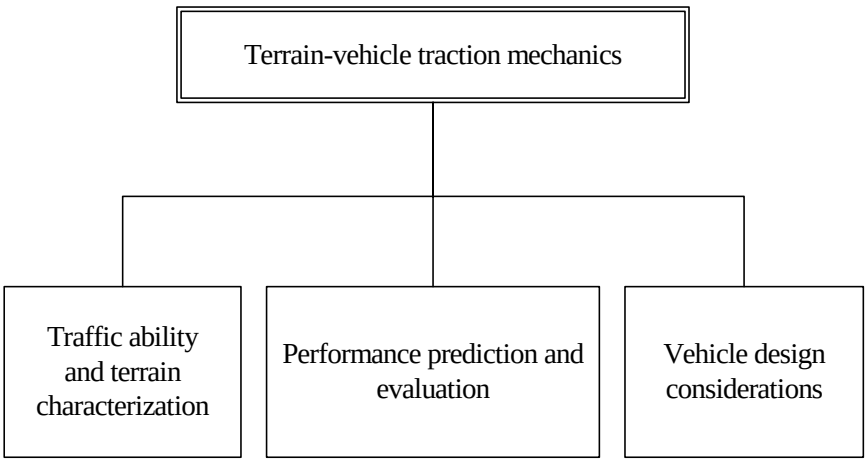

Figure 1.1. The related areas of terrain-vehicle mechanics (Yong, 1984)

1.2 OPTIMIZATION OF NEW TRACTION SYSTEMS

In the past, the choice of conventional tractive elements used for off-road vehicles to generate tractive effort was mainly restricted to either pneumatic tyres or steel tracks.

It is commonly recognized that tracked vehicles are better draught tractors because they are capable of producing high drawbar pull at a lower slip value and high tractive efficiency, even under difficult conditions such as on very soft surfaces. The large ground contact areas of the tracks result in low ground pressure and good stability on steep slopes. However, steel tracks have adverse characteristics when compared to pneumatic tyres from the point of view of steerability, manoeuvrability, noise, driver fatigue, maintenance and limited speeds. Additionally, travel on public roads is restricted in most areas due to road surface damage from penetration by the steel track grousers.

The worldwide use of steel-tracklayer tractors in the agricultural sector has declined since the introduction of large four-wheel-drive tractors. Four-wheel-drive tractors are characterized by moderate drawbar pull, high speeds, better ergonomics and good

performance, increasing the productivity over steel-tracked ones. Pneumatic tyres also allow comparatively high speed traveling on public roads. With low-pressure tyres fitted onto wheeled tractors, the compaction of soil can also be reduced.

For many years there has been an interest in developing rubber tracks to be used on tractors to combine the good tractive performance and low ground pressure of the steel tracks with the non-abrasive features, higher speeds, and asphalt road-going capability of the pneumatic tyres. In recent years, the availability of rubber compounds and methods of steel reinforcement enabled manufacturers to construct rubber tracks of adequate strength and durability for use on agricultural tractors and even earth moving machines. These tracks are cost effective and lighter than the conventional steel tracks. When summarized and compared to steel tracks, rubber tracks offer additional advantages such as:

- lower noise and less hazardous vibration levels for the operator;
- relative simplicity and lighter construction;
- ability to be used on asphalt roads without damage to the road surface; and
- higher operating speeds.

The Caterpillar Challenger series of tractors represents the most successful use of rubber tracks.

Bridgestone's positive drive rubber-covered steel tracks, driven by sprockets are also popularly used, especially for the cases of modified conventional undercarriages.

The development of alternative types of traction systems is a continuous process for many research workers, striving for better traction characteristics with less compaction or other damage to the terrain.

1.3 THE PREDICTION AND EVALUATION OF TRACTIVE PERFORMANCE

M. G. Bekker (1956, 1960, 1969) pioneered the theoretical investigation into the tractive mechanism for off-road vehicles. Although numerous attempts and considerable progress has been made in the past few decades to quantify the soil-machine interaction, understanding of this phenomenon is still far from satisfactory. Generally, models for prediction and evaluation of traction performance can be currently categorized as:

- empirical models;
- semi-empirical models; and
- analytical models.

All three methods have been used for modelling the traction of both wheeled and tracked vehicles, with various advantages and disadvantages. The details of the research undertaken by different researchers will be reviewed in Chapter 2.

1.4. THE DEVELOPMENT OF A PROTOTYPE TRACK AND THE MOTIVATION FOR THE RESEARCH

In an effort to pursue comprehensively balanced running gear for a traction vehicle to be used in agriculture, construction and military sectors in South Africa, a prototype track was developed with the feature of cable-tightened and rubber-covered steel track elements. The track is driven by smooth pneumatic tyres through rubber-rubber friction. The tractive effort of the track is also developed by soil-rubber friction and to a limited extent shear between the rubber surface of the track elements and terrain surface. Based on the walking beam concept, the track was developed to achieve a more uniformly distributed and lower vertical contact pressure, thus reducing motion resistance and soil compaction, resulting in better tractive efficiency at lower track slip values.

The aim of the design concept was to achieve greatly improved tractive performance, reduced motion resistance and soil compaction, comparable to that of a rubber crawler tracks working on soft terrain surface. This will reduce the operation cost and increase the yield of agriculture, therefore providing a significant advantage in agricultural production.

One of the important construction features for this prototype friction-based track is that it is composed out of a number of rubber covered track elements which enables low-cost replacement and maintenance when the track is partly damaged. Most of the currently in use rubber tracks are constructed as one integral single piece, i. e. a steel reinforced rubber belt, necessitating a costly replacement of the complete unit, if partly damaged.

As for other wheeled and steel-tracklayer tractors, the evaluation and performance prediction for a vehicle equipped with this prototype track is of great interest. It will assist in further validation, design modifications and optimum application of the new track system.

CHAPTER II

LITERATURE REVIEW

2.1 SOIL CHARACTERIZATION FOR TRACTION MODELLING

For off-road vehicle engineering the measurement of the soil properties is one of the fundamental tasks for the prediction and evaluation of tractive performance. Performance evaluation of terrain-vehicle systems involves both the design parameters for the vehicle and the measurement and evaluation of the physical environment within which the vehicle operates. The soil mechanical properties can be categorized as soil physical properties and soil strength parameters.

Soil physical properties affect the tractive performance of a vehicle by changing the soil strength characteristics under different conditions. However, a universal standard method does not yet exist for the measurement of the specific soil parameters. The classification and the measurement of the soil physical properties therefore depend much on the requirements of the individual user.

By utilizing the basic concepts from geotechnical and civil engineering, Karafiath & Nowatzki (1978) quoted an extensive range of references, definitions and measurements of permanent and transient soil properties for off-road vehicle engineering. Among the soil physical properties described by Karafiath & Nowatzki (1978) and Koolen & Kuipers (1983), some are usually necessary for traction such as soil classification by composition, soil porosity, soil water content, and soil density.

When the vehicle travels over a soft terrain surface, soil strength parameters are the major factors affecting the supporting, floating, shear, friction and other abilities of the soil under the vehicle load. The prediction of off-road vehicle performance, to a large

extent, depends on the proper evaluation and measurement of the strength parameters of the terrain which has been one of the major objectives of terrain-vehicle mobility research.

In geotechnical engineering, the standard methods for measuring soil strength parameters usually involve laboratory experiments, carried out on relatively small soil samples. In off-road vehicle engineering, if the soil strength and deformation characteristics are to be closely related to the field conditions under which the performance of the vehicles are evaluated, it is essential to measure the soil parameters in the field. The techniques currently in use for measuring and characterizing in-situ soil strength properties including the cone penetrometer (ASAE, 1988), bevameter (Bekker, 1969; Wong, 1993) and other techniques (Chi, Tessier, McKyes & Laguë, 1993), adopted from civil engineering.

In the highly theoretical models, utilizing the elastic-plastic theory and the finite element method (Chi, Kushwaha & Shen, 1993; Shen & Kushwaha, 1998), the soil parameters are usually measured by laboratory experiments, adapted from civil engineering such as a triaxial test and a direct shear test. As much as eight parameters may need to be measured under laboratory conditions before the development of the model (Chi, Kushwaha & Shen, 1993). This probably is the reason why the purely theoretical methods have not been used extensively for practical applications. Therefore, for the in-situ measurement in the field, the cone penetrometer and bevameter techniques are still the two most frequently used for soil characterization for traction and mobility modelling.

2.1.1 The cone penetrometer technique for soil characterization

The cone penetrometer used to evaluate soil strength for trafficability studies was initially applied by the U.S. Army Engineer Waterways Experimental Station (WES) (Freitag, 1965). To interpret and compare the results, the design and use of the cone penetrometer for agricultural applications is standardized as ASAE S313.2 (ASAE,

1988). This ASAE standard also specifies the index application range for different penetrometer types, penetration speed and depth increments for soil characterization.

The penetrometer consists of a circular 30° stainless steel cone mounted on a circular stainless steel shaft as shown in Figure 2.1. Other standardized dimensions of the penetrometer and the components are also shown in Figure 2.1.

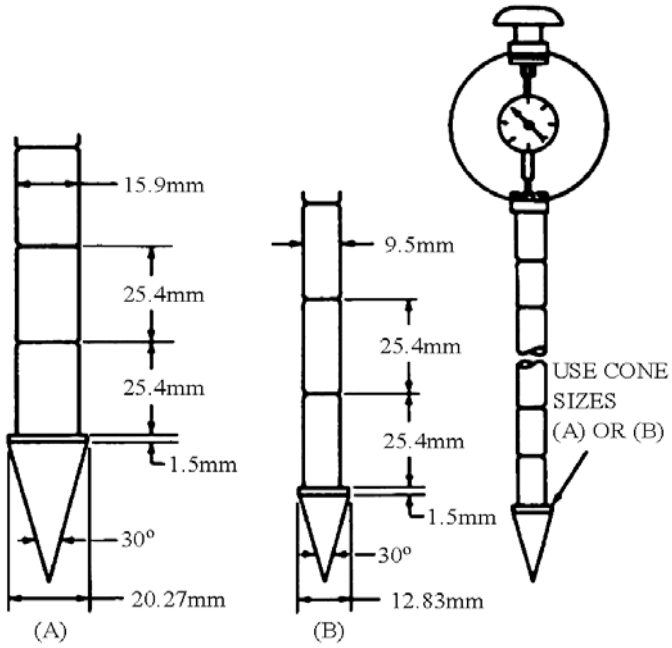

Figure 2.1. Cone penetrometer standardized by the ASAE S313.2.

The value of "Cone Index (CI)" represents the average penetration force per unit projected cone base area exerted by the soil upon the conical head when forced down to a specific depth at a penetration rate of about 3 cm/s as recommended by the ASAE standard S313.2 (ASAE, 1988). The cone index constitutes a compound parameter reflecting the comprehensive influence of shear, compression and even soil-metal friction.

The CI values may vary considerably with depth (Wismer & Luth, 1973). Therefore, the CI values usually used for traction prediction are the average value recorded over a depth corresponding to the maximum tyre or track sinkage.

For many years, the penetration test remained a very popularly used method applied by researchers for soil compaction and for some empirical traction studies. It is not only because of simplicity, convenience and ease of use, but also the provision of valuable information about the mechanical state of the soil. The value of such information can best be assessed when the CI is correlated to other information or parameters obtained from other test devices such as triaxial tests or the bevameter techniques. Although the CI value is important for soil characterization, it is questionable whether only the one value of CI is sufficient to represent the sophisticated phenomenon of soil reaction under vehicle traffic.

2.1.2 The bevameter technique for soil characterization

The bevameter technique, originally developed by Bekker (1956, 1960 and 1969) is well documented for characterizing soil strength and soil sinkage parameters relevant to tractive performance. Since a traction device or running gear applies both contact pressure and tangential stresses to the terrain surface to develop tractive effort, it seems reasonable to simulate the real phenomenon by applying loads in both directions. The bevameter technique attempts to represent this situation better than other currently available techniques (Wong, 1989, 1993).

The bevameter technique consists of:

- a plate sinkage test to determine the pressure-sinkage relationships of the soil; and
- a shear test to determine the in situ shear strength parameters of the soil.

A complete bevameter is illustrated schematically in Figure 2.2.

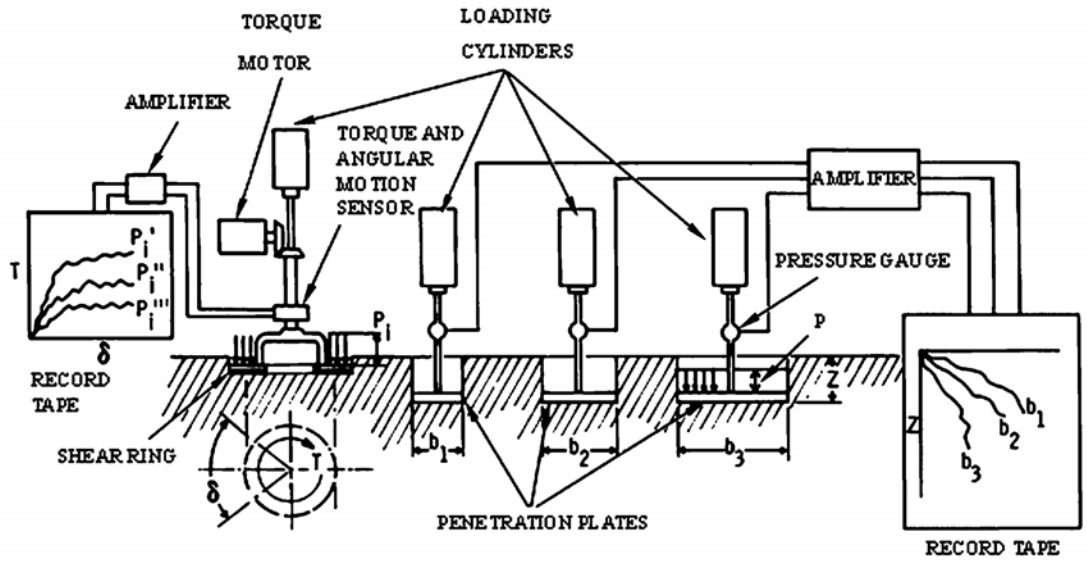

Figure 2.2. Schematic layout of a bevameter (Wong, 1993).

2.1.2.1 Measurement of pressure-sinkage relationships

By forcing rigid steel plates of different diameters or widths for rectangular plates into the soil surface for the specific test site, a typical family of pressure-sinkage curves can be generated as shown in Figure 2.3. In order to characterize the pressure-sinkage relationship for homogeneous terrain, the following equation was proposed by Bekker (1956):

$$p = (\frac{k_c}{b} + k_\phi)z^n \qquad (2.1)$$

where

p = contact pressure, (Pa).

b = width of a rectangular sinkage plate or radius of a circular sinkage plate, (m).

z = sinkage, (m).

k_c, k_ϕ and n = empirically determined pressure-sinkage soil characteristics.

In equation (2.1), k_c and k_ϕ have dimensional terms of N/m^{n+1} and N/m^{n+2} respectively and the parameters are related to soil cohesion and internal friction. The values of p and z are measured while the parameters k_c, k_ϕ and n are derived by fitting experimental data to the above equation (2.1) (Wong, 1989, 1993).

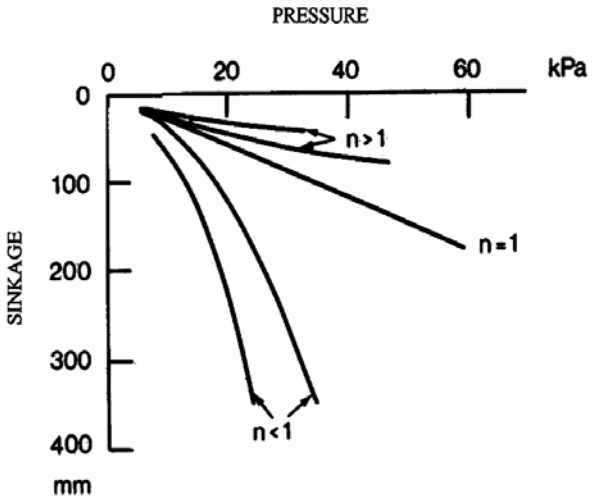

Figure 2.3. Typical pressure-sinkage curves (Bekker, 1969).

To obtain the parameters in equation (2.1), the results of a minimum of two tests with two plates having different widths or radii are required. The two tests produce two curves represented by two equations that can be rewritten in logarithmic form. They represent two parallel straight lines of the same slope on the log-log scale, where n is the slope of the lines. The values of k_c and k_ϕ are then calculated from the contact pressure for the two plates at z=1 (Wong, 1989).

It often happens that the pressure-sinkage curves may not be quite parallel on the log-log scale, probably due to the nonhomogeneity of the terrain and possible experimental errors. It is recommended by Wong (1989) that under the circumstances of two n values, the mean of the two values is usually accepted as the correct n value.

To improve the speed and efficiency of measurement and soil characterization for the bevameter technique, Wong (1980, 1989) developed a more rigorous and automated

data processing approach based on the weighted least squares method to derive the values of n, k_c and k_ϕ. In Wong's processing approach, the parameters in relation to repetitive pressure-sinkage loading-unloading were also taken into consideration. Although the technique improved the efficiency of obtaining k_c, k_ϕ and n, inherent problems still exist such as differences in behavior of a metallic plate compared to that of a rubber tyre or track, the effect of strain rate, speed of penetration and the fact that the plate can only characterize surface soil characteristics. The parameters k_c and k_ϕ in equation (2.1) also depend on the value of the exponent n.

To simplify equation (2.1) dimensionally, Reece (1965-1966) proposed the following alternative equation for the pressure-sinkage relationship:

$$p = (ck_c' + \gamma_s b k_\phi')\left(\frac{z}{b}\right)^n \tag{2.2}$$

where

k_c', k_ϕ' and n = dimensionless constants.

γ_s = unit weight of soil, (N/m^3).

c = soil cohesion, (Pa).

He also carried out a series of penetration tests to verify the validity of the principal features of the above equation. The sinkage plates used by Reece had various widths with aspect ratios of at least 4.5.

To measure the soil shear strength parameters, Reece (1965-66) built the apparatus as shown in Figure 2.4. One of the advantages of Reece's method and apparatus was that the sinkage caused by shear or so called slip-sinkage was also taken into consideration.

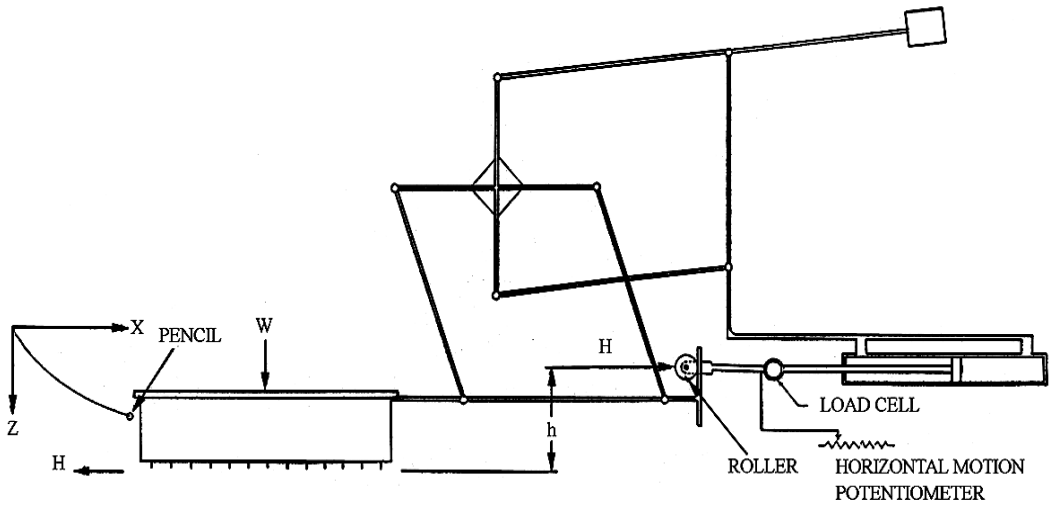

Figure 2.4. Reece's linear shear apparatus to measure soil shear strength and sinkage (Reece, 1965-1966).

Wong (1989) proved for various mineral terrains tested that the values of n, in both Bekker's equation and Reece's equation, were identical. It was also indicated that almost the same goodness-of-fit is resulted by fitting the same set of pressure-sinkage data with equation (2.1) or equation (2.2). Therefore, both Bekker's and Reece's equations were of similar form and comparable for the mineral terrain encountered for most operating conditions. As the bevameter technique was simpler and the parameters were easier to record and process, the bevameter method was more popularly used for traction studies.

Youssef and Ali (1982) reported that the accuracy of the plate sinkage analysis was affected by the size and shape of the plate used, as well as the soil strength parameters. They concluded that in order to achieve a more realistic result, the plate penetration rates ought to always be uniform and at a speed so as to simulate the situation under a track or a wheel. However, in practice, it was difficult to apply the load at such a high loading rate so as to simulate traffic. It was proved that the results from circular and rectangular sinkage plates were comparable.

Other researchers (Sela and Ehrlich, 1972; McKyes and Fan, 1985; Holm et al, 1987; Okello, 1991) also evaluated and investigated various pressure-sinkage relations for soil characterization. They were either very similar to Bekker's method or more complicated in processing than Bekker's method. Currently, the pressure-sinkage relationship, as proposed by Bekker, is still the popularly used expression for traction and is therefore chosen for the research.

2.1.2.2 Measurement of soil shear characteristics

Soil shear characterization is the second test constituting the bevameter technique. By the analysis of Bekker, a vehicle applies a shear to the terrain surface through its running gear, which results in the development of thrust and associated slip. To determine the shear strength of the terrain and to predict the tractive performance of an off-road vehicle, it is essential to measure the shear stress versus shear displacement relationship under various contact pressure conditions.

Bekker (1956) initially proposed the following equation to describe the shear stress versus shear displacement relationship for "brittle" soils with shear diagrams of a form similar to the aperiodic damped vibration:

$$\begin{aligned}\tau &= \frac{\tau_{\max}}{Y}\left(e^{(-K_2+\sqrt{K_2^2-1})K_1 j} - e^{(-K_2-\sqrt{K_2^2-1})K_1 j}\right) \\ &= \frac{c+\sigma\tan\phi}{Y}\left(e^{(-K_2+\sqrt{K_2^2-1})K_1 j} - e^{(-K_2-\sqrt{K_2^2-1})K_1 j}\right)\end{aligned} \tag{2.3}$$

where

τ = shear stress, (Pa).

τ_{max} = maximum shear stress, (Pa).

c = soil cohesion, (Pa).

ϕ = angle of soil internal shearing resistance, (degree).

σ = contact pressure, (Pa).

K_1, K_2 = empirical constants for soil shear.

j = shear displacement, (m)

Y = the maximum value of the expression within the bracket.

Based on the data for a large number of field shear tests on a variety of natural terrain surfaces, Wong (1989, 1993) concluded that three basic forms of shear stress-shear displacement relationships, which varied from Bekker's basic equation, were encountered.

A. The first type of the shear stress-shear displacement relationship exhibited the characteristics that the shear stress initially increased sharply and reached a "hump" of maximum shear stress at a particular shear displacement, and then decreased and approached a more or less constant residual value with a further increase in shear displacement (Figure 2.5). This type of shear curve may be expressed by:

$$\tau = \tau_{max} K_r \{1 + [\frac{1}{K_r(1-e^{-1})} - 1] e^{1-j/K_\omega}\} (1 - e^{-j/K_\omega}) \qquad (2.4)$$

where K_r is the ratio of the residual shear stress τ_r to the maximum shear stress τ_{max} and K_ω the shear displacement where the maximum shear stress τ_{max} occurs.

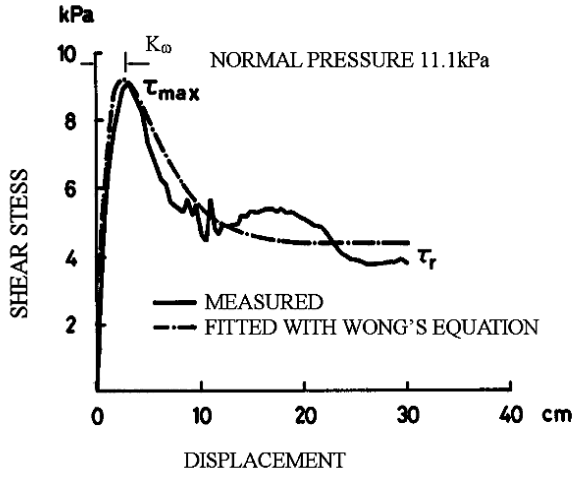

Figure 2.5. A shear curve exhibiting a peak and constant residual shear stress (Wong, 1989).

B. The second type of soil stress versus shear displacement relationship exhibited the characteristics that the shear stress increased with the shear displacement and reached a "hump" of maximum shear stress, and continued to decrease with a further increase in shear displacement as shown in Figure 2.6. It may be described by the following equation:

$$\tau = \tau_{max} (j / K_{\omega}) e^{1 - j / K_{\omega}} \tag{2.5}$$

where K_{ω} is the shear displacement where the maximum shear stress τ_{max} occurs. The rest of the symbols are as defined for equation (2.3).

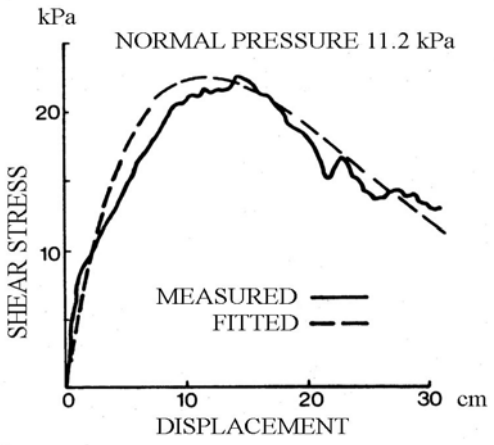

Figure 2.6. A shear curve exhibiting a peak and decreasing residual shear stress (Wong, 1989).

C. The third type of shear stress-shear displacement relationship was another modified version of Bekker's equation [equation (2.3)] containing only one constant. It was proposed by Janosi and Hanamoto (1961) as an exponential function. In practice, it is still the most popularly used expression.

$$\begin{aligned} \tau &= \tau_{max} (1 - e^{-j/K}) \\ &= (c + \sigma \tan \phi)(1 - e^{-j/K}) \end{aligned} \tag{2.6}$$

where K is referred to as the shear deformation modulus.

This relation did not display a hump but the shear stress increased with shear displacement and approached a constant value with a further increase in shear displacement as shown in Figure 2.7. The value of K determines the shape of the shear curve. Practically, the value of K can be measured directly from the shear curve or obtained from the calculation of the slope of the shear curve at the origin by differentiating τ with respect to j in equation (2.6):

$$\left.\frac{d\tau}{dj}\right|_{j=0} = \left.\frac{\tau_{\max}}{K} e^{-j/K}\right|_{j=0} = \frac{\tau_{\max}}{K} \tag{2.7}$$

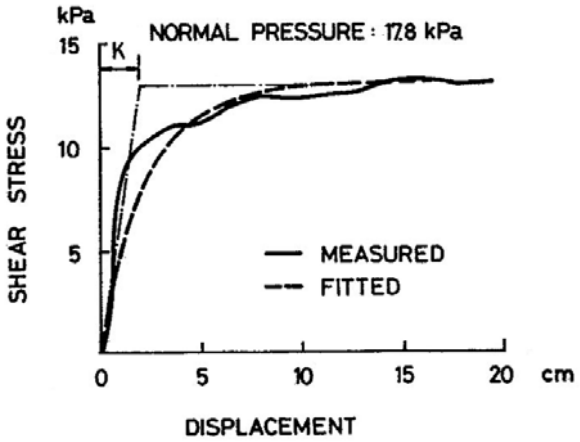

Figure 2.7. A shear curve exhibiting a simple exponential form (Wong, 1989).

The maximum shear stress for the curve is referred to as soil shear strength. The relation between the maximum shear stress and the corresponding contact pressure can be adequately described by the Mohr-Coulomb equation:

$$\tau_{\max} = c + \sigma \tan\phi \tag{2.8}$$

By plotting the measured values of the maximum shear stress versus the values of the corresponding applied contact pressure, a straight line may be obtained as shown in Figure 2.8. Therefore, the angle of soil internal shear ϕ and the soil cohesion c can be determined respectively by the slope of the straight line and the intercept of the straight line with the shear stress axis. Based on a large number of test results as shown

in Figure 2.8, Wills (1963) concluded that the shear strength parameters obtained from various shearing devices including the translational shear box, shear ring, rectangular shear plate, and rigid track were comparable.

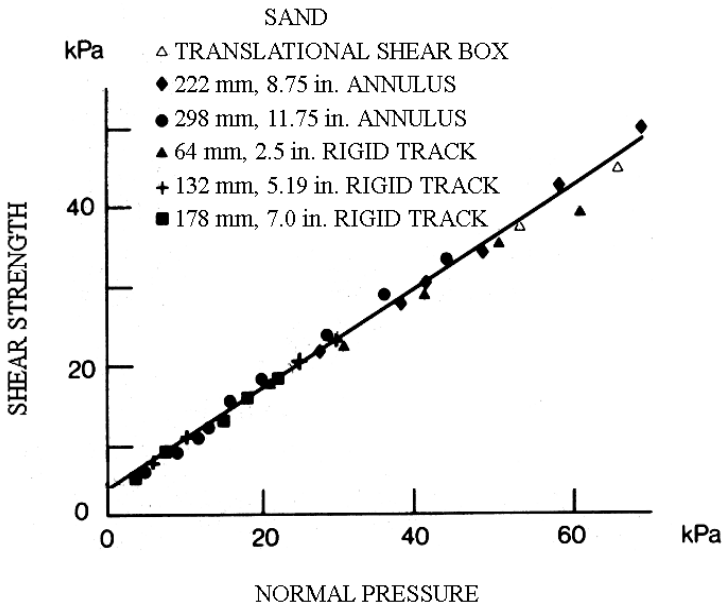

Figure 2.8. Shear strength of sand determined by various methods (Wills, 1963).

Summarized from the above literature review, it is obvious that the *in situ* measurement methods are preferable to the laboratory methods from the point of view of minimum disturbance of the soil sample. Furthermore, the *in situ* methods represent the real soil state in the field better than the methods of samples tested in a laboratory.

The cone penetrometer is perhaps the simplest in situ method and the most widely used technique. However, as only one parameter is used to describe the sophisticated phenomenon, the cone index is not sufficient to replace the soil strength parameters for representing the interaction between the running gear and the terrain surface. Despite its limitations to interpret the comprehensive soil property, the cone penetrometer with further modification and validation can efficiently be used for traction prediction. Alternatively it is also more suitable for the evaluation of soil compaction studies.

2.1.3 Friction and adhesion characterization for the soil-rubber contact surface

When a rubber tyre travels on a comparatively hard surface or a rubber track with a smooth surface travels on a terrain surface, minimal shear action occurs within the soil. The soil-rubber friction and the adhesion at the contact surface are the dominant factors for developing tractive thrust. Thus the characterization of rubber-soil friction and adhesion is of importance in developing a traction model for the track.

For describing the maximum friction and adhesion between a solid material surface and soil, the following equation, proposed by Terzaghi (1966), can be used:

$$\tau_{f\,max} = c_a + p\tan\delta \tag{2.9}$$

Where

τ_{fmax} = maximum friction stress, (Pa).
c_a = adhesion on the contact surface, (Pa).
p = normal pressure, (Pa).
δ = angle of friction between the rubber surface and soil, (degrees).

Equation (2.9) has the same form as equation (2.8), but the terms are different in physical definition.

Neal (1966) reported results of an investigation to compare the parameters in equations (2.8) and (2.9). As shown in Table 2.1, he concluded that the coefficient of soil to rubber friction, tan δ was, if not exactly the same, only slightly different from the coefficient of internal soil shear resistance, tan ϕ. However, the adhesion between rubber and soil c_a was less than the internal cohesion of the soil c, except for sand with both values negligibly small, which was not listed in the data. The value of c_a changed considerably with the soil water content. Reece's (1965-1966) research lead to the same conclusion as Neal's. This indicates that in sandy soils, where the values of rubber-soil friction coefficient are similar to the values of the coefficient of soil

internal shear resistance, the performance of a friction-based traction device is expected to be almost similar to that of shear-based traction device.

Table 2.1. Comparison of soil internal shear and soil-rubber frictional parameters (Neal, 1966).

Soil water content, %	Internal frictional angle for soil shear ϕ, degrees	Soil internal cohesion c, kPa	Soil-rubber frictional angle δ, degrees	Soil-rubber adhesion c_a, kPa
17.9	31.9	0.62	28.4	0.55
13.4	29.1	2.59	29.9	0.69
10.69	29.9	0.34	28.7	0.69
8.73	29.9	1.38	30.0	0.69

From the statistical data by Wong (1989), it was proved that the adhesion accounts for only a small portion of the total value of τ_{fmax}. Wong (1989) also concluded that among the soil shear parameters, although the specified test apparatus were not explained, the angles for soil-soil shearing resistance and rubber-soil friction were very similar, while the values of adhesion for rubber-soil were generally smaller than the soil-soil cohesion.

`

2.2 TRACTION PERFORMANCE MODELLING FOR WHEELED VEHICLES

2.2.1 Empirical methods for traction performance modelling

To predict the performance of vehicles, empirical methods are mainly based on the soil cone index (CI) as the single soil strength parameter to be measured. One of the well-known empirical models based on CI were originally developed during World War II by the US Army Waterways Experiment Station (WES) (Rula and Nuttall, 1971) as a means of measuring trafficability of terrain on a "go/no go" basis.

In developing the WES model (Rula and Nuttall, 1971), numerous tests were performed for a range of terrain types on primarily fine- and coarse-grained soils. The measured data for vehicle performance and terrain conditions were then empirically correlated, and a model known as the WES VCI was proposed for predicting vehicle performance on fine- and coarse-grained inorganic soils. The methods applied in the WES VCI models were very similar for wheeled and tracked vehicles (Rula and Nuttall, 1971).

With the widespread use of similitude and dimensional analysis in the early 1960's (Freitag, 1965; Turnage, 1972, 1978), an empirical model for the performance of a single tyre, based on dimensional analysis was developed at WES. In this model, two soil-tyre numerics, the clay-tyre numeric N_c and the sand-tyre numeric N_s were defined as below:

$$N_c = \frac{Cb_t d}{W} \times \left(\frac{\psi}{h}\right)^{1/2} \times \left(\frac{1}{1 + b_t / 2d}\right) \tag{2.10}$$

and

$$N_s = \frac{G(b_t d)^{3/2}}{W} \times \frac{\psi}{h} \tag{2.11}$$

where

b_t = tyre section width, (m).

CI = cone index, (Pa).

d = tyre diameter, (m).

h = tyre section height, (m).

W = tyre vertical load, (N).

G = sand penetration resistance gradient, (Pa/m).

ψ = tyre deflection, (m).

A soil-tyre numeric N_{cs} was proposed for cohesive-frictional soils by Wismer and Luth (1973) as:

$$N_{cs} = \frac{CIb_t d}{W} \tag{2.12}$$

The above mentioned three equations, especially equation (2.12), are the most commonly used empirical relationships to predict traction performance for wheels. On the bases of test results, mainly from soil bin tests in laboratories, the soil-tyre numerics were correlated with the three traction performance parameters for tyres. Among the parameters used in this equation, rolling resistance is a parameter often correlated with the soil-tyre numerics.

Wismer and Luth (1973) developed the following generally used equations for not highly compactible soils:

$$\rho = \frac{R_r}{W} = \frac{1.2}{N_{cs}} + 0.04 \tag{2.13}$$

$$\mu_g = \frac{T}{r_r W} = \frac{F_t}{W} = 0.75(1 - e^{-0.3 N_{cs} S}) \tag{2.14}$$

where

R_r = motion resistance, (N).

N_{cs} = wheel numeric, (CIbd/W).

T = applied torque, (Nm).

r_r = rolling radius based on a zero condition when net traction is zero at zero slip on a hard surface, (m).

F_t = gross tractive force, (N).

W = vertical load, (N).

ρ = motion resistance ratio.

μ_g = gross traction coefficient.

For the determination of r_r in the above equation, the slip is defined as:

$$i = (1 - \frac{V}{r\omega}) \times 100\% \tag{2.14a}$$

where

V = velocity of the wheel centre, (m/s).

r = radius of the wheel, (m).

ω = angular velocity, (rad/s).

Thus, the wheel pull coefficient or traction coefficient μ was calculated from:

$$\mu = \frac{F_t - R_r}{W} = \mu_g - \rho \tag{2.15}$$

For its simplicity and as only one parameter needed to be measured, the above described empirical method based on cone index used by many users to evaluate wheeled tractors under some given conditions. However, as pointed out by Wong (1989), the original concept of using the simple measurement of cone index is limited by the lack of information for the terrain conditions. The application is also strictly limited to cases which are similar to the conditions under which the original tests were undertaken. The exact range of soil conditions for which soil numerics are applicable also remains to be determined. This method should therefore be used with caution if the tyre or conditions differ from those under which the data were collected.

2.2.2 Analytical methods for traction performance modelling

Based on the parameters measured by the bevameter technique, Bekker originally developed one of the best known and most commonly used analytical methods - also known as a semi-empirical method for traction (Bekker, 1956, 1960, 1969; Wong, 1989, 1993). The principle of this analytical method was based on the assumptions that the vertical deformation in the soil under load was analogous to the soil deformation under a sinkage plate and that the shear deformation of the soil under a traction device was similar to the shear action performed by a rectangular or torsional shear device. The motion resistance of the running gear on a soft soil surface was predicted by assuming that the resistance was mainly caused by compacting the soil and the energy dissipated in forming a rut in the soil below the running gear. The total tractive effort was predicted by integrating the horizontal component of shear stress beneath the running gear in the direction of travel.

In the basic model proposed by Bekker (1956), a towed rigid wheel was analyzed based on the configuration of the contact surface as shown in Figure 2.9. For this simplified model, the motion resistance resulting from soil compaction was predicted as:

$$R_c = b_w \int_0^{Z_r} \left(\frac{k_c}{b} + k_\phi\right) z^n dz$$

$$= \frac{(3W)^{(2n+2)/(2n+1)}}{(3-n)^{(2n+2)/(2n+1)}(n+1)(k_c + b_w k_\phi)^{1/(2n+1)} D^{(n+1)/(2n+1)}} \qquad (2.16)$$

where

R_c = motion resistance, (N).

Z_r = depth of the rut, (m).

b_w = width of the wheel, (m).

W = wheel load, (N).

D = diameter of the wheel, (m).

k_c, k_ϕ and n = empirically determined pressure-sinkage soil characteristics.

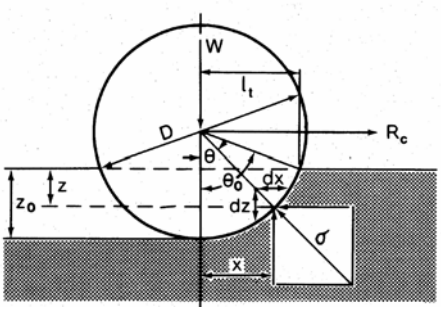

Figure 2.9. Simplified rigid wheel-soil interaction model by Bekker (1956).

This generalized equation is valid for moderate sinkage (i.e., $z_0 \leq D/6$) for any rigid wheel or highly inflated tyre with minimal deflection in homogeneous soft soils of any type. It is more accurate for larger wheel diameters and limited sinkage in soft soil. The sinkage of such a wheel z_0 is also determined from the following equation (Bekker, 1956):

$$z_0 = \left[\frac{3W}{(3-n)(k_c + b_w k_\phi)\sqrt{D}} \right]^{\frac{2}{2n+1}} \tag{2.17}$$

where

z_0 = sinkage of the wheel, (m).

b_w = width of the wheel, (m).

The rest of the symbols are as defined in equation (2.16).

For a pneumatic tyre, when the terrain is firm and the inflation pressure is sufficiently low, significant tyre deformation occurs (Figure 2.10). The sinkage of the tyre z_0 in this case can be determined by applying the following equation together with Bekker's sinkage equation:

$$z_0 = \left(\frac{p_{ti} + p_c}{(k_c / b_w) + k_\phi} \right)^{1/n} \tag{2.18}$$

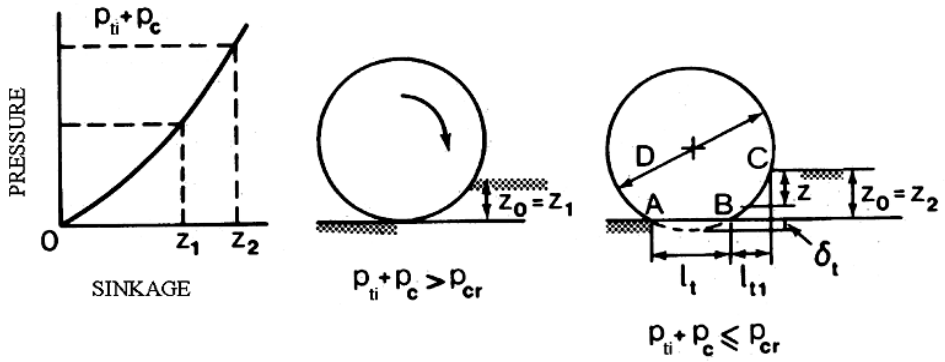

Figure 2.10. Deformation of a pneumatic tyre in different operating modes (Wong, 1989).

Under these circumstances, the motion resistance is given by:

$$R_c = \frac{b_w(p_{ti}+p_c)^{(n+1)/n}}{(n+1)(k_c/b_w+k_\phi)} \tag{2.19}$$

where

p_{ti} = inflation pressure, (Pa).

p_c = pressure due to the stiffness of the carcass, (Pa).

As proposed by Wong & Reece (1967), the analysis for the shear displacement developed along the contact area of a rigid wheel based on the analysis of the slip velocity V_j is shown in Figure 2.11 and is described by:

$$V_j = r\omega[1-(1-i)\cos\theta] \tag{2.20}$$

where

i = slip of the wheel as defined in equation (2.14a), (%).

r = wheel radius, (m).

ω = angular velocity of the wheel, (rad/s).

It is shown that the slip velocity for a rigid wheel varies with the angle θ and slip i.

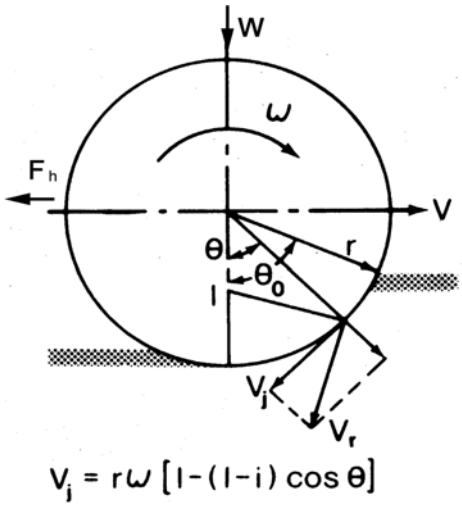

Figure 2.11. Analysis of shear displacement under a wheel (Wong, 1993).

The shear displacement along the interface is given by:

$$j = \int_0^t V_j dt = \int_0^{\theta_0} r\omega[1-(1-i)\cos\theta]\frac{d\theta}{\omega}$$
$$= r[(\theta_0 - \theta) - (1-i)(\sin\theta_0 - \sin\theta)] \qquad (2.21)$$

where θ_0 is the entrance angle of the wheel.

By applying the relationship of shear stress and shear displacement, as proposed by Janosi and Hanamoto (1961), the shear stress can be described as:

$$\tau(\theta) = [c + p(\theta)\tan\phi](1 - e^{j/K})$$
$$= [c + p(\theta)\tan\phi][1 - e^{-(r/K)[\theta_0 - \theta - (1-i)(\sin\theta_0 - \sin\theta)]}] \qquad (2.22)$$

By integrating the horizontal component of the stresses in the direction of travel over the entire contact area, the total tractive effort F_t can be determined:

$$F_t = \int_0^{\theta_0} \tau(\theta)\cos\theta d\theta \qquad (2.23)$$

To take into consideration the effect of shear stress on the vertical load and the effect of normal stress on the horizontal force, the equations for predicting the vertical load

and drawbar pull for a rigid wheel are given by equations (2.24) and (2.25) (Wong, 1993) respectively.

For vertical load,

$$W = rb_w \left[\int_0^{\theta_0} p(\theta) \cos \theta d\theta + \int_0^{\theta_0} \tau(\theta) \sin \theta d\theta \right] \quad (2.24)$$

For available pull,

$$F_h = rb_w \left[\int_0^{\theta_0} \tau(\theta) \cos \theta d\theta - \int_0^{\theta_0} p(\theta) \sin \theta d\theta \right] \quad (2.25)$$

Generally speaking, the methods for predicting the tractive performance for a pneumatic tyre are mainly dependent on the individual mode of operation. Other key issues for a wheel also include the distribution of normal and shear stress, and the profile of the contact patch.

2.3 TRACTION MODELLING FOR TRACKED VEHICLES

2.3.1 Empirical methods for traction performance modelling

Empirical methods are still playing an important role for the evaluation of the performance of tracked vehicles. The empirical methods are mainly based on cone penetrometer values as originally developed by WES (Rula and Nuttall, 1971). They follow similar methods used for the wheeled vehicles reviewed in the previous section.

2.3.2 Analytical methods for traction performance modelling

One of the most popular analytical methods for the performance of a track system was originally developed by Bekker (1956, 1960, 1969) based on the assumption that the track in contact with the terrain is similar to a rigid footing. By using Bekker's

pressure-sinkage equation (2.1), for a rigid, relatively smooth, uniformly loaded track, as shown in Figure 2.12, the track sinkage z_t is given by:

$$z_t = \left[\frac{p}{(k_c/b)+k_\phi}\right]^{1/n} = \left[\frac{W/bL}{(k_c/b)+k_\phi}\right]^{1/n} \tag{2.26}$$

The motion resistance of the track due to soil compaction R_c is:

$$R_c = \frac{1}{(n+1)(k_c/b+k_\phi)^{1/n}}\left(\frac{W}{L}\right)^{(n+1)/n} \tag{2.27}$$

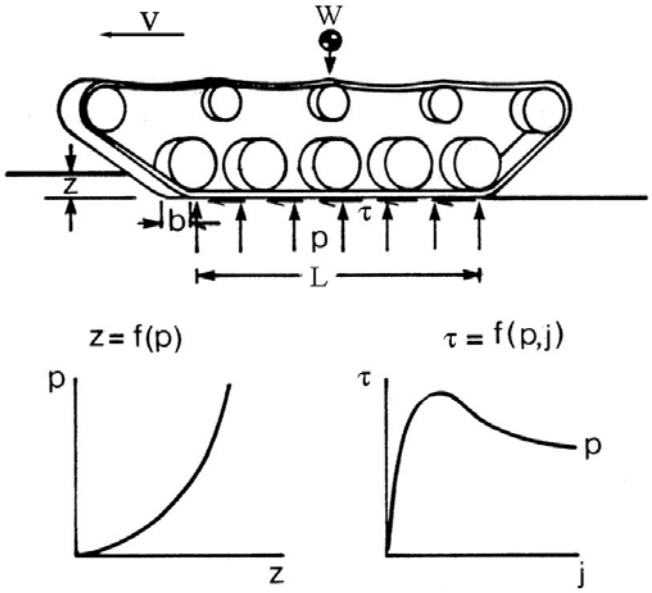

Figure 2.12. Simplified model for track-soil interaction (Wong, 1989).

If the contact pressure is uniformly distributed and the shear stress-shear displacement has a simple exponential relationship as shown in equation (2.6), the tractive effort of a track with contact area of A can be determined from:

$$\begin{aligned} F_t &= b\int_0^L (c + \frac{W}{bL}\tan\phi)(1 - e^{-ix/K})dx \\ &= (Ac + W\tan\phi)\left[1 - \frac{K}{iL}(1 - e^{-iL/K})\right] \end{aligned} \tag{2.28}$$

Using the maximum shear strength τ_{max} defined by equation (2.8), the maximum tractive effort F_{tmax} is therefore determined as:

$$\begin{aligned} F_{t\,max} &= A\,\tau_{max} \\ &= A[\,c + p\tan\phi\,] \\ &= Ac + W\tan\phi \end{aligned} \tag{2.29}$$

Thus the available pull F_h and the maximum pull F_{hmax} in horizontal direction are expressed by:

$$\begin{aligned} F_h &= F_t - R_c \\ &= (Ac + W\tan\phi)\left[1 - \frac{K}{iL}(1 - e^{-iL/K})\right] - \frac{1}{(n+1)(k_c/b + k_\phi)^{1/n}}\left(\frac{W}{L}\right)^{(n+1)/n} \end{aligned} \tag{2.30}$$

and

$$\begin{aligned} F_{h\,max} &= F_{t\,max} - R_c \\ &= (Ac + W\tan\phi) - \frac{1}{(n+1)(k_c/b + k_\phi)^{1/n}}\left(\frac{W}{L}\right)^{(n+1)/n} \end{aligned} \tag{2.31}$$

Practically, the distribution of normal stress on the track-terrain interface plays an important role for predicting the performance. In order to verify the theoretical assumption, Wills (1963) used a specially designed cantilever-type track link dynamometer to determine the distribution of normal pressure under a uniformly loaded rigid track by measuring the vertical and the horizontal forces between a track link and a track plate. The magnitude and distribution of horizontal shear force developed under the track were also measured. The effects of other different values of normal stress distribution (Figure 2.13) on tractive efforts were also investigated by Wills (1963).

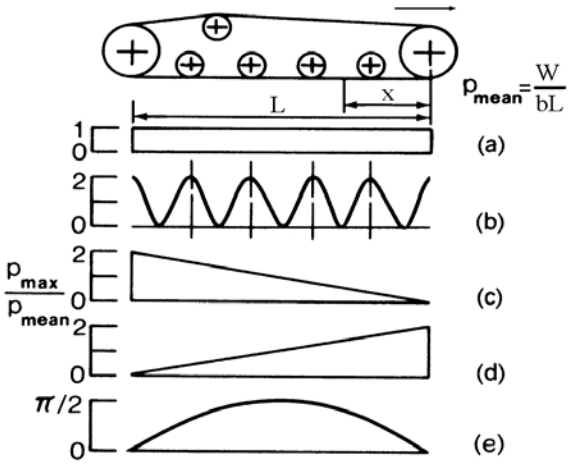

Figure 2.13. Various patterns of idealized contact pressure distribution under a track (Wills, 1963).

It proved that the normal stress distribution beneath a rigid track influenced the development of the tractive effort. In the case as shown in Figure 2.13(b), the normal pressure p has a multi-peak sinusoidal distribution expressed by:

$$p = \frac{W}{bL}\left(1 + \cos\frac{2n_p\pi x}{L}\right) \tag{2.32}$$

where n_p is the number of periods as shown in Figure 2.13. In a frictional soil with c=0, the shear stress developed along the contact length is expressed by:

$$\tau = \frac{W}{bL}\tan\phi\left(1+\cos\frac{2n_p\pi x}{L}\right)(1-e^{-ix/K}) \tag{2.33}$$

and the tractive effort is calculated as:

$$\begin{aligned} F_t &= b\int_0^L \frac{W}{bL}\tan\phi\left(1+\cos\frac{2n_p\pi x}{L}\right)(1-e^{-ix/K})dx \\ &= W\tan\phi\left[1+\frac{K}{iL}(e^{-iL/K}-1)+\frac{K(e^{-iL/K}-1)}{iL(1+4n_p{}^2K^2\pi^2/i^2L^2}\right] \end{aligned} \tag{2.34}$$

The tractive effort of a track with other contact pressure distribution patterns can be also predicted in a similar way. In the case of (c) (Figure 2.13), the pressure increases linearly from front to rear p=2[W/(bL)](x/L), and the tractive effort of a track in frictional soil is given by:

$$F_t = W\tan\phi\left[1-2\left(\frac{K}{iL}\right)^2\left(1-e^{-iL/K}-\frac{iL}{K}e^{-iL/K}\right)\right] \tag{2.35}$$

In the case of a contact pressure increasing linearly from rear to front, represented by p=2[W/(bL)](l-x)/L) as shown in Figure 2.13(d), the tractive effort of a track in frictional soil is calculated from:

$$F_t = 2W\tan\phi\left[1-\frac{K}{iL}\left(1-e^{-iL/K}\right)\right] - W\tan\phi\left[1-2\left(\frac{K}{iL}\right)^2\left(1-e^{-iL/K}-\frac{iL}{K}e^{-iL/K}\right)\right] \tag{2.36}$$

In the case of a sinusoidal distribution with maximum pressure at the center and zero pressure at the front and rear end (p=(W/bL)(π/2)sin(πx/L), as in Figure 2.13(d)), the tractive effort in a frictional soil is determined by:

$$F_t = W\tan\phi\left[1-\frac{e^{-iL/K}+1}{2(1+i^2L^2/\pi^2K^2)}\right] \tag{2.37}$$

Figure 2.14 shows the variation of the tractive effort with slip of a track with various types of contact pressure distribution on sand, as mentioned above (Wills, 1963). It can be seen that the contact pressure distribution has a noticeable effect on the development of tractive effort, particularly at low values of slip when the tractor is usually operated. In this point of view, the bottom one of the pressure distribution patterns as shown in the figure is most preferred for larger value of drawbar pull at lower value of slip. In fact, the distribution of normal pressure and shear stress are among the most important issues in the analytical models based on Bekker's method.

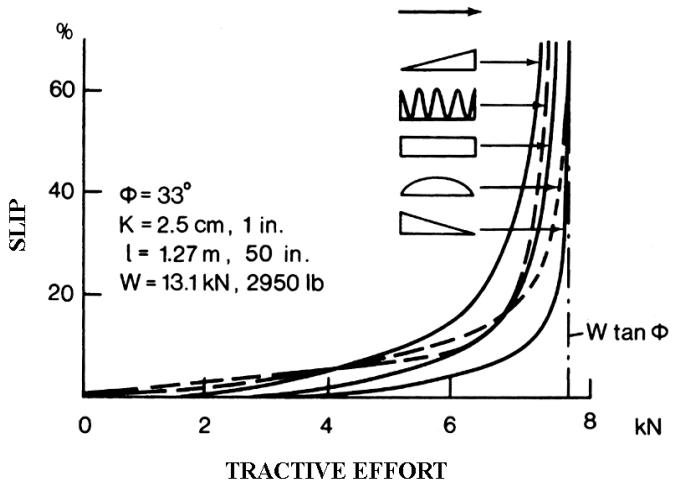

Figure 2.14. Effect of contact pressure distribution on the tractive performance of a track in sand (Wills, 1963).

The experiments performed and the results obtained by Wills (1963) in the laboratory with full size rigid tracks are important because in these experiments both the vertical and the horizontal forces acting on a track link were measured simultaneously. However, due to the practical difficulties to mount force transducers onto a track, little effort has since been made to measure the normal and horizontal forces simultaneously on the track. Other experiments aimed at the determination of the pressure distribution under tracks were only restricted to the measurement of normal stresses.

Wong (1989, 1993) developed a model based on the analysis of track-terrain interaction to predict the performance of the traditional steel track. In Wong's model, the contact pressure distribution was predicted by determining the shape of the deflected track in contact with the terrain. In the analysis, the track is assumed to be equivalent to a flexible belt and the assumed track-road wheel system travelling on a deformable terrain under steady-state conditions is shown in Figure 2.15. The magnitude of the slip velocity V_j of a point P on a flexible track is expressed by:

$$\begin{aligned} V_j &= V_t - V\cos\alpha \\ &= r\omega - r\omega(1 - i)\cos\alpha \\ &= r\omega[1 - (1 - i)\cos\alpha] \end{aligned} \tag{2.38}$$

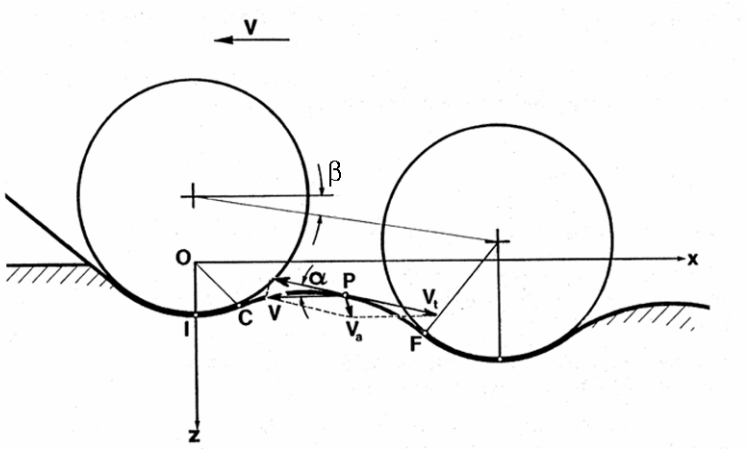

Figure 2.15. Deformation of the interaction surface used in Wong's model (Wong, 1993).

The shear displacement j along the track-terrain interface for contact length is given by:

$$\begin{aligned} j &= \int_0^t r\omega\,[\,1-(\,1-i\,)]\,dt \\ &= \int_0^{\ell} r\omega\,[\,1-(\,1-i\,)]\,\frac{d\ell}{r\omega} \\ &= \ell - (1-i)x \end{aligned} \tag{2.39}$$

The shear stress distribution is expressed by:

$$\tau(x) = [\,c + p(x)\tan\phi\,]\left\{1-\exp\left[-\left(\frac{\ell-(1-i)x}{K}\right)\right]\right\} \tag{2.40}$$

where p(x) is the contact pressure on the track and is a function of x.

In this model, for a vehicle with two tracks, the external motion resistance R_e is given by

$$R_e = 2b\int_0^{\ell_t} p\,\sin\,\alpha\,d\ell \tag{2.41}$$

And the tractive effort F_t for a vehicle with two tracks is given by:

$$F_t = 2b\int_0^{\ell_t} \tau \cos\alpha d\ell \tag{2.42}$$

In Wong's model, the response to repetitive loading was also included in the analysis.

According to the reported results, a close agreement between the measured and predicted contact pressure distribution values as well as drawbar performance was recorded.

It was mentioned by Wong (1993) that for a track with rubber pads, the part of the tractive effort generated by rubber-terrain interaction could be predicted by taking into consideration the portion of the vehicle weight supported by the rubber pads, the area of the rubber pads in contact with the terrain, and the characteristics of rubber-terrain frictional slip. However, there was no further description given in this respect.

2.4 DEVELOPMENT OF AND TRACTION CHARACTERISTICS FOR RUBBER TRACKS

Initially, the idea of rubber tracks was proposed in the early 1970's. The first type was a pneumatic rubber track tested by Taylor and Burt (1973). The pneumatic rubber track consisted of a circular shaped, and nylon reinforced flexible tyre, mounted over stretching wheels fixed to a frame. In their study, the traction performance and soil compaction was compared for a steel track, a pneumatic rubber track and a pneumatic tyre in a soil tank. The tractive efficiencies for various soil types ranged from 80% to 85% for both the steel and the pneumatic rubber tracks and from 55% to 65% for the pneumatic tyre. Maximum tractive efficiencies occurred at less than 10% slip for the tracks and between 15% and 25% for the tyre. In general, both the steel and pneumatic tracks had comparable traction performance characteristics. However, the performance of both tracks was much higher than that for a pneumatic tyre.

Evans and Gove (1986) reported the test results comparing the tractive performance and soil compaction for a rubber belt track and a four-wheel drive tractor. The tests were conducted in tilled soil and firm soil and proved that the rubber belt tractor, in comparison to the four-wheel drive tractor, developed higher tractive efficiencies at a specified pull ratio and generated an equivalent drawbar pull at lower slip levels. The maximum tractive efficiency in tilled and firm soil was 85% and 90% for the rubber belt tractor and 70% and 85% for the four-wheel drive tractor. The reported results for soil compaction tests conducted in the tilled soil showed that the rubber belt tractor and the four-wheel drive tractor caused similar increases in cone penetration resistance as they had equal mass. However, the measurement of subsoil pressure proved that at the same depth, peak subsoil vertical stresses were twice as high for the four-wheel drive tractor as for the rubber belt tractor. The rubber track also depicted a more uniformly distributed contact pressure under the track than for the wheel.

Culshaw (1988) reported about two experiments in which the tractive performance of rubber tracks were compared to that of tractor drive tyres. The first experiment was a comparison between a friction drive rubber track and a conventional radial type tractor tyre. The tests were conducted by alternatively mounting the track and the tyre on a single wheel tester. The results proved that the rubber track produced about 25% more drawbar pull than the tyre. The second experiment was a comparison between a small dumping truck running on rubber tracks and a conventional two-wheel drive tractor with a similar mass. It was proved that the truck produced twice the pull of the wheeled tractor with similar tractive efficiencies and caused less rutting on a soft soil.

Esch, Bashford, Von Bargen and Ekström (1990) reported a comprehensive traction performance comparison between a rubber belt track tractor and a four-wheel drive tractor equipped with dual wheels, having comparable power and mass. The drawbar tests were performed on four ground surface conditions: untilled oats stubble, disked oats stubble, plowed oats stubble, and maize stubble. The tractive performance was compared based on relationships of dynamic traction ratio to slip, tractive efficiency to slip and tractive efficiency to dynamic traction ratio. It showed that the rubber belt

track offered small advantages over the four-wheel drive tractor on firm surface but significant advantages under soft surface conditions.

In the research reported by Okello et al (1994), it was found that the rubber tracks had higher rolling resistance than the tractor driving wheel tyre apparently due to the internal power losses in the track unit. Accordingly, the tractive efficiencies of the rubber tracks were lower than that of the tyre because of the higher rolling resistance for the track.

Dwyer et al (1993) reviewed the research on rubber tracks at the Silsoe Research Institute. Two mathematical models, namely an infinitely stiff and infinitely flexible track (Figure 2.16), were described for predicting the tractive performance. The contact pressure at each point on the ground contact surface was calculated from the pressure-sinkage relationship in equation (2.1). The shear stress-shear displacement relationship in equation (2.6) was applied to predict the tangential stress. The equations of equilibrium were established by using the track deformation assumptions for two extreme flexibility situations. The equilibrium equations for the infinitely stiff model are as follow:

In the vertical direction:

$$W = b\int_0^L (p\cos\beta + \tau\sin\beta)dx \tag{2.43}$$

In the horizontal direction:

$$R_r = b\int_0^L p\sin\beta dx \tag{2.44}$$

and

$$F_t = b\int_0^L (\tau\cos\beta - p\sin\beta)dx \tag{2.45}$$

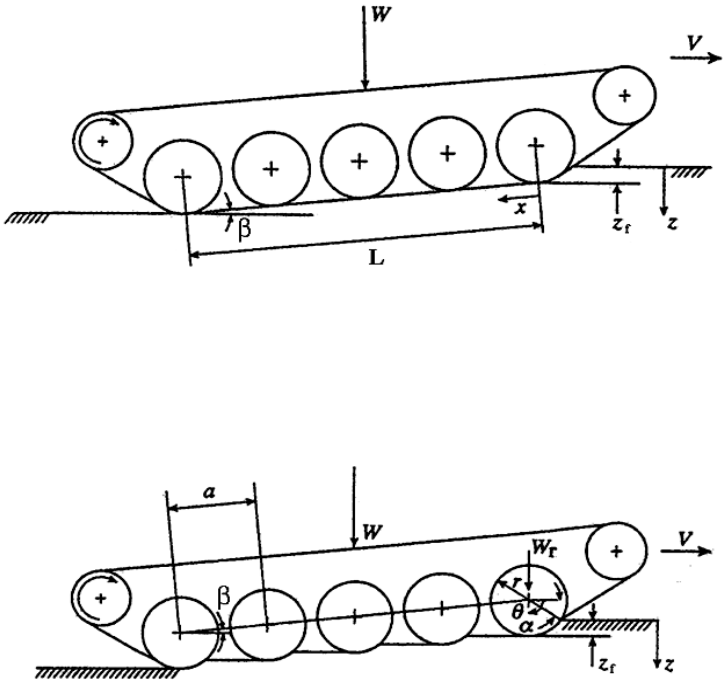

Figure 2.16. The infinitely stiff and the infinitely flexible models by Dwyer *et al.* (1993).

With the infinitely stiff assumption, the solution was independent of the diameter or spacing of the ground rollers and the ground contact area was a flat and rectangular plate. With the infinitely flexible model, the track unit behaved like a multi-wheel vehicle, as if there was no track at all, and the performance depended entirely on the number and diameter of the ground rollers. The results of the field tests with the experimental track unit on a single-wheel tester proved that the tractive performance of the rubber track was over-predicted by the infinitely stiff model and considerably under-predicted by the infinitely flexible model. The method, based on Wong's procedure, was used in the analysis. They determined that the profile of ground contact surface and thus the stress distribution was the major factor causing the difference.

A model was developed by Okello et al (1998) to study the traction performance and ground pressure distribution of a rubber track unit on soft agricultural soils. By closely following Wong's method of steel tracks, the model made use of relevant soil characterization parameters obtained by applying shear and sinkage tests based on the

bevameter technique. The effect of repetitive loading was also taken into consideration by the procedure suggested by Wong (1989). For their research a rubber track unit was mounted on a structure similar to the one for a traditional steel track. The theoretical model was validated against the experimental results by attaching the rubber track unit to the rear of a single-wheel tester. For two of the four soil conditions tested, the results from the theoretical prediction and the experimental data were compared and showed close agreement with a maximum difference of only 7.5%. For other two soil conditions, the predicted results were not provided for the reason of failed soil shear tests.

In recent years, the rubber tracks became more popular for their combined advantages when compared to conventional steel tracks and the wheels, as summarized in Chapter 1. The rubber tracks are currently mainly used on agricultural tractors and some construction machinery. However, they are also used on combines.

After the development over a decade, the Challenger tractor series equipped with rubber belt tracks from Caterpillar became the major rubber track crawler tractors available on the market. The historical development and the technical features for the Challenger Series were reported in the relevant ASAE lectures (Caterpillar Inc., 1995). A friction drive is utilized to transmit the power from the sprocket to the rubber belt tracks and the rubber tracks have lugs in contact with soil to generate the thrust effort.

According to the design principle, if the track tension is set higher than the maximum traction effort developed by the track, slip will not occur between the track and the driving wheel and the efficiency will not be reduced. Overloading of friction drives may lead to slipping of the rubber belt, but with minimal belt damage. However, a combination friction/positive drive unit leads to a longer service life for the rubber belt and positive safe transmission of driving power (Dudzinksi & Ketting, 1996). Besides the success of the Challenger crawler tractors, other types of rubber tracks are also being pursued for improved tractor construction. It is still too early to reach a conclusion whether the friction driven tracks used on the Challenger series is superior to the positive drive rubber track with sprocket as developed by Bridgestone.

As can be seen from the above review, the previous research was mainly concentrating on the comparison of performance for the rubber tracks and conventional traction devices. Further research needs to be done on the prediction of performance and traction modelling to develop a better understanding of the traction mechanism and to guide further improvement of the design for rubber tracks if they are to be utilized on a larger scale.

2.5 MEASUREMENT OF THE DISTRIBUTION OF CONTACT AND TANGENTIAL STRESSES BELOW A TRACK

2.5.1 Track link dynamometer by Wills (1963)

In order to verify the assumptions of different contact pressure distributions, Wills designed and built a cantilevered dynamometer beam as shown in Figure 2.17. By the application of strain gauge transducers, the distribution and magnitude of the contact pressure and horizontal shear force below a steel track was measured simultaneously. The results in sand for different distribution types were also compared.

The results from Will's research work are currently still cited by many researchers.

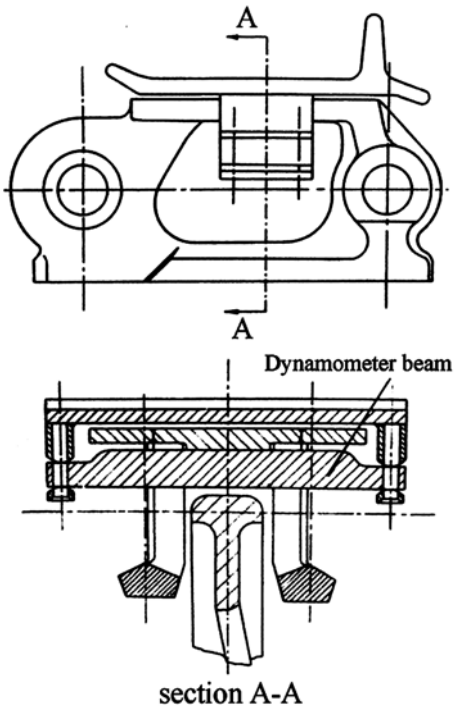

Figure 2.17. Track link dynamometer by Wills (1963).

2.5.2 Applications of extended octagonal ring transducers for measuring two perpendicular forces

The principle of the circular ring is used as the basis for the measurement of two orthogonal forces in its plane of symmetry (Lowen & Cook, 1956). As shown in Figure 2.18, with the circular ring and the properly arranged strain gauge bridge circuits, it is possible to measure the two orthogonal forces P and F independently. The octagonal form of the ring (Figure 2.18, top right) results in greater stability for the measurement of both forces. The most useful form is obtained by extending the octagonal ring by $2L_o$ (Figure 2.18, bottom). The extended octagonal ring ensures sufficient stability for most practical applications. It also minimizes the bending effects and maintains as nearly as practicable the condition of zero rotation of the top surface. The extended octagonal ring transducers have been used in agricultural engineering by many researchers (Godwin, 1975; O'Dogherty, 1975; Thakur & Godwin, 1988; Girma, 1989).

In Figure 2.18, the strain and stress at the inside and the outside surfaces of the ring due to the forces P and F are zero at θ=nodal angles, ϕ_P and ϕ_F respectively. With the strain gauges mounted in these positions and connected into the Wheatstone bridge circuits, the gauges 1-4 will measure the force F, eliminating the influence of the force P, while the gauges 5-8 will measure the force P, eliminating force F.

Although no exact solutions exists for the strain of an extended octagonal ring, the following approximate equations were suggested by O'Dogherty (1996) to predict the value of the strain caused by force P and F respectively:

Force P:

$$\varepsilon_{90^\circ} = \frac{k_P P r_o}{E b_o t_o^{\,2}} \tag{2.46}$$

Force F:

$$\varepsilon_{\phi_f} = \frac{k_F F r_o}{E b_o t_o^{\,2}} \tag{2.47}$$

In equation (2.46), k_P is the constant for P, in practice ranging from 1.50 to 1.78 with a mean value of 1.70. In equation (2.47), k_F is the constant for F, ranging from 1.66 to 2.02 with mean value of 1.80, while ϕ_P is the nodal angle at which stress, due to force P is zero. The value of ϕ_P ranges from 34° to 50° according to various researchers. For a specific application ϕ_P rather needs to be determined by calibration. E is the modulus of elasticity of the ring material.

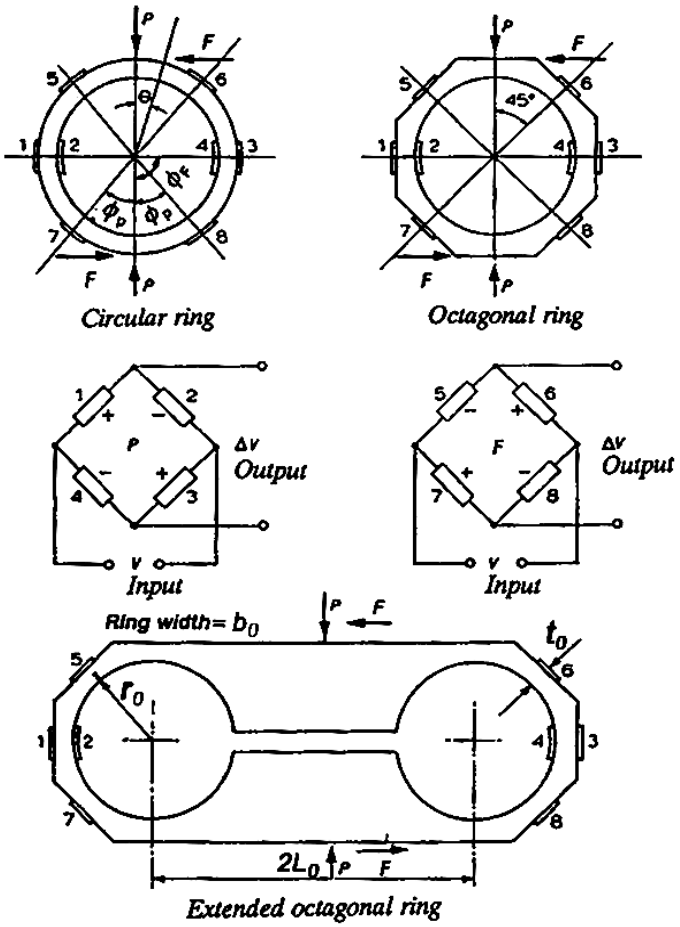

Figure 2.18. The Extended octagonal ring transducer (Godwin, 1975)

2.6 DEVELOPMENT OF THE PROTOTYPE TRACTION SYSTEM BASED ON SOIL-RUBBER FRICTION

A rubber-surfaced and friction-based track system, initially named a Bi-pole traction system (two pole wheels used at the ends of the oval track), was developed and mounted on a prototype tractor based on a new Allis Chalmers four-wheel drive tractor (Barnard, 1989).

As described by du Plessis (1996), the prototype traction concept was invented to have the terrain effect of a very large diameter wheel (Figure 2.19). This was achieved by

constructing an articulated beam type track which resists inward articulation, but allows outward articulation carried by two pairs of pneumatic wheels (N) for each track.

By using the middle wheels (M) on the track, the tractor was also expected to have significantly reduced steering resistance and damage to the ground surface when steered (Figure 2.19). It offers the additional advantage that the individual track elements can easily be replaced at low cost when compared to damaged rubber belt tracks. As the prototype track represents an alternative principle to achieve the same characteristics as the rubber belt tracks, it has the potential to be competitive to other similar mechanisms.

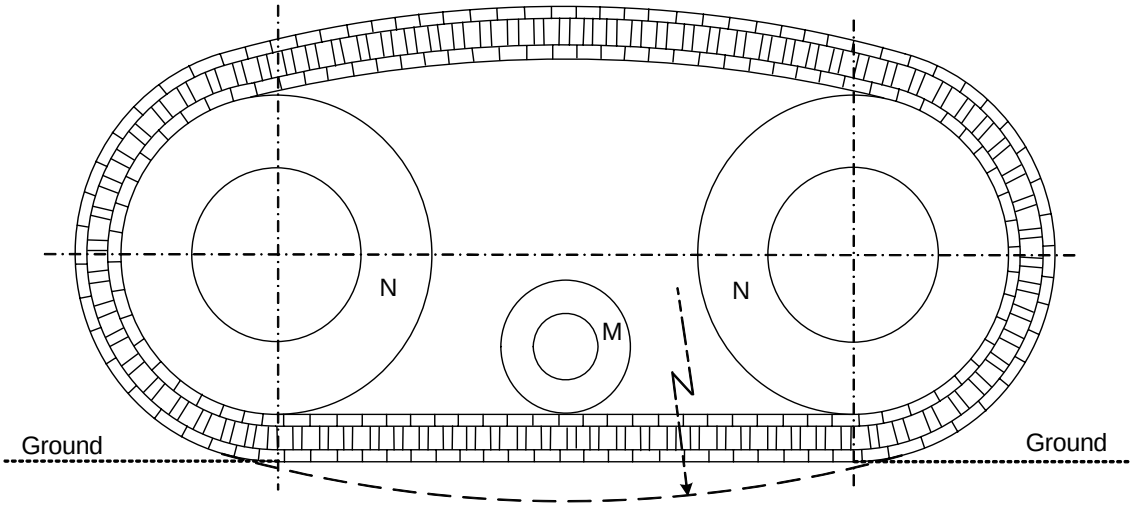

Figure 2.19. The construction concept of the prototype track to achieve the effect of a very large diameter wheel.

The initial field performance tests for the tractor equipped with this prototype track system proved that the maximum drawbar pull and power on a concrete surface at a chosen speed was notably higher than for the equivalent four-wheel drive tractor (du

Plessis, 1996). Other performance parameters were also enhanced by the prototype tracks as summarized in the report (Barnard, 1989).

2.7 JUSTIFICATION FOR CONDUCTING THIS STUDY

The literature review indicates that extensive information has been published on the subject of vehicle-terrain interaction, especially the analytical approaches pioneered by Bekker. However, there is no idealized universal approach to adequately predict and evaluate the new traction device. There is also very limited literature available for in depth research about rubber tracks.

The utilization of the rubber tracks is still in the early and rapidly developing stage (Evans and Gove, 1986. ASAE, 1995). Extensive efforts need to be made for improving the design principle of rubber tracks. It is obvious that any research and study work on this newly developed traction device would be beneficial and valuable to the future design of the traction device.

The reviewed literature has led to the following proposed approach for this study undertaken:

- The bevameter technique is a realistic approach to characterize the soil properties for analytical traction modelling.

- Based on the previous study, an analytical model to predict the contact pressure distribution below the track, as well as the tangential stress, will be derived.

- The measurement of vertical contact pressure and the tangential stress was done some years ago. The extended octagonal ring transducers are suitable to measure the vertical and the horizontal forces on the track elements.

- The shape of the terrain contact surface of the prototype track is different from that of previous traction devices. Thus the rationale of such a traction system needs to be evaluated for further improvement.

- From Neal's research (1966), it was indicated that in sandy soils, where the values of rubber-soil friction coefficient were similar to the values of the coefficient of soil internal shear resistance, the performance of a friction-based traction device such as the prototype track in this research was expected to be almost similar to that of shear-based traction device, i. e. the traditional steel tracks or wheels.

- According to the research by Wills (1963) as shown in Figure 2.14, the contact pressure distribution had a noticeable effect on the development of tractive effort, particularly at low values of slip when the tractor was usually operated. It was preferred to keep the pressure distribution in the pattern that the magnitude of the pressure at the rear end was maximum whilst at the front end the pressure was close to zero.

- The prototype track system designed by Barnard (1989) based on frictional principle was expected to have comparable tractive performance to the performance of a traditional steel track system.

2.8 OBJECTIVES

After the above literature review, the specific objectives of this study were:

- to develop an appropriate analytical model to predict the drawbar performance for the prototype track based on the friction-shear principle between rubber and soil on a soft terrain surface;

- to build the necessary measurement and instrumentation system to acquire the distribution of the contact and the tangential stresses under the prototype track;

- to measure the required soil and rubber characteristics necessary for traction modelling;

- to undertake the field tests for validation of the data from the traction modelling and the experiments under various soil conditions;

- to evaluate the effects of the design features of the prototype traction system on the tractive performance; and

- to proof that the performance of a shear-based and a friction-based traction mechanism is almost similar.

The soil parameters required for the development of the analytical model were obtained by using the instrumented apparatus applying the bevameter technique. Particularly, the characterization of the rubber-soil friction and shear were undertaken by using a standard track element. A computerized data acquisition system was used to record all the *in situ* test results for the soil characterization and the full size drawbar tests.

The special transducers to measure the distribution of the contact pressure and the friction-shear stress were built according to the principle of the extended octagonal ring. The structure of the prototype track was modified to accommodate the installation of these transducers.

After the validation of the results from the field tests and the modelling, some design features such as the frictional drive principle, the track tensioning and the function of the middle wheels were evaluated.

Figure 2.20 shows the flow chart of the procedure by which the above objectives were achieved.

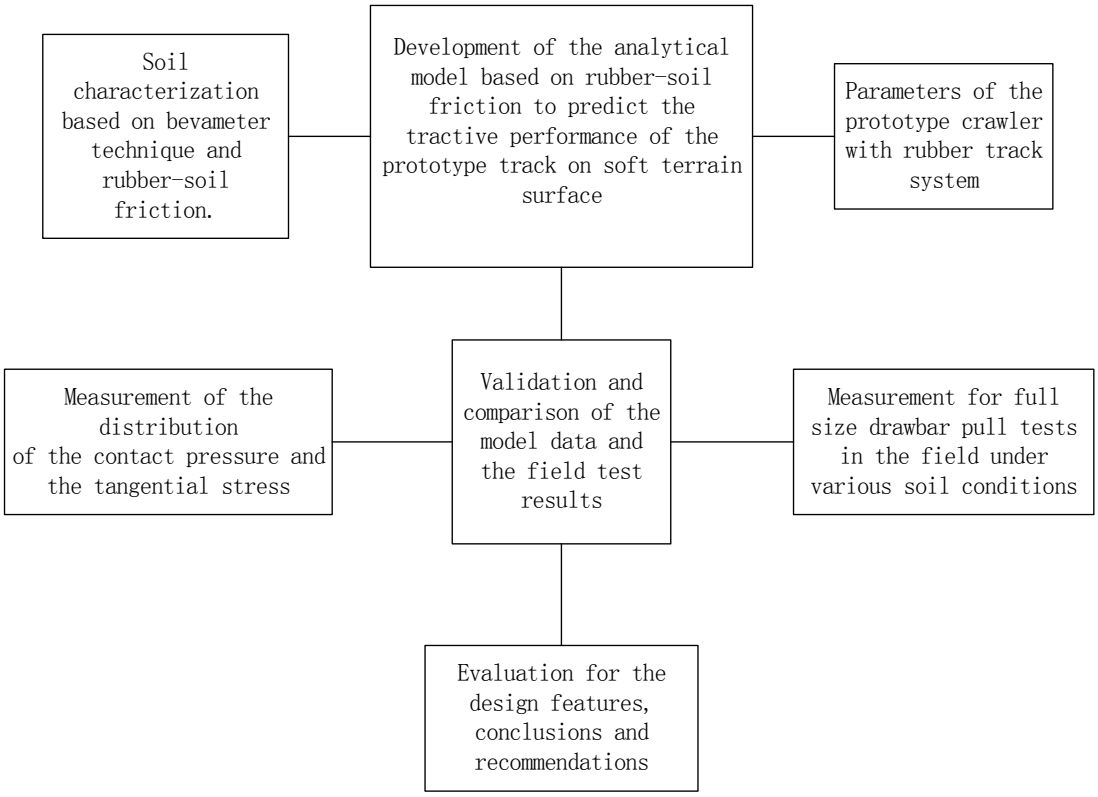

Figure 2.20. Flow chart of the proposed research procedure.

CHAPTER III

CONSTRUCTION OF THE PROTOTYPE RUBBER-FRICTION TRACTION SYSTEM

3. 1 INTRODUCTION

The crawler tractor, equipped with the prototype rubber-friction track under investigation was initially named “Di-Pole Tractor” by the inventor (Barnard, 1989). It was based on a four-wheel drive Allis Chalmers 8070 tractor with a 141 kW engine (du Plessis, 1996). Compared to the popularly used Caterpillar Challenger tractors, the prototype crawler under investigation had a common feature, namely the rubber contact surface with the terrain. However, the thrust generating rationale for the prototype crawler was based on friction, whilst the Caterpillar Challengers was based on soil shear. In addition to the advantages of the rubber contact surface with the ground, the prototype track system also had as features:

- rubber-covered track elements, linked by five parallel cable loops forming each of the two tracks as articulated walking beams;
- a friction drive between the pneumatic drive wheels and the track and between the track and the terrain surface;
- track tension adjusted by horizontally mounted hydraulic cylinders on the track suspension;
- a steering control system with automatic differential lock;
- two ground wheels at the centre of each track, applying a vertical force to ease the steering operation;
- achieving pivot steering about its own vertical axis; and
- considerably reduced specific ground pressure for this prototype tractor in comparison to a similar wheeled tractor.

Some comparative performance test results between the Di-Pole and conventional four-wheel drive tractors are given in Table 3.1.

Table 3.1 Comparative test results for the prototype Di-Pole and conventional Allis Chalmers 8070 four-wheel drive tractor on sandy soil (Barnard, 1989).

Tractor Type	Tractor speed (km/h)	Drawbar pull (kN)	Implement width (tilled) (m)	Cultivation rate (h/ha)	(ha/h)	Diesel consumption (l/h)	(l/ha)
Di-Pole	6.5	39	2.45	0.63	1.59	37	23.38
AC Conventional	6.5	31	1.94	0.79	1.26	29	22.95
Di-Pole	5.5	55	4.12	0.44	2.27	41	18.11
AC Conventional	5.5	43	3.22	0.56	1.77	31	17.51
Di-Pole	4.25	74	10.10	0.23	4.29	41	9.55
AC Conventional	4.25	55	7.51	0.31	3.19	32	10.03
Di-Pole	3.2	105	16.24	0.19	5.20	41.5	7.98
AC Conventional	3.2	62	9.59	0.32	3.07	29	9.45

The above test results proved that under comparable conditions, the modified crawler with rubber-covered track elements had a much higher drawbar pull and working rate when compared to the original conventional tractor using the same engine. With higher drawbar pull, the engine for the modified crawler was better loaded with a higher torque applied to the tracks and therefore, the total fuel consumption in liter per hour was higher, but almost the same in liter per hectare. At lower speeds, the slip losses probably influenced the total fuel consumption for the conventional four-wheel drive tractor negatively, resulting in higher fuel consumption in liter per hectare. Unfortunately, no values of slip versus pull were supplied in the report. Although the comparison may scientifically be questionable, Barnard (1989) intended a comparison under typical farm conditions.

In this Chapter, the technical and constructional features of the prototype track, as tested on the modified tractor, will be described.

3.2 THE PROTOTYPE TRACK

3.2.1 The fundamental construction and layout

As the basic component of the track, each track element has a steel base plate (B) with a rubber pad (A) bonded to it (Figure 3.1).

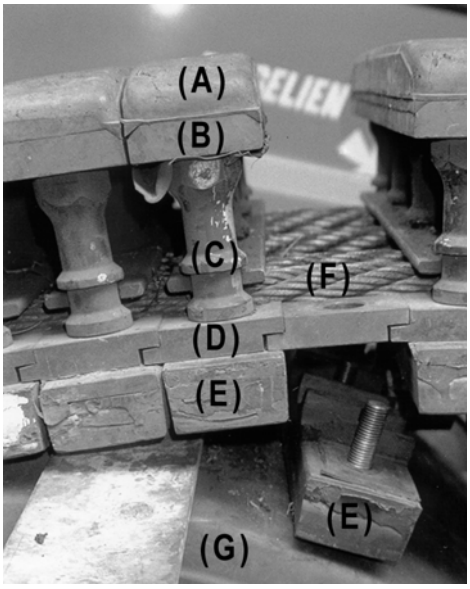

(A) rubber pad to form track surface (B) steel base plate to carry rubber pad

(C) steel stud (D) steel plate carried by steel cables

(E) inner rubber pad to form inner friction surface

(E) replaceable inner rubber pad and its steel plate (F) steel loop cables

(G) rubber tyre

Figure 3.1. The fundamental components of the prototype track.

In practice, it proved that the structure of the track element was robust enough as the rubber pad never got detached during the durability tests. The steel base plates (D) fixed to the track element by studs (C) are kept in position by five steel cable loops (F). The inner rubber pad (E) is bonded to a thinner steel plate, and is linked by a bolt through the holes to steel plate (D) and threaded into the centre of the steel column (C). By rotating the column (C), the track element (A) together with (B) and the rubber pad (E) can be separated from the base plate (D).

Figure 3.2 shows an individual rubber-covered track element removed from the track assembly. As the track is composed of 101 individual track elements, instead of an integral belt, as used by other rubber tracks, any track element can be replaced individually within a reasonable breakdown time. The track therefore need not be replaced as a complete unit when partially damaged.

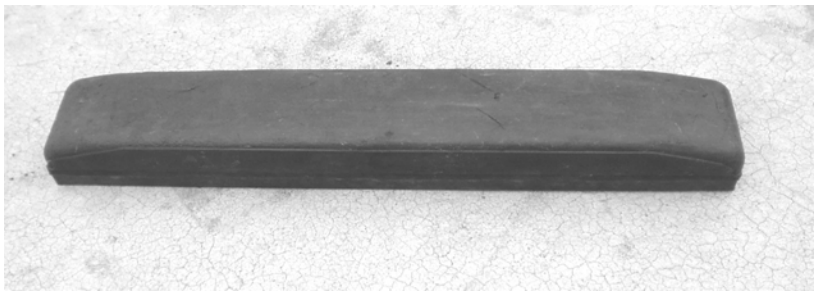

Figure 3.2. The individual track element.

Figure 3.3 shows the side view of the tractor equipped with the track. Two double rear wheels (Figure 3.3 (A)) with smooth pneumatic biasply tyres are fixed to the rear drive shafts on each side to provide rear wheel propulsion by frictional contact with the rubber-covered inner surface of the track. In comparison to the active drive, this frictional drive automatically protects the mechanical system against overload. Unfortunately, slipping losses may be caused by decreased track tension and propulsion force when the tractive load is high or the frictional properties deteriorates, caused by operational circumstances such as heat, water, soil or other

foreign inclusions. It was found from the initial tests that the slip was increased by low track tension.

To prevent damage at the interference by mud entering the friction surface, the friction drive periphery of the prototype track is positioned 200mm above the ground level. The height of the track elements and the rubber pad (Figure 3.3) lifts the internal rubber frictional surface of the track well above ground level, making it less susceptible to inclusion of foreign material like mud at the driving surface. This also prevents a bulldozing effect occurring when steering.

(A) Rubber tyre (B) Centre ground wheel (C) Dividing flanges
(D) Swinging axle mounting (E) Hydraulic ram adjusting the track tension
(F) Locking device

Figure 3.3. Side view of the prototype track fitted to the tractor.

3.2.2 The centre ground wheels

Hydraulically activated centre ground wheels (Figure 3.3 (B)), with solid rubber tyres, can be lifted or pushed down when necessary. During steering, the centre ground wheels are forced against the lower portion of the track so as to increase the curvature of the track and thus decrease the contact area. Pivot steering is approached by the two wheels on each side, fixed to a single axle. For sharp turns, when one track was driven forwards and the other rearwards with the centre wheels pushed down onto the tracks, tractor turned along in a circular path around the vertical axis of the tractor with minimal damage to the soil surface.

Under normal operational conditions for straight line travel, the centre wheels (B) may be moderately pushed down onto the track to help achieve a more evenly distributed ground contact pressure. However, this was not the original design purpose of the centre wheels.

3.2.3 Track mounting, tensioning and driving friction at interface

The tracks are carried by two vertically swinging axle mountings (Figure 3.3 (D)) pivoted around the original rear axle extensions with the cranks loaded by rubber springs at the front. This facilitates the use of the original tractor T-frame for mounting the two track assembly units on to the original frame of either side shaft, without necessitating any changes to the existing drive system. Frictional propulsion is generated by contact of the flat-treaded pneumatic tyres (Figure 3.3 (A)) with the inner track elements consisting of compression–molded composite of a carboxylated nitrite.

The track is laterally constrained by dividing flanges (Figure 3.3 (C)) at the centre of the inner track surface fitting into the gap formed between the side walls of the two pneumatic drive wheels and the two pneumatic tensioning wheels.

By extending the centre distance between the driving wheels and the driven wheels by means of permanently mounted hydraulic rams (Figure 3.3 (E)), the track tension necessary for the driving friction can be set by applying the correct pressure to the tension cylinders. The mechanical locking device (Figure 3.3 (F)) maintains the tension during normal operation. However after several hours of use, it may lose grip and must be retensioned. The frictional propulsion of the track is also assisted by the deflection of the tyre side walls clamping the central dividing flanges (C) when the tyre side walls are deflected outwards by the vertical load.

3.2.4 The beam effect

In order to achieve the so called "walking beam effect", the track elements were designed with dimensions A<B<C<D as shown in Figure 3.4. It was claimed to function in a way that when a series of wedge-shaped track elements were linked by the five close loop cables, an oval shape, as seen from side, was formed by the track. The curvature of the upper and lower portions of the track is therefore obtained from the slightly wedged shape of the track elements, extending outwards beyond the inner peripheries of the steel cables. The lower free span of the track in contact with the soil behaved like a compound beam, stressed by the mass of the tractor. The radius of the ground contact arc depended on the load and according to the designer varied between about 30 meters and infinity, but the claim was not proofed. The elastic resistance of the straightened track was expected to provide a more uniform pressure distribution underneath the track than for a conventional flexible rubber track supported only by road wheels.

As reported by du Plessis (1996), the walking beam effect was reduced, probably due to cable strain and wear on the contact surfaces between track elements. During tests flat metal spacers were inserted between the track elements to restore the beam effect, but they were soon damaged (Figure 3.4 (E)) and the beam effect was lost again.

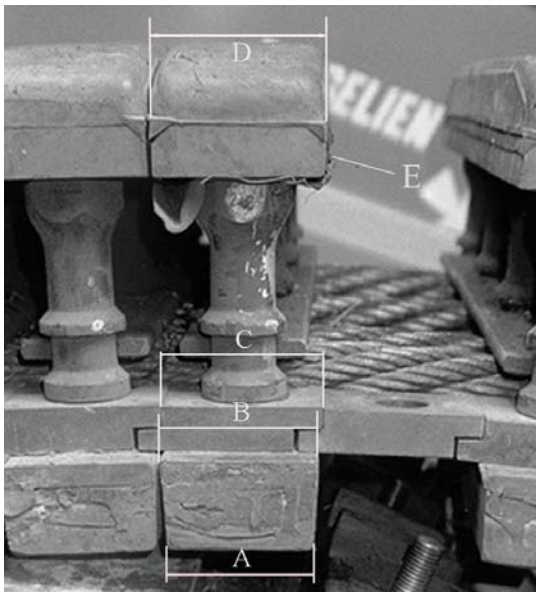

Figure 3.4. The wedge-shaped track elements to enable the beam effect.

3.3 THE DRIVE TRAIN, STEERING CONTROL AND AUTOMATIC DIFFERENTIAL LOCK

The patented drivetrain featured with the automatic differential lock, the differential steering system and the swing mounted track carriers constitute an important part of the design. The schematic layout of the drive train of the tractor, equipped with the prototype track, is shown in Figure 3.5 (du Plessis, 1996).

The control differential (S) consisted of nitride spur gears, driven by the input shafts K_1 and K_2 (Figure 3.5a). The input ring gear (R) is mounted around a circular cage (K) and a pair of half shafts (H_1 and H_2) with spur gears (R_1 and R_2) (Figure 3.5 b) at their inner ends. Spur pinions (A) are provided as two identical pairs in a diametrically opposite arrangement on a pitch circle about the half shafts H_1 and H_2. The spur pinions (A) are meshed with the spur gears (R_1 and R_2) and with each other.

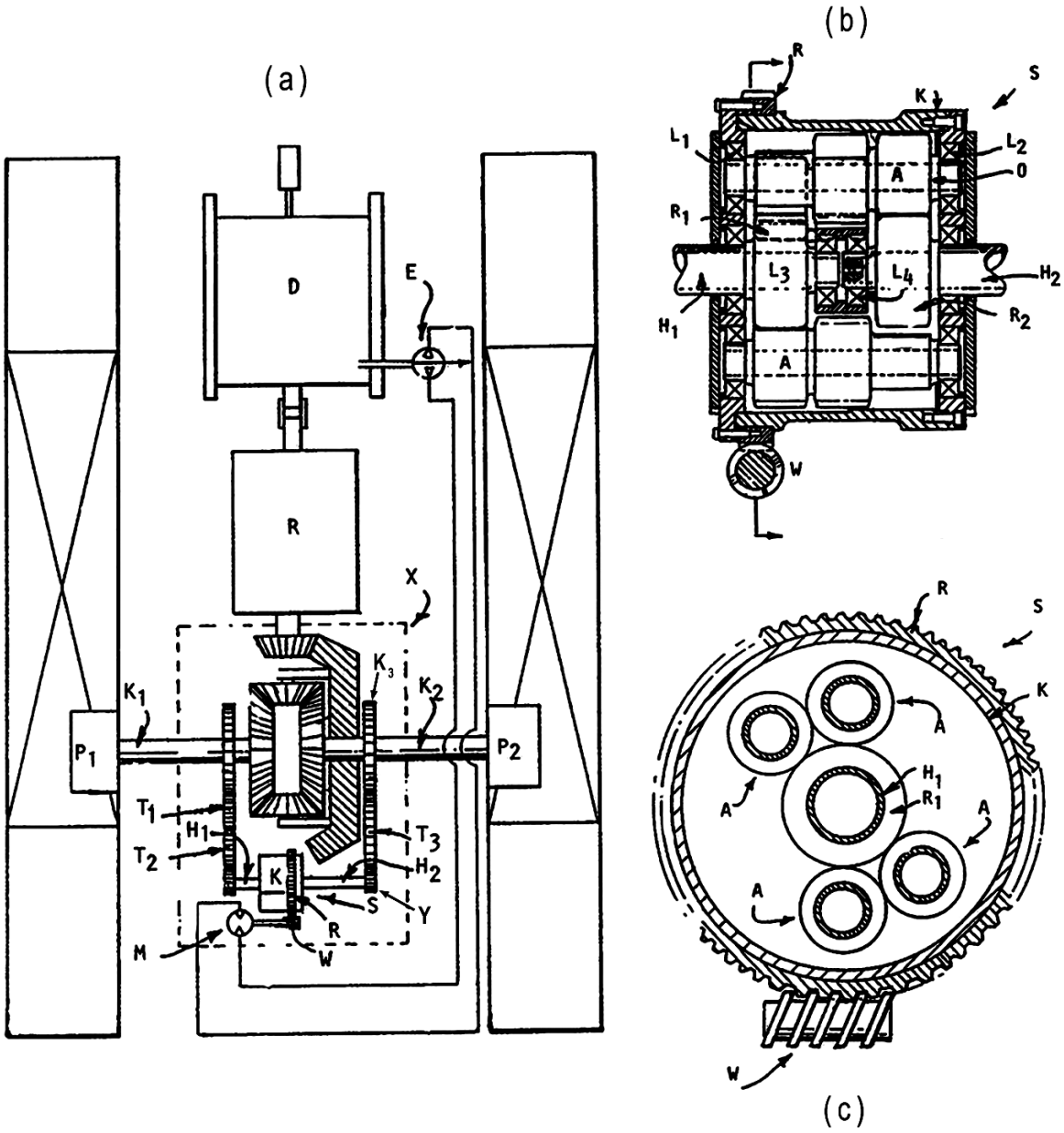

Figure 3.5. The drive train and the differential lock.

In the control differential (S), the half shafts (K_1) and (H_1) are interconnected by spur pinions (T_1) and (T_2) to accommodate the distance between the shafts. Spur gear (K_3) is fixed to the half shaft (K_2) and spur pinion (Y) is fixed to the half shaft (H_2) with idler gear (T_3) to form a gear train driving (K_2) and (H_2) in the same direction. With a gear ratio of about 6:1 the shafts (H_1 and H_2) rotate in opposite directions at a speed six times that of K_1 and K_2, thus reducing the shaft diameter and mass.

For straight line travel the half shafts (K_1) and (K_2) rotate at the same speed and direction and the spur pinion (A_1) and (A_2) in an opposite direction at equal but a higher speed, but at zero torque. They do not orbit and the ring gear (R) is stationary. The spur pinions are driven by (H_1) and (H_2), but are also interlocked as shown on the end views and the differential is automatically locked.

When steering, the variable displacement hydraulic piston pump (E), and the motor (M) drives the control differential via a worm gear (W) in a desired direction and speed, corresponding to the steering angle. The force from the inside track is thus transferred to the outside track via the control differential (S) and regeneration takes place. One track may even move forward and the other rearwards.

With an asymmetrical resistance, one track would tend to slow down and the other to speed up, due to differential operation. This unequal torque tends to rotate the differential (S), the ring gear (R), gear (W) and the motor (M). With a closed hydraulic valve, or a worm gear (W) with a speed ratio of at least 6:1, the control differential is locked and unstable steering action is thus prevented.

For straight travel, the spur pinions (A) spin at a high speed and conventional differentials with bevel gears are not suitable. Contrary to the standard cantilever arrangement, the spur pinions (A) are also supported on either side by bearings (L_3 and L_4). Large diameter thin-walled hollow shafts (H_1 and H_2) are used to enhance the load carrying capacity and resilience with minimal inertia.

The design features as explained enable regeneration and replace complex devices such as a null shaft.

3.4 DIMENSIONS OF THE PROTOTYPE TRACK

Based on the original design, the relevant dimensions of the track are shown in Figure 3.6. The distance between the front and the rear axles can be adjusted up to 2000 mm at maximum by hydraulic cylinder (E) as shown in Figure 3.3.

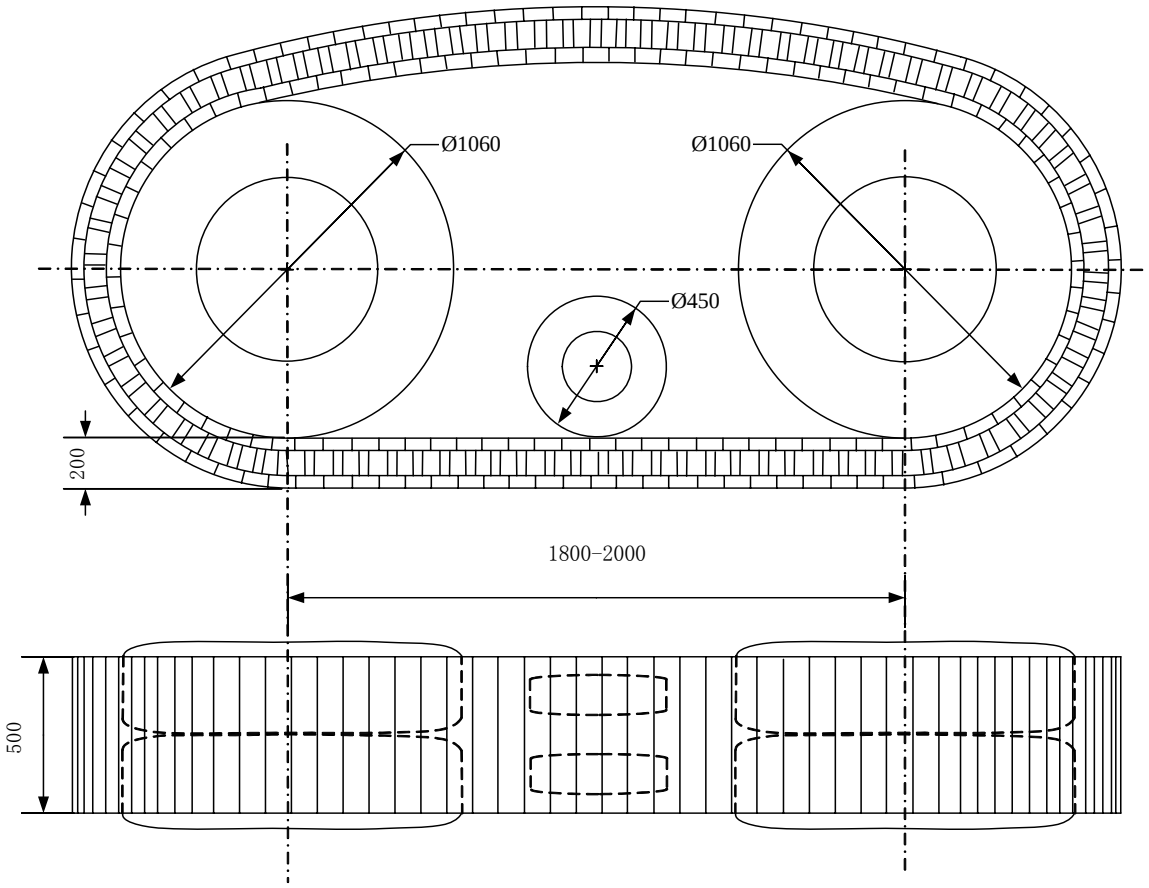

Figure 3.6. The dimensions of the prototype track.

3.5 PRELIMINARY TESTS AND ASSESMENT OF TRACTIVE PERFORMANCE

Tests carried out to evaluate the handling and performance characteristics of the prototype track system were reported by du Plessis (1996). The test results for this field performance evaluation are shown in Table 3.2. The engine for the wheeled

tractor was used and the crawler had a new engine, thus the dynamometer measured power for the two engines were slightly different.

Table 3.2. The comparative test results for the prototype crawler and a four-wheel drive tractor (du Plessis, 1996).

Type	Conventional four-wheel drive tractor (used Allis Chalmers 8070)	Di-Pole crawler (Based on new Allis Chalmers 8070 tractor)
Engine power tests		
Maximum engine power (kW)	132kW@2400rpm	141kW@2400rpm
Maximum torque (Nm)	600Nm@1800rpm	645Nm@1800rpm
Test on a soft surface		
Gear for maximum power	4 Low	4 Low
Maximum drawbar power (kW)	58	63
Drawbar pull (kN)	31	53
Speed (km/h)	6.8	4.3
Rolling resistance (kN)	9	14
Wheel or track/soil slip (%)	Front 19.0, rear 21	5.9
Slip between drive wheels and track (%)	-	9.4
Test on a concrete surface		
Gear	4 Low	4 Low
Maximum drawbar power (kW)	77	79
Drawbar pull (kN)	38	55
Speed (km/h)	7.3	5.2
Rolling resistance (kN)	8	9.5
Wheel or track/road slip (%)	Front 4.7, rear 4.4	1.0
Slip between drive wheels and track (%)	-	3.4

The engine for the conventional four-wheel drive tractor was used whilst that for the crawler was new, thus the difference in power existed. The results showed that on both a concrete and a soft surface, most of the performance characteristics for the prototype crawler were superior to that of the conventional four-wheel drive tractor equipped with a similar specification, but used engine. Particularly for the test on a soft surface, the slip of the crawler tractor was at 5.9% whilst the wheeled tractor at 20%. However, the rolling resistance for the crawler was higher than for the standard

four-wheel drive tractor for both hard and soft surfaces. The friction between the track and the drive wheels for the crawler was another factor which influenced the performance of the crawler negatively. The distribution of the contact pressure as observed was uneven and the beam effect, as was envisaged by the original design, did not materialize (du Plessis, 1996).

3.6 SUMMARY AND REMARKS

Based on the description of the design and construction in this chapter, it is shown that the prototype crawler featured with the friction-based track and the patented drive train system is uniquely distinct from other wheeled tractors or crawlers currently in use. Theoretical traction performance modelling had not been carried out for such a tractor. The assessment of factors influencing the traction performance would also be of interest. Therefore, the following conclusions were drawn:

- The rubber-rubber and rubber-terrain friction-based track played an important role in distinguishing the prototype crawler from other tractors.

- The drive train including the automatic differential lock performed well.

- More specialized tests needed to be conducted if the tractive performance of the track was to be evaluated or validated by modelling.

- The walking beam effect could be restored partly by means of inserting some flat metal sheet spacers between track elements to restore the outer circular length of the track. However, they were soon damaged and the beam effect was lost again.

CHAPTER IV

DEVELOPMENT OF THE TRACTION MODEL FOR THE PROTOTYPE TRACK

4.1. INTRODUCTION

Based on the literature review in Chapter 2, analytical methods of modeling were preferred to other method for this research. For analytical methods fewer parameters were needed to be measured with than methods such as the finite element analysis (FEM). Analytical methods also offered closer simulation to the real tractive phenomenon than the empirical approaches such as the methods based on cone index.

After years of research and assessment by researchers, analytical methods for soil characterization and traction modelling based on the bevameter technique is still a preferred technique. For its feasibility and simplicity, the approach based on bevameter technique was therefore chosen for this research.

To develop the traction model by applying analytical methods based on the bevameter technique, characteristics of the friction between the track and the terrain surface, limited soil shear characteristics, and the pressure-sinkage relationship had to be determined. The soil parameters and the distribution of the contact pressure could be applied for the prediction of the tractive performance. By applying Bekker's analysis of motion resistance, mainly caused by soil compaction and the loss from internal track friction, the total motion resistance could be predicted.

The distribution of the contact and tangential stresses relies mainly on the deformation of the track and the terrain surface. When the bevameter technique was applied to predict the distribution and magnitude of the ground contact pressure under the track, the shape of the deflected track in contact with the terrain surface

was of importance. A detailed analysis of the pressure distribution at the track–terrain interface was made. For traction modelling the relationship between the relevant vehicle parameters associated with the deformed track shape in contact with the terrain and the soil characteristics was established.

4.2 CHARACTERIZATION OF RUBBER-SOIL FRICTION AND SOIL SHEAR WITH DISPLACEMENT

As reviewed and discussed in the preceding chapters, the thrust between the running gear and the terrain surface, for a traditional tractive device, is usually developed by the internal soil shearing action associated with relative slip. It is the rationale that the prototype track generates tractive thrust mainly by friction between the smooth rubber surface and the terrain surface whilst the soil-soil shear is minimal. The characterization of the relationship for soil shear stress versus shear displacement, and soil-rubber friction versus displacement was thus required for the proposed modelling procedure.

When the shear action occurs in the soil, which is typical for a tractive device with grousers moving over a soft terrain surface, the maximum shear stress τ_{max} can be described by the Mohr-Coulomb failure equation, i.e. equation 2.11.

The Mohr-Coulomb equation describes the shear strength of soil to soil, therefore it is valid when used to simulate the shearing action of a tyre or track with lugs penetrating into the soil. Shear action in the soil is caused by the moving lugs when the running gear propels the vehicle. However, when the surface of the running gear is smooth and the slip action apparently occurs at the soil contact surface, it is more appropriate to describe the phenomenon as frictional. Thus it is better expressed by applying another equation of similar form but with different parameters for the maximum frictional stress τ_{fmax} at the frictional contact surface as expressed by:

$$\tau_{fmax} = c_a + p \tan \delta \tag{4.1}$$

where

c_a = soil-rubber adhesion on the interacting surface, (Pa).

p = contact stress on the interacting surface, (Pa).

δ = angle of soil-rubber friction, (degrees).

From the preparatory field measurements in this research, the values of the soil shear parameters obtained from steel shear grousers were different from the measured friction-shear parameters obtained by using the rubber-coated track element as a friction plate with a smooth rubber surface (Yu, 1996). It was also found that the values of the coefficient of soil to rubber surface friction tan δ, and the internal shearing resistance of the soil tan φ were very similar as shown in Table 4.1. The adhesion between rubber and soil was less than the internal cohesion of the soil. This was in accordance with values reported by Neal (1966) and Wills (1963). Therefore the two cases of soil shear and rubber-soil friction must be considered differently for traction modelling.

Table 4.1. Comparison of soil internal shear and soil-rubber friction parameters (Yu, 1996).

Soil water content (dry basis), %	Internal frictional angle for soil shear ϕ, degrees	Soil internal cohesion c, kPa	Soil-rubber frictional angle δ, degrees	Soil-rubber adhesion c_a, kPa
10.9	33.9	1.62	29.4	1.55
21.6	31.1	2.59	29.9	2.69
35.3	30.9	3.34	28.7	2.49

The tractive thrust for the prototype track under investigation is generated by the smooth rubber surface when the track, composed of individual track elements, develops pull on soft terrain surface. For the interaction between the track element and the soil surface, the soil-rubber frictional action is dominant, rather than the

internal soil shear action applicable for conventional steel tracks with grousers. The rubber-soil friction characterization can adequately represent the interaction between the prototype track and soil surface.

According to the measured data for the rubber track element collected during the *in situ* tests, the tangential frictional stress initially increased rapidly with the increase in displacement, and then approaches an approximately constant value for a further increase in displacement as shown in Figure 4.1 (Yu & du Plessis, 1997).

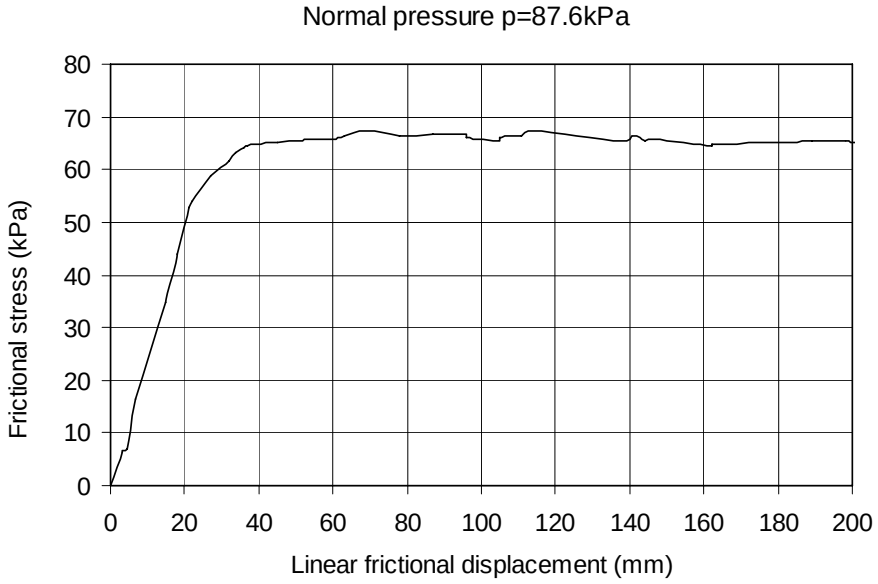

Figure 4.1. Frictional stress versus displacement for a track element test.

Such type of relationship between the shear-friction stress and the displacement as shown in Figure 4.1 can be expressed as equation (2.6) (page 2-11) by an exponential equation similar to the one proposed by Janosi and Hanamoto (1961). This equation can be modified to express the relationship of rubber-soil friction versus corresponding displacement as follow:

$$\begin{aligned} \tau_f &= \tau_{f\,max}\,(1 - e^{-j/K}) \\ &= (c_a + p\tan\delta)(1 - e^{-j/K}) \end{aligned} \tag{4.2}$$

where

τ_f = rubber-soil frictional stress, (Pa).

j = relative tangential displacement for soil-rubber friction, (m).

K = frictional deformation modulus, (m).

Equation (4.2) reflects the relationship between the horizontal contact frictional stress and the corresponding slip below the prototype track and soil and is thus used as the basic soil-rubber frictional characterization.

When compared to the Janosi-Hanamoto equation (2.6), equation (4.2) has the same format for the equation and also the number of parameters. However, the terms of the parameters in the equation have different physical meanings. It is the fundamental relationship for calculating the total tractive effort in the horizontal direction in this research.

To obtain the parameters related to the frictional characteristics from the field tests, the method based on the bevameter technique and the procedure reported by Wong (1989, 1993) and Upadayaya (1994) was adapted.

4.3 CHARACTERIZATION OF THE RELATIONSHIP BETWEEN CONTACT PRESSURE AND SINKAGE

The maximum shear or frictional stress between the tractive device and the terrain surface directly depends on the applied contact pressure. On a soft terrain surface the contact pressure is usually related to the sinkage. As reviewed in Chapter 2, several efforts have been made to identify the exact relationship for contact pressure versus sinkage in both agricultural engineering and civil engineering applications. To describe the relationship of the contact pressure and the corresponding sinkage, the expression proposed by Bekker is still the most common one applied for analytical modelling methods to predict vehicle performance, especially for the case of soft terrain surfaces.

The relationship of contact pressure and sinkage expressed by equation (2.1) can be used to calculate the contact pressure at each point on the ground contact surface under the track. In equation (2.1), k_c and k_ϕ are parameters related to steel-soil cohesion and soil-soil friction respectively, while n is the exponent for sinkage deformation.

For the experimental work, the parameters obtained and the resulted curves from the field tests are presented in the results.

4.4 ANALYSIS OF THE DISTRIBUTION OF TRACK-SOIL CONTACT PRESSURE

The analysis by Wills (1963) proved that the contact pressure distribution influences the development of tractive effort. The prediction of the distribution of the contact pressure is therefore one of the most important issues in analytical traction modelling for wheels and tracks.

To a large extent, the shape of the track in contact with the terrain surface governs the distribution of contact pressure. Several typical track deformation shapes can be considered.

4.4.1 Tractive effort for uniform and trapezoidal pressure distribution

The initial design of the prototype track tested in this project was aimed to achieve an ideally almost uniform contact pressure distribution by applying the walking beam concept. For most of the conventional steel tracks, however, the pressure distribution for a uniformly loaded track was far from being uniform, as reported by many researchers (Wills, 1963; Wong, 1989). For the practical situations, several factors influence the pressure distribution at the contact surface including vehicle and track physical parameters, soil homogeneity and other soil physical properties and in particular the weight transfer of the tractor. To counterbalance the effect of weight

transfer, some means of automatic adjustment of the vertical load and consequently the centre of gravity must be utilized, which is not yet realized for practical field operations.

When any drawbar pull is applied, the intensity and the distribution of the ground contact pressure below the track is influenced by weight transfer. To take into account the effect of the weight transfer, the position of the centre of gravity (CG) of the test tractor was designed to be located in front of the centre of the track contact length. When a drawbar pull is applied, the load distribution center of the ground contact pressure for the track moves rearwards, caused by weight transfer.

In this research project, two simple models of contact pressure distribution are initially validated and analyzed. One is a uniform distribution whilst the other a dynamic trapezoidal distribution (Figure 4.2). In the dynamic trapezoidal model, to predict the distribution of the vertical load, the effect of the weight transfer caused by drawbar pull is taken into consideration.

For the uniform distribution of the contact pressure, as shown in Figure 4.2 (b), the value of the ground contact pressure p (Pa) can be calculated from:

$$p = W / A \tag{4.3}$$

where

W = the total vertical load on one track including track weight, (N).

A = the total contact area of one track, (m^2).

For the trapezoidal contact pressure distribution, as shown in Figure 4.2 (a) and (c), the contact pressure changes when the drawbar pull increases. For the static state and without drawbar pull, the centre of gravity for the vehicle is located in front of the centre point of the track, thus the contact pressure has a larger magnitude at the front end and decreases rearwards. As the drawbar pull increases to a specified value, the transient state of ideal uniform distribution for the contact pressure below the track

may be reached as shown in Figure 4.2 (b). When the drawbar pull increases further, the magnitude of the contact pressure at the front end of the track decreases and is smaller than at the rear (Figure 4.2 (c)).

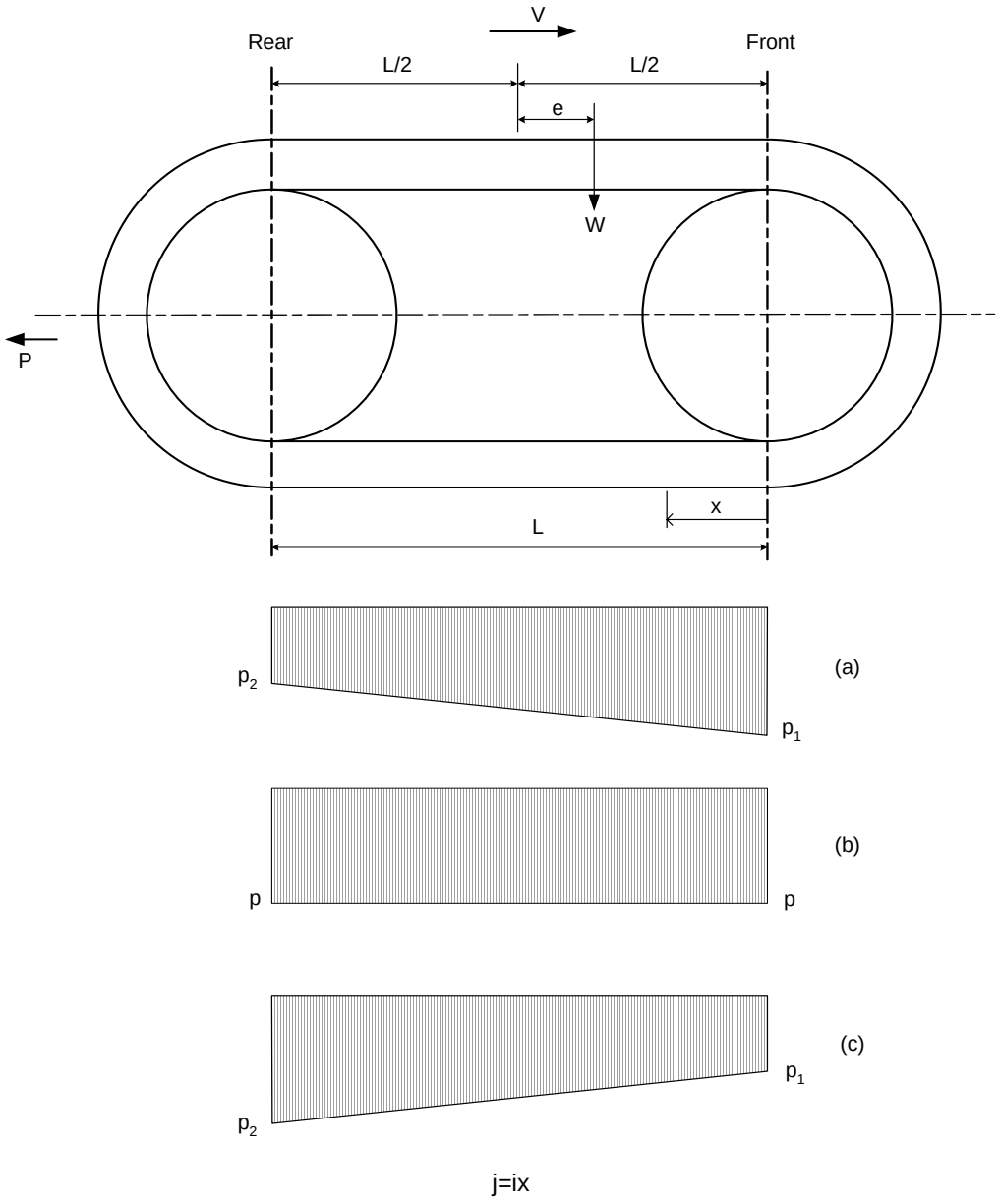

Figure 4.2. The idealized distribution of contact pressure under a track.

In both cases of distribution (a) and (c), if it is assumed that the tractor does not tilt, one obtains:

$$p = \frac{p_1 + p_2}{2} = \frac{W}{A} = \frac{W}{bL} \tag{4.4}$$

Where b is the width (m) and L (m) the contact length of one track.

In Figure 4.2 (a), the contact pressure p(x) for any point at a distance x from the track front contact point can be calculated from:

$$p(x) = p_2 + (p_1 - p_2)\frac{L - x}{L} \tag{4.5}$$

where p(x) is the contact pressure at a distance x from the track front contact point.

Similarly, in Figure 4.2 (c), p(x) can be calculated from:

$$p(x) = p_1 + (p_2 - p_1)\frac{x}{L} \tag{4.6}$$

For either a uniform or trapezoidal contact pressure, it is assumed that the friction-shear displacement j is linearly proportional to the track slip i. At any point below the track, with distance x to the front end of the track, the value of the friction-shear displacement between track and soil, as shown in Figure 4.2, is given by:

$$j = ix \tag{4. 7}$$

where i is the slip of the track.

Substituting equation (4.7) into equation (4.2),

$$\begin{aligned} \tau_f &= \tau_{f\,max}(1 - e^{-j/K}) \\ &= (c_a + p\tan\delta)(1 - e^{-ix/K}) \end{aligned} \tag{4. 8}$$

where the contact pressure p is also a function of x and is expressed by one of equations (4.3) to (4.6).

When the frictional stress τ_f is integrated along the contact length, the total tractive effort F_t can be predicted as:

$$F_t = 2\int_0^L \tau_f(x)dx$$
$$= 2\int_0^L [c_a + p(x)\tan\delta](1 - e^{-ix/K})dx \quad (4.9)$$

4.4.2 Tractive effort for a rigid track model with tilt angle

On a deformable terrain surface, however, the track-soil contact surface is usually inclined towards the rear of the track, depending on the drawbar height and drawbar pull. With further assumption of a tilt angle β, the parameters to describe the track-soil interaction are illustrated in Figure 4.3.

As shown in Figure 4.3, for equilibrium in the vertical direction:

$$W = b\int_0^L [p(x)\cos\beta + \tau_f(x)\sin\beta]dx \quad (4.10)$$

For equilibrium in the horizontal direction:

$$F_t = b\int_0^L [\tau_f(x)\cos\beta - p(x)\sin\beta]dx \quad (4.11)$$

and the rolling resistance R_r:

$$R_r = b\int_0^L p(x)\sin\beta dx \quad (4.12)$$

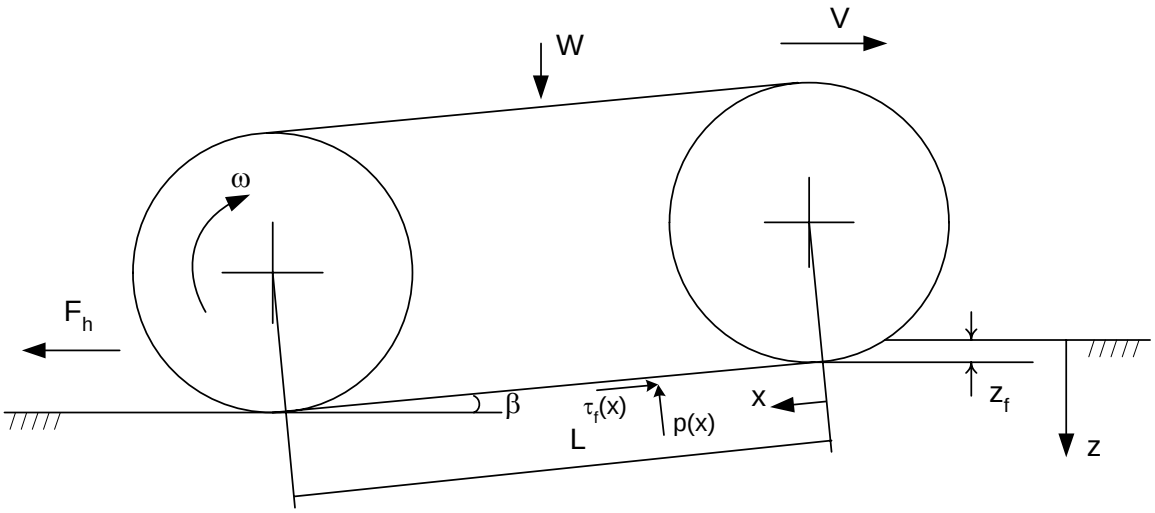

Figure 4.3. Side view of the track-soil interaction with the inclusion of a tilt angle.

In the above equations (4.10-4.12), the contact pressure of the track at any point in contact with the terrain depends on the corresponding sinkage at the specific point, whilst the sinkage can be calculated from the initial sinkage of the front wheel z_{f0} and the tilt angle β.

By substituting the values of $\tau_f(x)$ and $p(x)$ into the above equations, the tractive effort F_t and the rolling resistance R_r can be predicted.

The calculation for traction can be initiated by assuming that the front and rear wheels support the total static vertical load proportionally. The static sinkage of the front and the rear wheels can be calculated by applying the equation proposed by Bekker (1960). The tilt angle can also be calculated according to the load distributed on the front and rear wheels respectively.

To avoid a negative tilt angle, the tilt angle is initially assumed to be zero, due to the fact that the CG of the tractor is located in front of the middle point of the track in a longitudinal direction. The tilt angle remains zero until the vertical load is distributed equally between the front and the rear wheels. With further increase in drawbar pull, the load on the rear wheels increases and the load on the front wheels decreases by the same numeric value which was derived from the weight transfer. The tilt angle is

taken into consideration as soon as the load on the rear wheels is larger than the load on the front wheels.

Therefore, one of the advantages of this model is that the effect of load transfer can be accounted for when the drawbar pull changes, in addition to the uniform or trapezoidal contact pressure distributions.

4.4.3 Tractive effort for the flexible track model

If the designed walking beam effect of the prototype track materializes, the track operates similar to a wheel of very large diameter which may result in a very uniform distribution of contact pressure. The track-soil interaction can be solved by applying one of the idealized models as shown in Figures 4.2 and 4.3.

However, when the centre wheels were not forced onto the track, it was difficult to achieve the idealized uniformly distributed contact pressure as envisaged by the original design concept. Most likely, the track was flexible and be deformed at the section between the front and the rear wheels, being influenced by several factors, particularly the terrain characteristics and the track tension. When the track tension was not automatically adjusted or not sufficient to form the large circle in equilibrium with the terrain, the section of the track between the front and rear wheels would be deflected upwards and form a curved interacting shape with the terrain surface. The shape of this interaction surface would, to a large extent, govern the distribution of the contact pressure.

While the ideal contact pressure distribution is as shown in Figure 4.2, based on the practical observations and preparatory tests on a soft terrain surface (Yu and du Plessis, 1997) definitive peak pressures were observed below the front and rear wheels. The shape of the flexible interaction surface between the track and the soil was assumed to be as shown in Figure 4.4.

For the shape shown in Figure 4.4, the contact surface of the track and deformable terrain can be divided into two typical segments, one in contact with both the wheel and terrain, such as segments of ABC and FGH, and another in contact only with the terrain, such as segment CDEF.

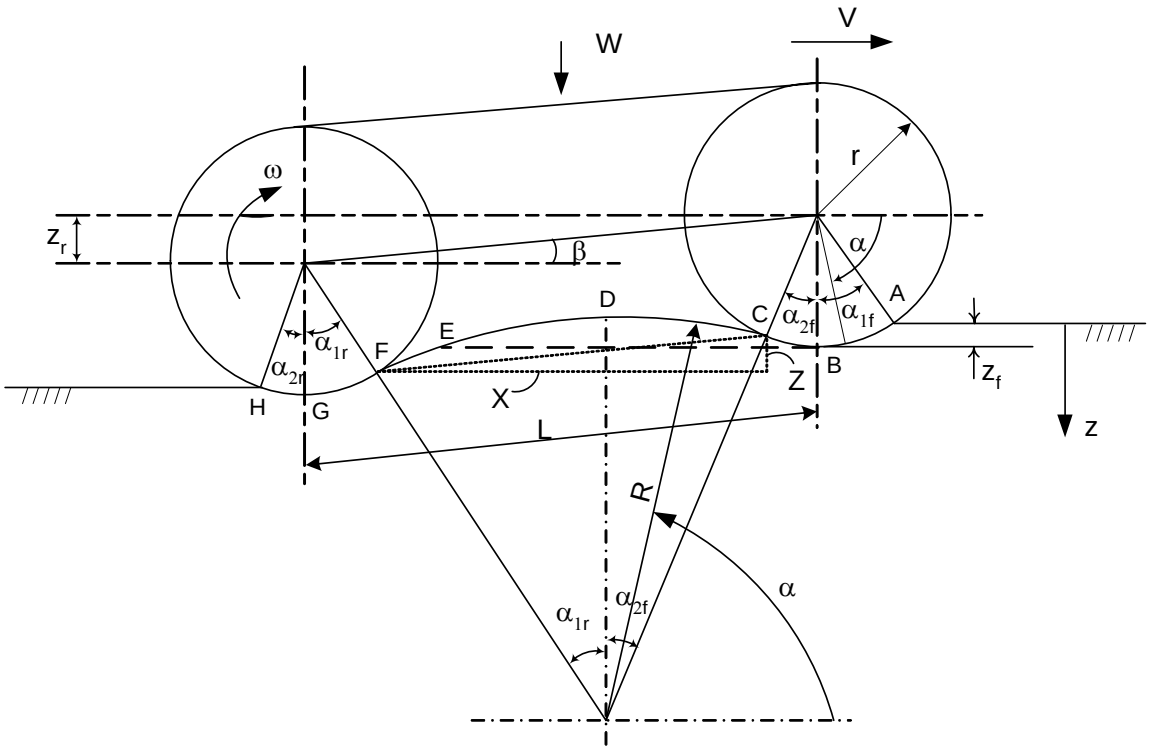

Figure 4.4. The flexible deformation model for track-soil interaction.

It was assumed that the front wheels initially had a sinkage of z_f, and the shape of the curve between the front and the rear wheels, i.e. the segment CDEF in contact only with the terrain surface, was circular in shape, with radius R.

On a soft terrain surface, the inflation pressure of the driving and tension wheels was relatively high to optimize the friction drive. It is, therefore, reasonable to assume that the wheels have characteristics similar to that of rigid wheels. The shape of the contact segments ABC and FGH therefore are circular, with the same diameter as the tyres.

On the basis of the assumptions above, the following relevant geometrical parameters were derived from the track-soil configuration as illustrated in Figure 4.4.

$$\alpha_{1f} = \cos^{-1}(1 - \frac{z_f}{r}) \tag{4.13}$$

$$R = \frac{\sqrt{X^2 + Z^2}}{2\sin[(\alpha_{1r} + \alpha_{2f})/2]} \tag{4.14}$$

where

$$X = L\cos\beta - r(\sin\alpha_{1r} + \sin\alpha_{2f}) \tag{4.15}$$

and

$$Z = L\sin\beta - r(\cos\alpha_{1r} - \cos\alpha_{2f}) \tag{4.16}$$

$$\beta = \sin^{-1}((z_r - z_f)/L) \tag{4.17}$$

$$\alpha_{1r} = \alpha_{2f} + 2\beta \tag{4.18}$$

If a rigid wheel on a soft terrain was accepted, the sinkage of the front and the rear wheels could be determined by applying the analysis as proposed by Bekker (1956, 1960):

The sinkage

$$z_f = \left[\frac{3W_f}{b(3-n)(k_c/b + k_\phi)\sqrt{2r}}\right]^{2/(2n+1)} \tag{4.19}$$

and sinkage

$$z_r = \left[\frac{3W_r}{b(3-n)(k_c/b + k_\phi)\sqrt{2r}}\right]^{2/(2n+1)} \tag{4.20}$$

where W_f and W_r represented the vertical load on the front and the rear wheels respectively whilst b was the track width

In the above analysis, the radius of the deformed track segment in contact with the terrain surface directly depended on the exit angle of the front wheels, the distance between the front and the rear wheels and the wheel diameter.

Wong (1989) indicated that the entrance and the exit angles for a pneumatic tyre were interrelated and the relationship was governed by the terrain response to repetitive contact loading, but the relationship was not specified or suggested. Due to the fact that the rebound of the terrain was limited by the track tension and the track was not definitely flexible, the exit angle was expected to be smaller than the value calculated for the case of a pneumatic tyre.

Okello et al (1998) proposed the use of a constant C to relate the entrance and the exit angles as:

$$\alpha_{2r} = C\alpha_{1f} \tag{4.21}$$

However, no method to determine the value of C was mentioned.

From the curves of the repetitive contact loading, it could be seen that when the terrain stiffness was larger, the contact pressure decreased more rapidly during the unloading cycle and the elastic rebound of the terrain took a shorter period of time. It was considered that the slope angle of the unloading curve could be used to derive the exit angle. No practical conclusions on the entrance and exit angles were drawn from the unloading-reloading curves and it needs more experimentation to proof such a relationship.

Karafiath and Nowatzki (1978, pp 386-387) proposed that the exit angle be taken as 10 degrees for entry angle variations from 30 to 60 degrees. For entry angles of less than 30 degrees, it should be reduced by half the difference between the entry angle

and 30 degrees. Based on this method, the exit angle was therefore calculated as 0 when the entry angle was less than 10 degrees. By considering the effect of the track tension on soft terrain for the proposed model, the exit angle was determined as one third of the entry angle.

The track contact surface was divided into n segments of different configuration, and the equilibrium equations for the track were expressed as:

In the vertical direction,

$$\begin{aligned} W &= \sum_{i=1}^{n} W_i \\ &= \sum_{i=1}^{n} b\int_0^{l_i} (p_i \sin\alpha + \tau_{fi}\cos\alpha)dx \\ &= \sum_{i=1}^{n} b\int_{\alpha_i}^{\alpha_{i+1}} r_i(p_i \sin\alpha + \tau_{fi}\cos\alpha)d\alpha \end{aligned} \tag{4.22}$$

In the horizontal direction,

$$\begin{aligned} F_t &= \sum_{i=1}^{n} F_{ti} \\ &= \sum_{i=1}^{n} b\int_0^{l_i} (p_i \cos\alpha + \tau_{fi}\sin\alpha)dx \\ &= \sum_{i=1}^{n} b\int_{\alpha_i}^{\alpha_{i+1}} r_i(p_i \cos\alpha + \tau_{fi}\sin\alpha)d\alpha \end{aligned} \tag{4.23}$$

In the above equations, the subscription i indicates the i^{th} segment which has the length of ℓ_i with radius of r_i, entrance angle of α_i and exit angle of α_{i+1} under consideration, as illustrated in Figure 4.4. It can be seen that all the variables in the above equations can be expressed as functions of the angle α of the wheels.

To describe the relationship of the frictional-shear stress versus the slippage (j), an analysis based on Wong's model for a steel track with ground wheels (Wong, 1993), was adopted.

The slip velocity of any point on the surface of the track-soil interaction, relative to the terrain surface, was the tangential component of the absolute velocity:

$$\begin{aligned} V_j &= V_t - V\sin\alpha \\ &= r\omega - r\omega(1-i)\sin\alpha \\ &= r\omega[1-(1-i)\sin\alpha] \end{aligned} \tag{4.24}$$

The friction-shear displacement (j) along the track-terrain interface was obtained by integrating the slip velocity from the point where friction-shear started to the specified point under consideration:

$$\begin{aligned} j &= \int_0^t r\omega[1-(1-i)\sin\alpha]dt \\ &= \int_{\pi/2-\alpha_{1f}}^{\alpha_i} r[1-(1-i)\sin\alpha]d\alpha \\ &= \ell - (1-i)x \end{aligned} \tag{4.25}$$

where ℓ is the contact length between the specified point to the point where soil contact started, and x was the corresponding horizontal distance between the specific point and the initial soil contact point. The rotational angle α for each segment was considered. The value of α_i was calculated according to the corresponding configuration of the segment. Therefore the integrated value of j was also calculated for any point within each segment. For instance, for the segment ABC, the friction and shear displacement j at any point was calculated as:

$$\begin{aligned} j &= r[(\alpha-(\pi/2-\alpha_{1f}))+(1-i)(\cos\alpha-\cos(\pi/2-\alpha_{1f}))] \\ &= r[(\alpha-(\pi/2-\alpha_{1f}))+(1-i)(\cos\alpha-\sin\alpha_{1f})] \end{aligned} \tag{4.26}$$

Whilst for a point within the segment of the track in contact only with the terrain surface CDEF, j was calculated from:

$$\begin{aligned} j &= \int_{\pi/2-\alpha_{1f}}^{\pi/2+\alpha_{2f}} r[1-(1-i)\sin\alpha]d\alpha + \int_{\pi/2-\alpha_{2f}}^{\alpha} r[1-(1-i)\sin\alpha d\alpha \\ &= r[(\alpha_{1f}+\alpha_{2f})-(1-i)(\sin\alpha_{1f}+\sin\alpha_{2f})] \\ &\quad + r[(\alpha-(\pi/2-\alpha_{2f}))+(1-i)(\cos\alpha-\sin\alpha_{2f})] \end{aligned} \tag{4.27}$$

Similarly, for a point within the segment FGH, the displacement was determined from:

$$\begin{aligned} j &= \int_{\pi/2-\alpha_{1f}}^{\pi/2+\alpha_{2f}} r[1-(1-i)\sin\alpha]d\alpha + \int_{\pi/2-\alpha_{2f}}^{\pi/2+\alpha_{1r}} R[1-(1-i)\sin\alpha d\alpha \\ &\quad + \int_{\pi/2-\alpha_{1r}}^{\alpha} r[1-(1-i)\sin\alpha]d\alpha \\ &= r[(\alpha_{1f}+\alpha_{2f})-(1-i)(\sin\alpha_{1f}+\sin\alpha_{2f})] \\ &\quad + R[(\alpha_{2f}+\alpha_{1r})-(1-i)(\sin\alpha_{2f}+\sin\alpha_{1r})] \\ &\quad + r[(\alpha-(\pi/2-\alpha_{1r}))+(1-i)(\cos\alpha-\sin\alpha_{1r})] \end{aligned} \tag{4.28}$$

4.5 THE PREDICTION OF MOTION RESISTANCE

The motion resistance of the prototype track R_r can be expressed as:

$$R_r = R_e + R_i \tag{4.29}$$

Where R_e is the external resistance and R_i is the internal track resistance.

For the models as discussed in the Section 4.4.1 (page 4-5), the external motion resistance between the track and the terrain surface is mainly due to the soil compaction below the track. To simplify the procedure for predicting the performance, only the rolling resistance for soil compacting was taken into consideration.

If the contact pressure on the track-terrain interface is distributed uniformly, which is the case for an ideal ground pressure distribution based on the initial design, the motion resistance for compacting soil was expressed by Bekker (1960):

$$R_e = \frac{b}{(n+1)(k_c/b+k_\phi)^{(1/n)}}\left(\frac{W}{bL}\right)^{(n+1)/n} \tag{4.30}$$

Observations based on the preliminary test results (Yu and du Plessis, 1997) proved that the contact pressure distribution was not as uniform as expected. Other possible pressure distributions, such as the rigid and the flexible track models described in the preceding sections, should therefore also be considered. For both rigid and flexible models, the rolling resistance was attributed to the total horizontal component of the contact pressure in the direction opposite to travelling. The contact pressure was expressed as a function of the rotational angle of the track segment α for the flexible track model as shown in Figure 4.4. The motion resistance can be predicted by summation of the motion resistance generated by each segment of the track as shown in the following equation:

$$\begin{aligned} R_e &= \sum_{i=1}^{n} R_i \\ &= \sum_{i=1}^{n} b \int_0^{\ell_i} p(x) \sin \alpha \, d\ell \\ &= \sum_{i=1}^{n} b r_i \int_{\alpha_i}^{\alpha_{i+1}} p(x) \sin \alpha \, d\alpha \end{aligned} \tag{4.31}$$

In Equation (4.31), ℓ_i is the corresponding length of the i^{th} track segment, whilst r_i is either the radius of the wheels or the virtual radius of the circular curve of the track in contact only with the terrain surface.

The internal loss is mainly caused by friction and relative movement and associated friction between the track elements. The track tension of the prototype traction system was designed to be adjustable. If the track tension was adjusted to be higher than the maximum tractive effort between the track and terrain surface, the slip resulting would be kept to a minimum.

Under operational conditions, rubber materials have elastic characteristics. During this action extra internal losses were therefore caused by cyclic reshaping of the rubber tracks and the wheels with hysteresis and heat build up. An analysis of the internal resistance will be addressed in the next section.

The total motion resistance can be calculated based on equation (4.29) after the external and internal resistances are obtained.

4.6 INTERNAL TRACK RESISTANCE AND THE FRICTION DRIVE BETWEEN THE WHEEL AND THE TRACK

The prototype track is tensioned to a specified level by a hydraulic cylinder and locked by a threaded rod and lock nuts.

The track tension is a critical factor for the frictional torque transfer between the drive wheels and the internal track surface.

If the rubber surfaced track stretched by the drive wheels is considered as a rubber belt and a rubber pulley, the analytical results for belt conveyers and friction drives may be utilized to explain the relationship of tension and frictional drive force. When the rubber belt track travels on a smooth rigid surface and the traction force is assumed to increase linearly along the ground contact length of the track, as shown in Figure 4.5, the following relationship can be established according to basic theory of belt friction (Green, 1955):

$$\begin{aligned} F_t &= T_t - T_0 \\ &= T_0 e^{\pi' \mu_\varphi} - T_0 \\ &= T_0 e^{(\pi' \mu_\varphi - 1)} \end{aligned} \tag{4.32}$$

where

T_0 = track pre-tension, (N).

T_t = maximum track tention, (N).

F_t = tractive effort, (N).

μ_φ = friction coefficient between contact surfaces.

π' = wrap angle = 180°.

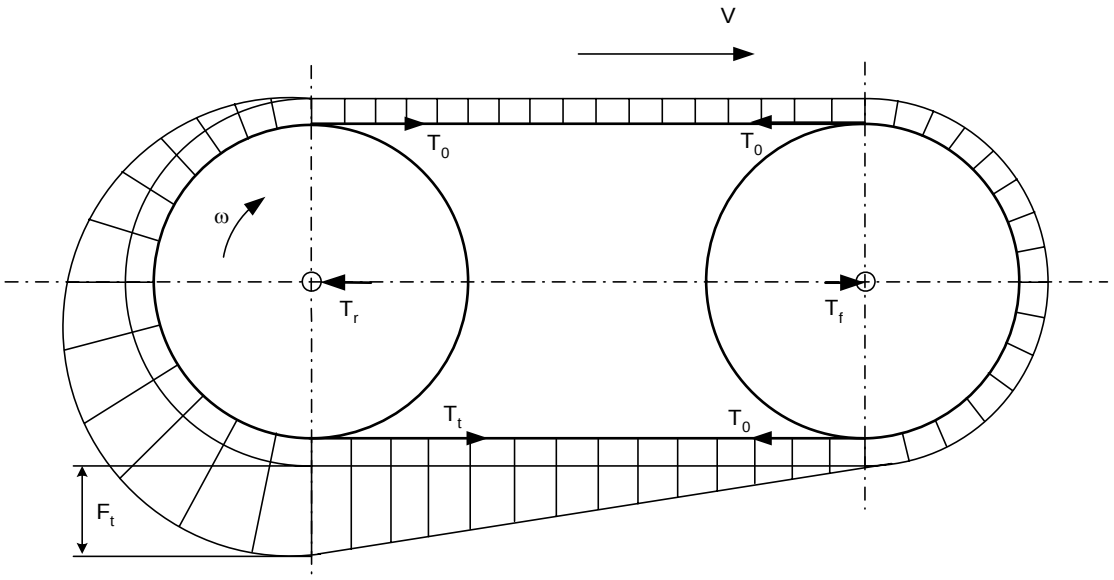

Figure 4.5. Simplified distribution of the track internal tension during forward movement.

When the values of the track pre-tension T_0, the wrap angle and the friction coefficient are set, the tractive effort F_t is the limitation within which slippage is minimized. Therefore the higher the track tension, the larger the traction that can be transfered. On the other hand, the magnitude of the track tension is limited by the dimensions of the sub-frame structure, the strength of the track and other design factors.

As observed in practice, small amounts of slippage occur as soon as the friction drive is loaded, although it is not easily measurable when the drawbar pull is small. The loss caused by this slippage may be accepted as 3-5% of the total power transmitted by the traction device which represents a typical situation for a rubber belt conveyer (Green, 1955).

In this research, to simplify the calculation for modelling, a decrease of 3% of the total tractive effort was accepted to account for internal bending and slip losses, regardless of the speed.

4.7 TOTAL DRAWBAR PULL OF THE PROTOTYPE TRACK

The total drawbar pull F_h is the difference between the tractive effort and the motion resistance and can be expressed as:

$$F_h = F_t - R_r \tag{4.33}$$

where F_t is the resultant total force in the direction of movement which can be obtained by integration or derived from the analysis of tangential stresses and contact pressure. R_r is the total motion resistance.

Since the contact pressure and the tangential stress are functions of the track sinkage and the track slip respectively, the track motion resistance R_r and the tractive effort F_t also vary with the track slip. Based on equation (4.33), the relationship of drawbar pull and the track slip can be predicted.

4.8 THE COEFFICIENT OF TRACTION AND TRACTIVE EFFICIENCY

The coefficient of traction C_{ct} is the ratio of tractive effort to the vertical load of the track and expressed by:

$$C_{ct} = \frac{F_t}{W} \tag{4.34}$$

The tractive efficiency η is the ratio of the output to input power of the track and expressed as:

$$\eta = \frac{P_{out}}{P_{in}} = \frac{F_h V}{2T\omega} \tag{4.35}$$

where

η = tractive efficiency.

P_{in} = input power, (kW).

P_{out} = output power, (kW).

F_h = total drawbar pull, (N)

V = travel velocity, (m/s)

T = input torque for one side shaft, (Nm).

4.9 MODELLING PROCEDURE

For both the flexible track and the rigid track models, the static vehicle weight was accepted to be supported only by the wheels. The sinkage of the front wheels were calculated based on Bekker's (1956, 1960) sinkage equation for solid wheels (equations 4.19 and 4.20). The sinkage of the rear wheels were accepted to be equal to that of the front wheels until the load increase caused by weight transfer, which lead to additional rear wheel sinkage.

The contact pressure at any point on the interacting surface was calculated based on the pressure sinkage relationship proposed by Bekker with equation (2.1) after which the sinkage at each point on the contact surface was determined by initial assumptions and the configuration of the track-terrain contact profile as described in the previous sections of this chapter. The tilt angle β was also taken into account for the contact pressure caused by sinkage.

The accumulated displacement j was calculated by equation (4.7) or equations (4.26) to (4.28). Equation (4.7) (p 4-9) was validated for the idealized contact pressure distribution. Equations (4.26) (p 4-17), (4.27) (p 4-17) and (4.28) (p 4-18) were applicable for the segments ABC, CDEF and FGH (Figure 4.4, p 4-13) respectively for the flexible track model. The tangential stress was then calculated from equation (4.2) (p 4-4), as described in the previous sections of this chapter. The total thrust for a specific level of slip was calculated by applying equation (4.11) (p 4-10) for the idealized uniform distribution or (4.23) (p 4-16) for the flexible track model. The parameters related to rubber-soil friction characterization were obtained from bevameter tests.

When the motion resistance was calculated by any of the equations (4.12) (p 4-10) for the uniform pressure distribution model, or equations (4.30) (p 4-18) and (4.31) (p 4-19) for the flexible track model respectively, the drawbar pull was the difference between the total tractive thrust and the calculated motion resistance.

The tractive thrust as well as the motion resistance could be calculated by either computer programming or spreadsheet coding. To utilize its advantage of simplicity, the spreadsheet method was mainly used for the calculations for this research.

The final results from the calculations were expressed as the relationship of either the tractive force or the drawbar pull versus the slip as was predicted.

CHAPTER V

INSTRUMENTATION, CALIBRATION AND EXPERIMENTAL PROCEDURE

5.1 INTRODUCTION

To prove the proposed theoretical model for the traction performance of the tracked vehicle on soft terrain surface based on the analytical method, *in situ* soil characterization was necessary. In this research project, the bevameter technique was used to acquire soil characteristics for shear strength, rubber-soil friction as well as the pressure-sinkage relationship.

For validation of the predicted results, a series of full-scale drawbar pull tests were conducted in the field. The parameters measured during the drawbar pull test included the drawbar pull, the torque to one side drive shaft of the tractor and the theoretical and actual travel speeds was based on which the total slippage was calculated. The slip between wheel and track measured manually by means of marks on the wheel and the track to derive the difference between the calculated wheel travel distances to the measured track travel distance after a certain number of revolutions of the wheel.

The contact and the tangential forces on the ground contact surface between a track element and the soil were also measured by using two small specially designed extended octagonal ring transducers, mounted on the track basis. From the measured contact force, the distribution of the contact pressure along the track was derived. The total tangential tractive effort was calculated based on the summation of the measured tangential forces.

All the experimental work was conducted under field conditions at the Experimental Farm, University of Pretoria. To identify the influence of the soil water content on drawbar performance it was decided to perform the tests under three different values of soil water content, controlled by irrigating the test site several days before a test. In order to achieve realistic test conditions as expected, the field was carefully chosen and disk ploughed. The tests were also conducted during the dry winter season to eliminate the influence of rainfall.

A computerized data acquisition and logging system was built and used to pre-process and record all the data concerned.

5.2 APPARATUS FOR SOIL CHARACTERIZATION

To obtain the soil parameters necessary for the traction modelling based on the analytical methods, an instrumented apparatus applying the bevameter technique was built in the Department of Agricultural Engineering, University of Pretoria (Yu, 1996). This linear shear and soil sinkage apparatus was similar to the one originally developed at the University of California, Davis Campus (Upadhyaya et al, 1993).

The instrumented apparatus as shown in Figure 5.1, can be used to measure:

- linear soil shear and frictional characteristics for steel-soil and rubber-soil contact respectively;
- soil contact pressure-sinkage parameters; and
- soil cone index.

The main frame (M) was carried by a front mounted tractor three point linkage (L).

A double acting hydraulic cylinder and set of loading blade springs (B) applied a predetermined constant vertical load to the main frame (M) and adjustable feet (A).

The grouser carrier frame (F) was moved horizontally by a hydraulic cylinder (H_2) supported by two horizontal brass bearings sliding over round stainless steel rod slides (S_2). To accommodate slip sinkage during the test the anchor of the traction cylinder (H_2) slides vertically on a brass bush and rod (S_3). To ensure minimal frictional influence on the horizontal shear force, measured by the load cell between the grouser carrier frame and piston assembly (H_2), the grouser was carried by four identical vertical adjustable arms (L_1) with ball joints.

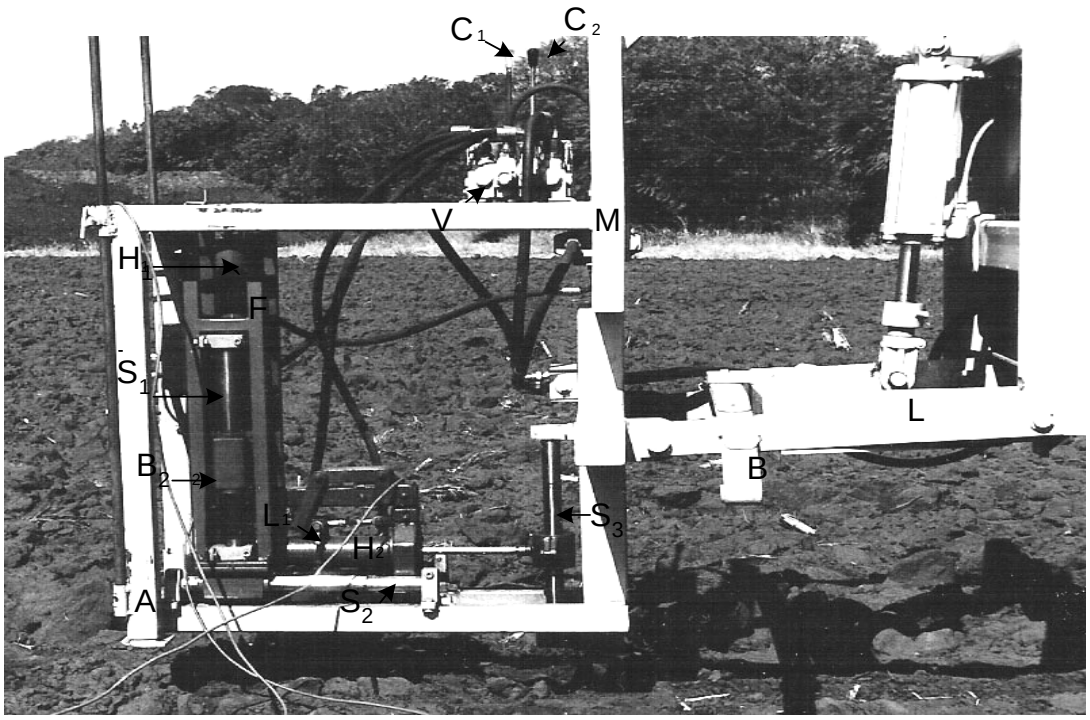

A – adjustable feet	B – loading blade springs	B_2 – moving blocks
C_1 – control lever	C_2 – second control lever	F – carrier frame
H_1 – vertical cylinder	H_2 – piston assembly	L – three point linkage
M – main frame	S_1 – vertical piston rod	S_2 – rod slides
S_3 – brass bush and rod	V – pressure control valve	

Figure 5.1. Linear shear meter used for soil shear, soil-rubber friction as well as sinkage characterization.

Two separate hydraulic circuits were used to prevent interaction between the vertical and horizontal loading. The vertical force was applied by a pump and circuit, with a hydraulic cylinder between the main frame (M) and unit with two parallel moving blocks (B_2). The vertical load cell was mounted between (B_2) and the grouser carrier.

The applied vertical force was kept constant during slip sinkage by supplying surplus oil and using a special adjustable pressure control valve (V). During the test the vertical load was applied with the supply control lever (C_1) fully open and the control valve (V) set at a specific release pressure, with the surplus oil flowing back to the tank.

The second control lever (C_2) activated the second hydraulic circuit and supplied oil to the horizontal cylinder (H_2) whilst the vertical hydraulic cylinder (H_1) followed the slip sinkage action and applied a constant vertical load. The vertical and horizontal displacement of the grouser was recorded via two rotational potentiometers with woven string and a rotary spring for automatic return.

Two industrial S-type weighing scale load cells were used to measure the applied vertical and horizontal loads independently. The shear grousers, sinkage plates and cone penetrometer with different shapes, dimensions, and surface materials could easily be removed and replaced when necessary.

The analog signals from the load cells and the potentiometers had to be pre-processed by an A/D converter before being recorded by the data acquisition system.

Three sinkage steel plates with different dimensions were used to characterize the soil pressure-sinkage relationships. Two different steel shear grousers were used to obtain the soil shear characteristics, whilst a standard rubber-covered track element was used to measure the rubber-soil frictional characteristics.

Figure 5.2 shows the grouser shear plates, the sinkage plates, the track element and the cone penetrometer used for soil characterization with the instrumented bevameter.

The dimensions of the shear grousers and the sinkage plates are shown in Table 5.1 and Table 5.2 respectively.

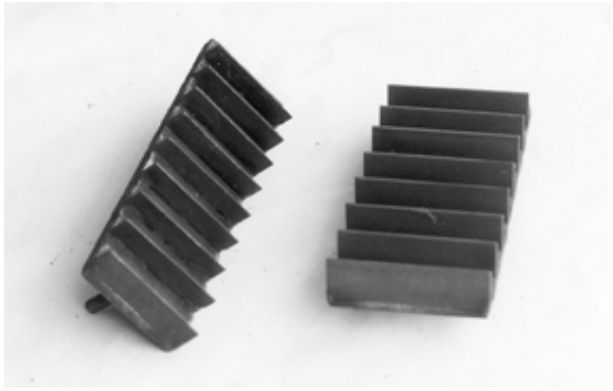

(a) shear grousers

(b) sinkage plates

(c) track element

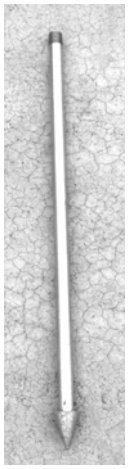

(d) cone penetrometer

Figure 5.2. Components used for soil characterization.

Table 5.1. Dimensions of the rectangular steel shear grousers and the rubber track element.

Dimension	Length, mm	Width, mm	Grouser height, mm
Steel shear grouser	240	60	10
Steel shear grouser	220	80	12
Rubber track element	500	70	Smooth rubber surface

Table 5.2. Dimensions of the steel sinkage plates.

Sinkage plate	Width, mm	Length, mm	Aspect ratio (L/W)
No. 1	70	210	3
No. 2	60	240	4
No. 3	55	285	5.18

5.3 THE EXTENDED OCTAGONAL RING TRANSDUCERS FOR MEASURING THE DISTRIBUTION OF CONTACT PRESSURE AND TANGENTIAL STRESS

5.3.1 Design of the transducer

Two identical extended octagonal ring transducers were built in order to measure the distribution of contact pressure and tangential stresses.

The basic shape and dimensions of the octagonal ring transducer are shown in Figure 5.3.

The values of L_o and r_o were chosen to accommodate the limited space available between the track element and the base plate over the track cable assembly. The value of b was chosen to provide for sufficient supporting area and stiffness to mount the transducer onto the track. The transducers were machined from a solid block of EN24 alloy steel, and heat-treated for an ultimate tensile strength of about 1500MN/m^2 on which the preliminary design was based. Both high sensitivity and sufficient stiffness within the elastic deformation range was necessary. By applying the equations as reviewed in Chapter 2, the thickness t_o, at the middle point of the flat surface was initially calculated as 1.9mm. The vertical force was accepted as 2000N with an allowable working stress of 750MN/m^2. For machining purpose, the value of

t_o was eventually adjusted to 2mm. The dimensions for the two transducers are shown in Table 5.3.

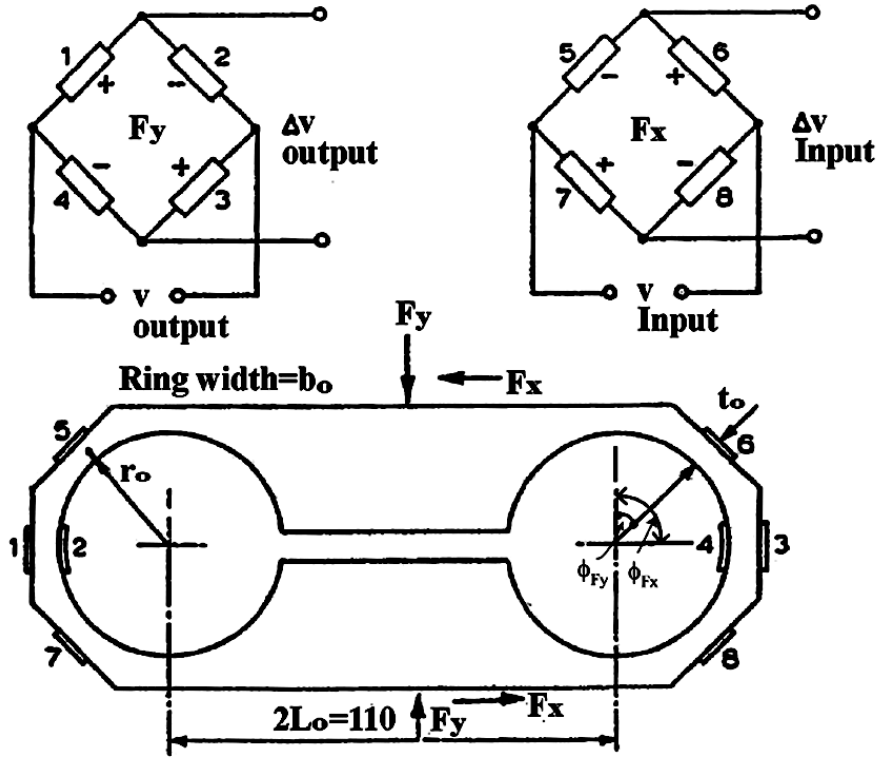

Figure 5.3. Design parameters and forces for the extended octagonal ring transducer.

Table 5.3. The dimensions of the octagonal ring transducers.

r_o, mm	L_o, mm	t_o, mm	b_o, mm	ϕ_{Fx}, deg	ϕ_{Fy}, deg
16	55	2	20	90	45

The nodal angle for force F_x was determined as 90° by trial and error fixing of the strain gauges at different angles with the least interference on force F_x by force F_y and vice versa,. For force F_y, the nodal angle was identified as 45°.

The ratio of r_o/t_o=8 is larger than 5 and is sufficiently large for thin ring theory to be accepted as valid on which the design was based (Godwin, 1975).

5.3.2 Calibration and installation of the transducers

For each extended octagonal ring transducer, eight 120Ω strain gauges were used to form two Wheatstone bridges. After the strain gauges were fixed and the circuits connected, the two transducers were calibrated using a special frame on which the horizontal and the vertical loads were applied independently. The excitation voltage to the bridges was 5 volt and the outputs for calibration were measured with a Hewlett-Packard high-sensitivity multi-meter.

The preliminary calibrations showed some unacceptably high cross sensitivity errors for the bridge measuring force F_y caused by force F_x (Yu & du Plessis, 1996). Further investigation and modifications were undertaken to correct the error by inserting two thicker steel spacers (B in Figure 5.4) on both mounting surfaces of the transducer to ensure that the elastic deformation of the transducer was not interfered with by improper constraints as shown in Figure 5.4.

Prior to the field tests, the two transducers were finally calibrated to obtain the results as shown in Figures 5.5 to 5.8. The regression data proved that the outputs for both transducers were highly linear with the correlation coefficients ≥ 0.998 over the full load range tested. The recorded cross sensitivity error for the two transducers was less than 2%. The line is shown at the bottom of each graph. The calibration results are shown in Table 5.4.

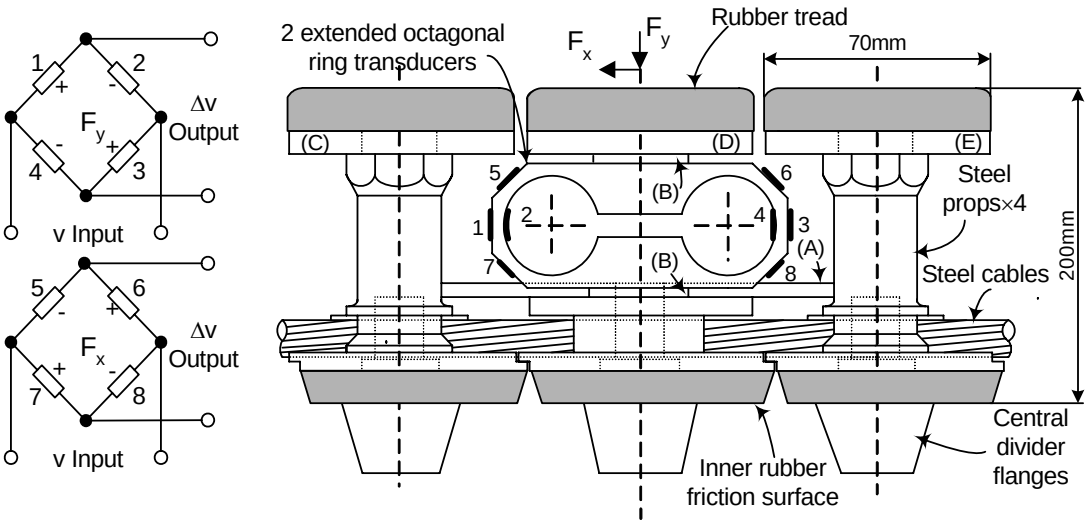

Figure 5.4. The installation of the octagonal ring transducers on the track element.

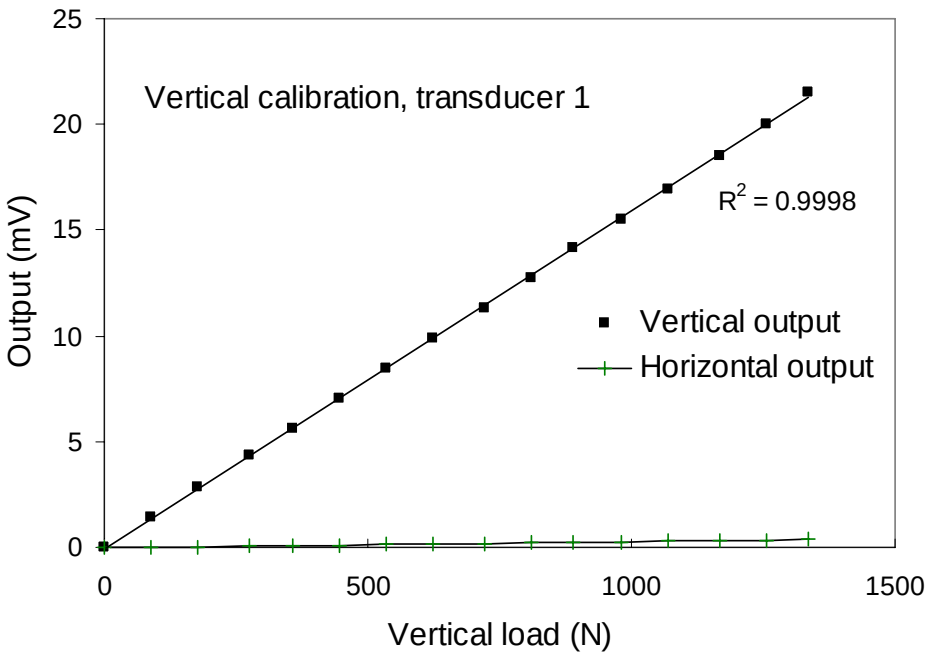

Figure 5.5. Vertical calibration of the octagonal ring transducer 1.

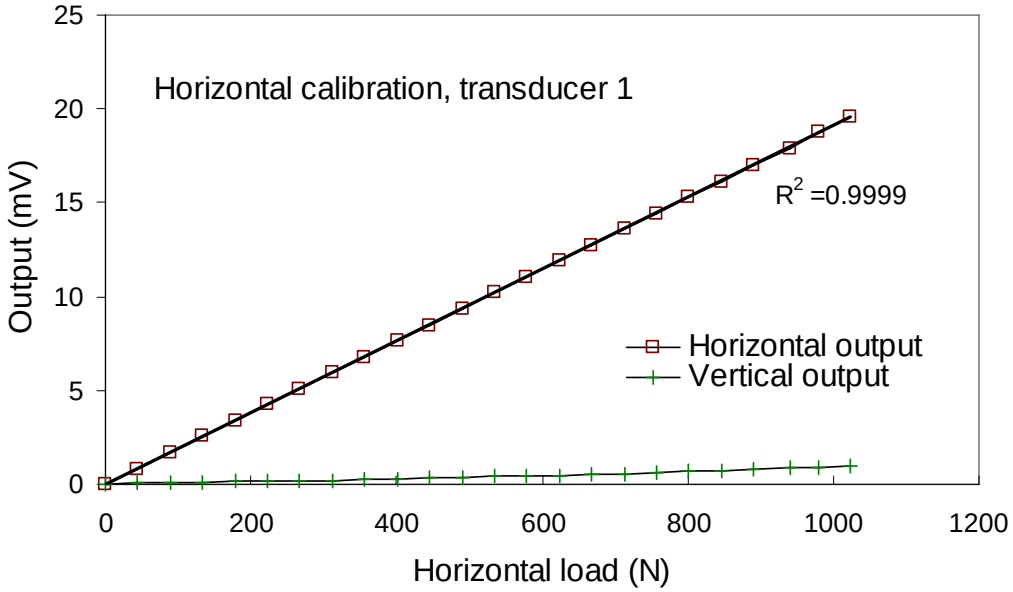

Figure 5.6. Horizontal calibration of the octagonal ring transducer 1.

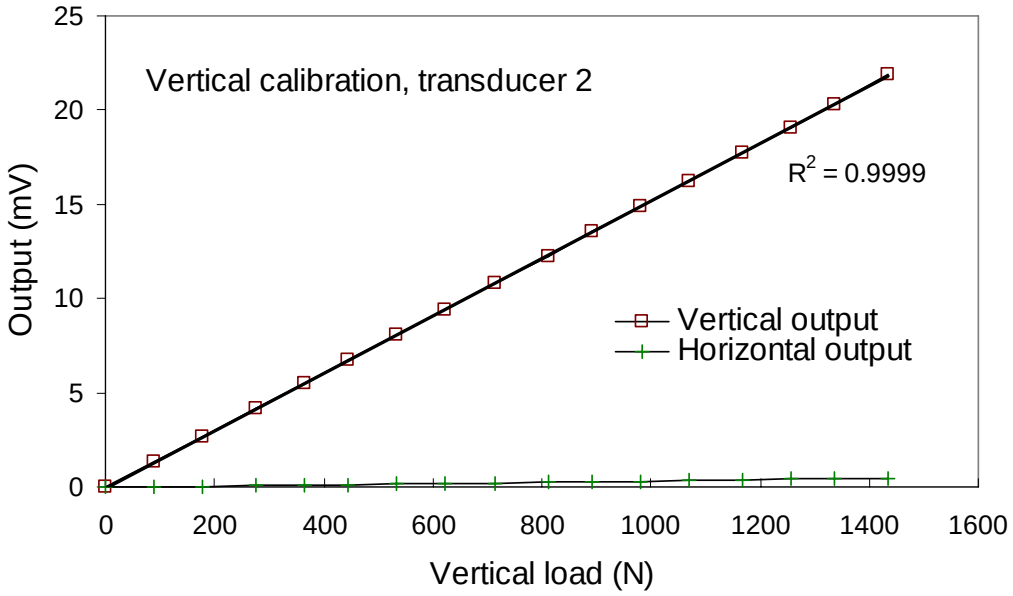

Figure 5.7. Vertical calibration of the octagonal ring transducer 2.

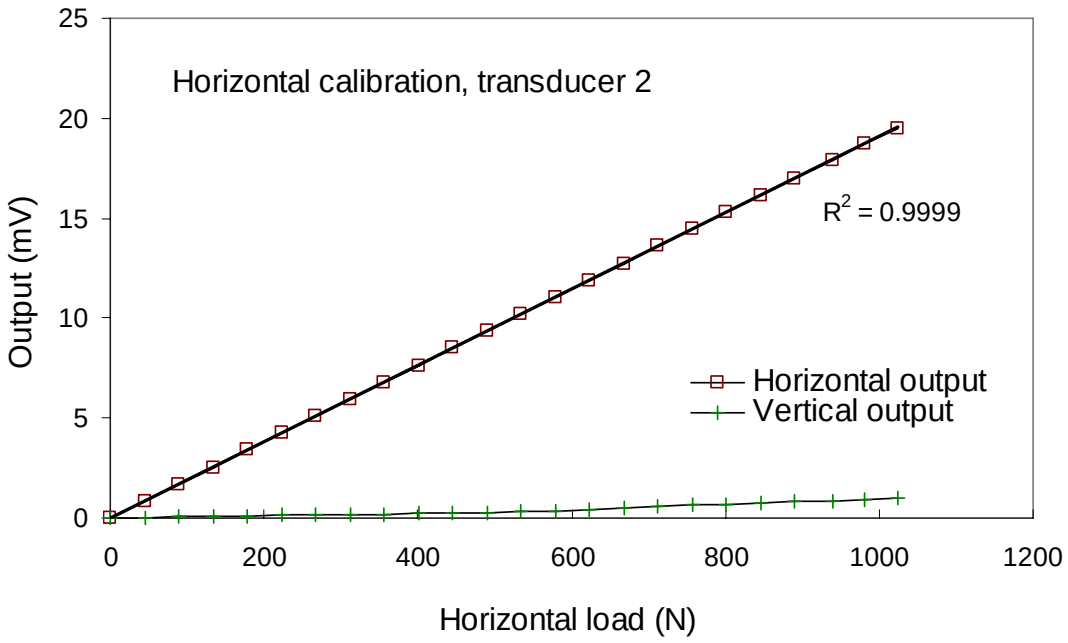

Figure 5.8. Horizontal calibration of the octagonal ring transducer 2.

Table 5.4. Calibration results for the two octagonal ring transducers.

	Transducer 1		Transducer 2	
	Vertical load F_V	Horizontal load F_H	Vertical load F_V	Horizontal load F_H
Sensitivity (mV/N·V)	0.62180	0.52453	0.65049	0.52534
Correlation coefficient	0.99981	0.99991	0.99995	0.99992

The two extended octagonal ring transducers were fitted between the track base assembly and the track element as shown in Figure 5.9 and Figure 5.10. Two steel plates (A) were inserted between the columns of the adjacent track elements to prevent them from touching the middle one onto which the transducers were mounted. In this way the tangential stress could be measured without interference from the neighboring track elements (Figures 5.9 and 5.10). By mounting the two transducers side by side along the width of the track, the total force on the track element could be measured by adding the outputs from the two transducers in vertical and tangential directions respectively. Accordingly, the contact pressure and the shear-friction stress could be calculated by dividing the corresponding load by the contact area.

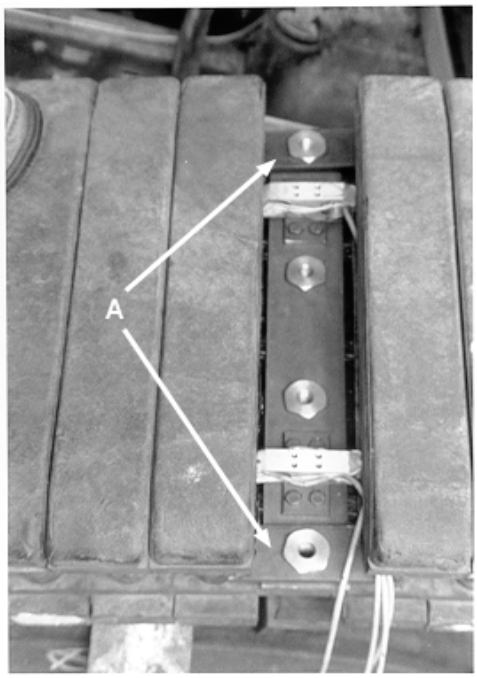

Figure 5.9. Top view of the two transducers installed side by side on the track.

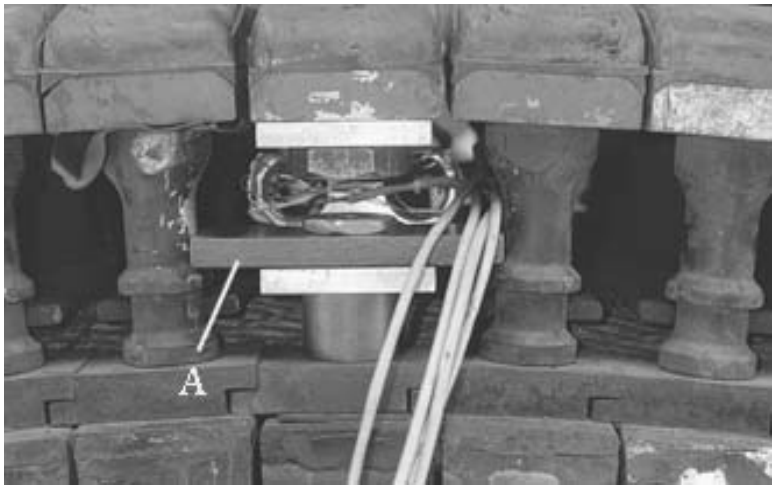

Figure 5.10. Side view of the two octagonal ring transducers installed between the track element and the track base assembly.

5.4 INSTRUMENTATION FOR MEASURING TORQUE, SLIP AND DRAWBAR PULL

5.4.1 Instrumentation for measuring the side shaft torque

By using a special differential system in the tractor drive train, the torque is equally divided between the two side shafts under normal operational conditions. The drive torque and speed are also equally split to the two side shafts for straight line traveling. To simplify the instrumentation for measurement, it was decided to measure the torque and the speed for only one side shaft as torque was equally split between the two side shafts by the interlinked differential.

Wire-type strain gauges were chosen to measure the side shaft torque and the circuit was connected into Wheatstone bridges (Figure 5.11). To reduce the noise errors during the signal transfer, the output signal for the torque was firstly amplified and conditioned by a circuit fixed to the rotating shaft. The amplified signal was transmitted via a slip ring and a cable system to the data acquisition system. The torque transducer was calibrated prior to the re-assembly of the drive axle by using a

three meter long steel arm fixed to the drive shaft and step by step loading it by standard weights. The calibration data for the torque transducer is shown in Figure 5.12.

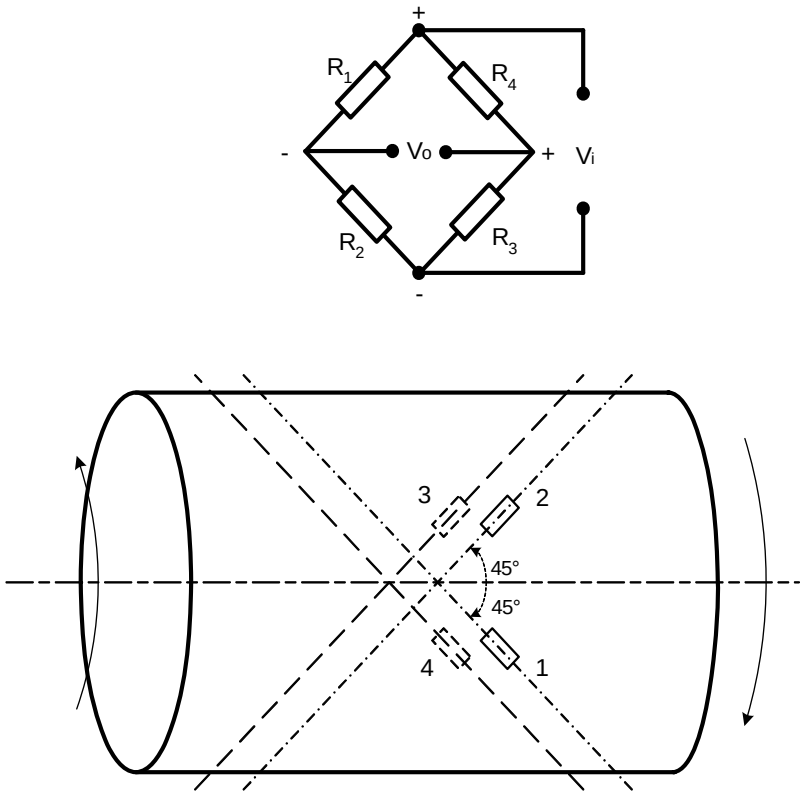

Figure 5.11. The strain gauges and the circuit to measure the side shaft torque.

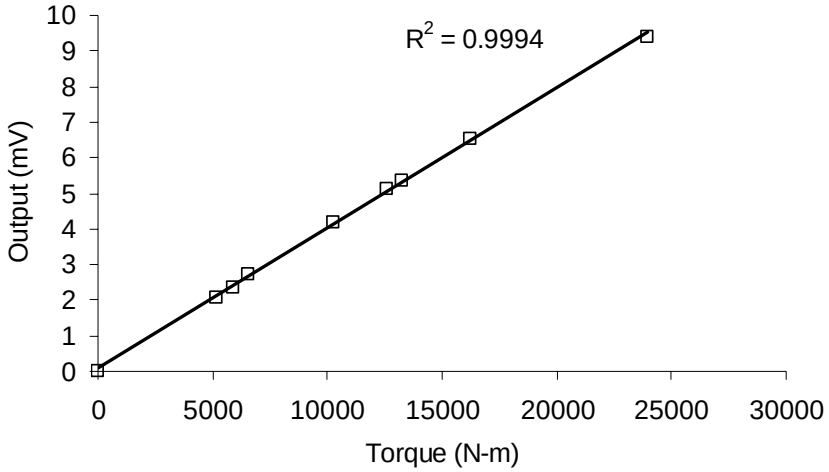

Figure 5.12. The calibration results for the torque transducer.

5.4.2 Instrumentation for measuring speed and slip

Two speed sensors using photoelectric counters were built to measure the speeds (Figure 5.13). The sensor consisted of a circular and thin transparent plastic disk with uniformly distributed radial black printed stripes at the outer edge (Figure 5.13, A) housed in a circular aluminum housing (B) and a micro optical emitting switch (C) on the side of the box. The optical switch sensed the number of the radial black stripes passing the slot which were subsequently recorded as a frequency signal by a special pulse counter circuit.

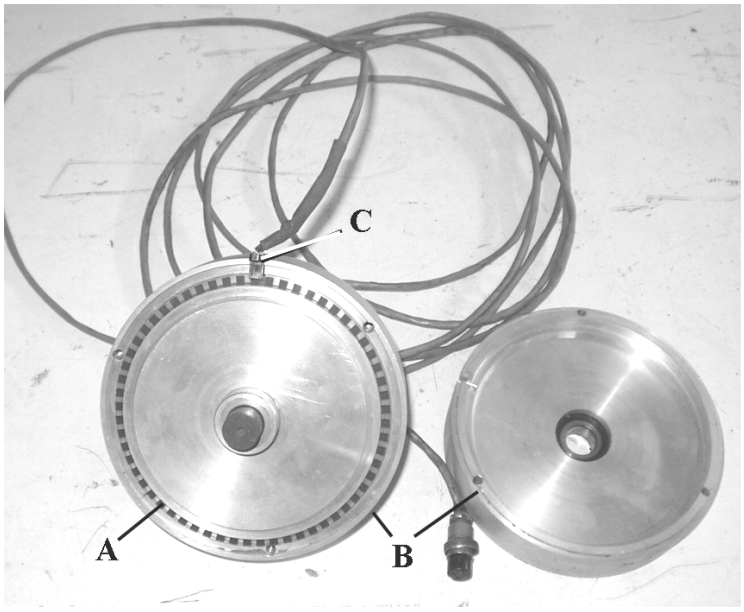

Figure 5.13. Construction of the speed transducers.

Figure 5.14 shows the two instrumented speed transducers mounted on the side shaft of the tractor.

The frequency signals from the speed transducers and the analog signals from the torque transducer on the side shaft were transferred via a slip ring unit (A) with special carbon brushes (Figure 5.14). The rotational speed of the rear side shaft was recorded by the speed transducer unit (B). The true ground speed was recorded by

the speed transducer unit (D) fixed to a drum driven by a cable and anchored to the soil surface. The cable was rewound by winch (C) and braked by (E) to prevent the cable from overrunning. Wheel (F) was used for changing the cable direction.

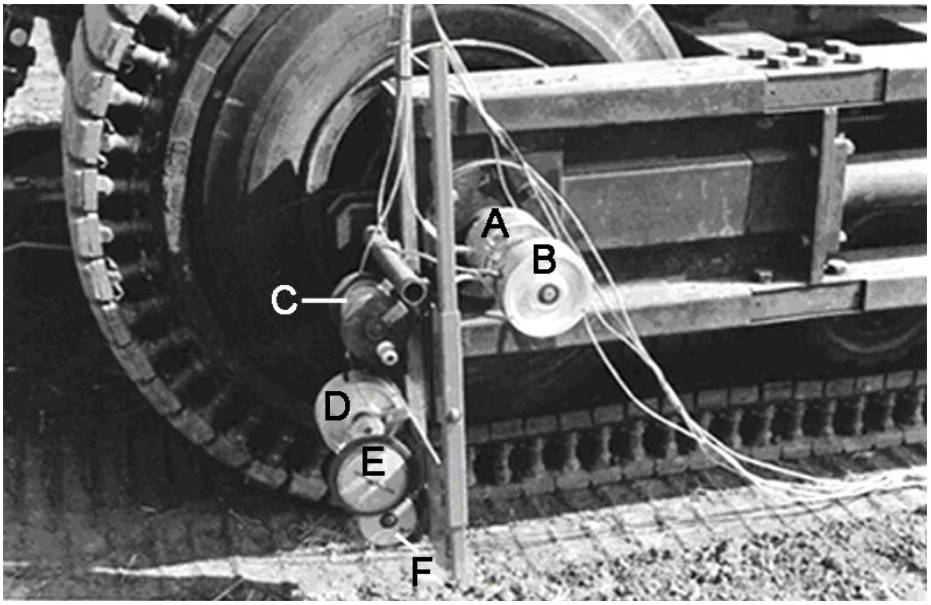

A - slip ring
B – speed transducer unit for theoretical speed
C – winch
D – speed transducer unit for actual speed
E – winch brake

Figure 5.14. The speed transducers, the brush and rotational slip ring unit mounted on the side shaft of the tractor.

The total slip of the track S_t, including wheel to track slip, was obtained by measuring the theoretical speed V_t and the ground speed V of the tractor.

$$S_t = \frac{V_t - V}{V_t} \times 100\% \tag{5.1}$$

The angular speed ω of the shaft of the aluminum unit was obtained based on the frequency of the speed pickup by applying equation (5.2):

$$\omega = 2\pi f / n \tag{5.2}$$

Where n is the total number of the black stripes for 360 degree engraved circle on the plastic sheet.

One of the two aluminum counter units was directly mounted on the extended part of the side drive shaft (Figure 5.13 (A)) and was used to measure the theoretical speed V_t as:

$$\begin{aligned} V_t &= 2\pi r_t \omega_t \\ &= 4\pi^2 r_t f_t \\ &= C_t f_t \end{aligned} \tag{5.3}$$

Where

r_t = the rolling radius of the track, (m).

ω_t = the theoretical angular speed, (rad/s).

f_t = the frequency recorded up by the theoretical speed sensor.

C_t = a constant.

The travel distance for a specified number of revolutions of the drive wheel N_t was measured when the crawler tractor was propelled by its own engine but with zero drawbar pull on concrete road surface. Then the travel distance for the same specified number of revolutions of the drive wheel N_t was measured again when the crawler tractor in neutral gear was towed by another tractor. The rolling radius of the track was calculated based on applying the average travel distance L_t from the above two runs.

Thus,

$$r_t = \frac{L_t}{2\pi N_t} \tag{5.4}$$

The effective radius of the drum was determined by taking the effect of cable diameter into account. When the drum was driven by cable winding over it, the revolutions of the drum N_d were counted and the corresponding travel distance of the cable L_d measured. The effective radius of the drum was therefore calculated by:

$$r_d = \frac{L_d}{2\pi N_d} \tag{5.5}$$

Similarly, the ground travel speed V can then be obtained as:

$$\begin{aligned} V &= 2\pi r_d \omega_d \\ &= 4\pi^2 r_d f_a \\ &= C_a f_a \end{aligned} \tag{5.6}$$

Where

r_d = effective radius of the drum, (m).

ω_d = angular speed of the pulley, (rad/s).

f_a = the frequency recorded by the actual speed sensor.

C_a = a constant to calculate the theoretical speed related to r_d and π.

For the above instrumented device, the recorded slip was the total slip including the wheel-track slip and the track-soil slip.

The wheel-track slip was measured for the field tests by manually marking the tyre surface and the track element. The first marks were made on the tyre and the specified track element at the same time. After several revolutions, the travel distances of the marked point on the tyre and the marked track element were measured and compared to obtain the difference between the two. Then the slip between the wheel and the track was determined.

5.4.3 Instrumentation for measuring drawbar pull

The drawbar pull was measured by mounting a 10 ton industrial load cell, from a local supplier, namely Load Cell Services, between the tested crawler tractor and one or two loading wheeled tractors in series as shown in Figure 5.15. To ensure that the effective drawbar pull was measured, the hitch points of the towing bars for the tractors were adjusted to be parallel to the ground surface.

The analog signal from the load cell was transmitted to the A/D card signal amplifier and conditioner and the data logging system via a cable.

Figure 5.15. The tractors in series for the drawbar pull tests.

5.5 THE COMPUTERIZED DATA LOGGING SYSTEM

All measured analog and digital signals for the field experiments were recorded by an IBM PC compatible computer via a PC30 A/D converter card.

The analog signals, e.g. the signals from the force transducers and octagonal ring transducers, were pre-processed or conditioned before data logging. A signal conditioner mainly composed of 1A31B IC chips from Analog Devices and other associated components were used for amplification and conditioning the signals. The analog signals were then amplified to a specified range for the PC30 card and the noise was filtered. By applying a specially designed circuit to accommodate the 1A31B IC chips, the excitation voltages to the analog transducers and to the frequency and digital transducers were adjustable to suit the display and recording range of the data logging system. As a routine task, the final signals to be recorded

by the PC based data logging system were observed and calibrated before each field test.

The only exception was the analog signal from the side shaft torque transducer which was pre-processed by another amplifying circuit, mounted inside the hub of the drive wheel. An instrumentation amplifier AD620 supplied by Analog Devices was used for the torque signal because of its compact size. By using a slip ring assembly, the amplified signal from the torque transducer was transferred from the rotating side shaft directly to the PC30 card.

In the computer, Stat30 and Waveview software were used to record the data from all the channels. The basic functions of the software included the pre-set and adjustment for sampling frequencies, recording time, offset of signals, channels for data recording, magnitude range of signals and other parameters. The recording of the data was triggered by one touch of the keyboard. The software was also capable of recording data in several specific formats including special graphic format, numeric format and plain text format for further processing with spread sheets or other software.

The flow chart for data processing and recording is shown in Figure 5.16. Figure 5.17 shows the hardware housed in the tractor cab.

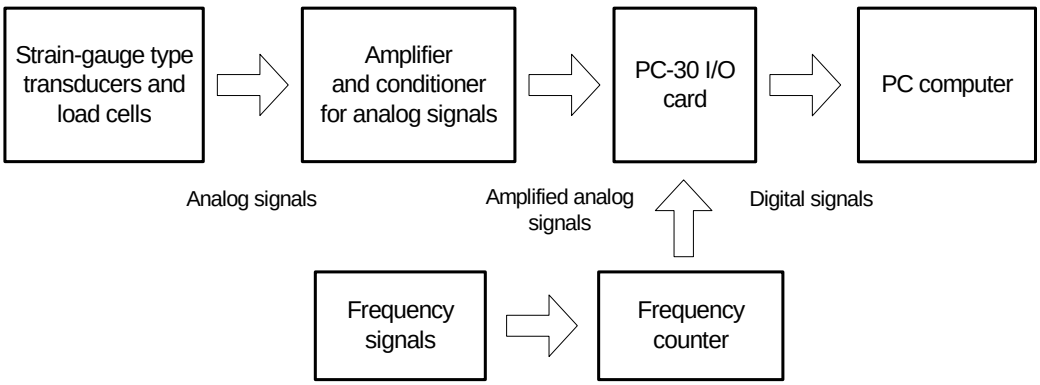

Figure 5.16. The flow chart for the data acquisition system.

Figure 5.17. The computer system in the cab ready for data logging.

CHAPTER VI

FIELD EXPERIMENTS AND DATA COLLECTION

6.1 MEASUREMENT OF SOIL PROPERTIES

6.1.1 Soil classification

Before the field tests, soil samples were randomly collected from the test plot for classification. The sieve analysis method was used to classify the soil according to the USDA textural triangle for soil classification (McKyes, 1989). The soil on the test plot was found to be classified as sandy loam containing 19% clay, 12% silt and 69% sand.

6.1.2 Soil density, soil water content and cone index

Different spots in the test plot were randomly selected for collecting soil samples by applying a cylindrical soil sampler of 60 mm diameter and 100 mm long which was forced into the soil surface and rotated to cut the soil sample. The soil samples were oven dried and the dried bulk density and the soil water content determined. In total ten samples were collected for each soil condition and the average of the readings, as well as other soil characteristics, are shown in Table 6.1.

The cone index was also measured to quantify the soil strength profile for reference purpose. The aim was to ensure that the soil strength was relatively uniform in the treatment areas. The average cone index for the range of depths to 400 mm was recorded for each penetration. The measurement was repeated ten times for each soil condition. The average values for the measurements and the standard deviations obtained were accepted as the final cone index and is shown in Table 6.1.

Table 6.1 Soil physical properties and other field conditions for the field tests

Field number	Soil classification	Surface coverage	Bulk density (dry basis, kg/m^3)	Soil water content (dry basis, %)	Average cone index (kPa)	Standard deviation for CI (kPa)
1	Sandy loam	None	1126	7.8	433	28
2	Sandy loam	None	1245	13.3	675	45
3	Sandy loam	None	1310	21	745	43

6.2 EXPERIMENTAL PROCEDURE FOR SOIL CHARACTERIZATION

6.2.1 Pressure-sinkage characterization for the test plot

The original bevameter technique, without considering the slip sinkage, according to the procedure proposed by Wong (1989, 1993) as reviewed in Chapter 2, was adapted in this research to obtain the soil parameters in equation (2.1). The parameters k_c, k_ϕ and n, were derived according to the method described by Wong (1989, 1993).

The instrumented test device and the sinkage plates, as described in Chapter 5, were used for soil characterization. Each of the three sinkage plates with dimensions as explained in Chapter 5, was loaded to penetrate into the soil at approximately 25 mm/s, as recommended by Wong (1989, 1993). The pressure-sinkage curves for the three soil water content conditions are shown in Figure 6.1 to Figure 6.3. The results of the sinkage tests were analyzed by applying the pressure-sinkage relationship equation proposed by Bekker (1958, 1965) and the values of k_c, k_ϕ and n determined.

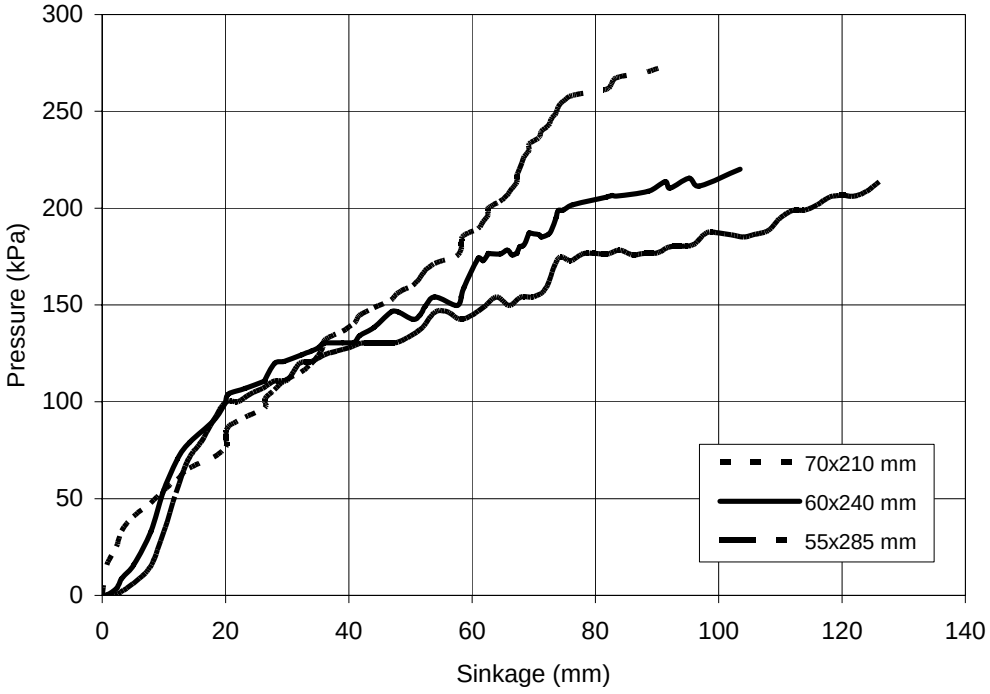

Figure 6.1. Contact pressure-sinkage curves for the sandy loam soil with soil water content 7.8% (dry basis).

The values of k_c, k_ϕ and n were calculated based on the results of at least two tests with two plates having different widths by plotting the p-z curves on log-log scale resulting in two parallel straight lines of the same slope. The proposed procedure by Wong (1989, 1993) was adapted to obtain values for the sinkage parameters.

The pressure-sinkage characteristics obtained from the measurements are shown in Table 6.2.

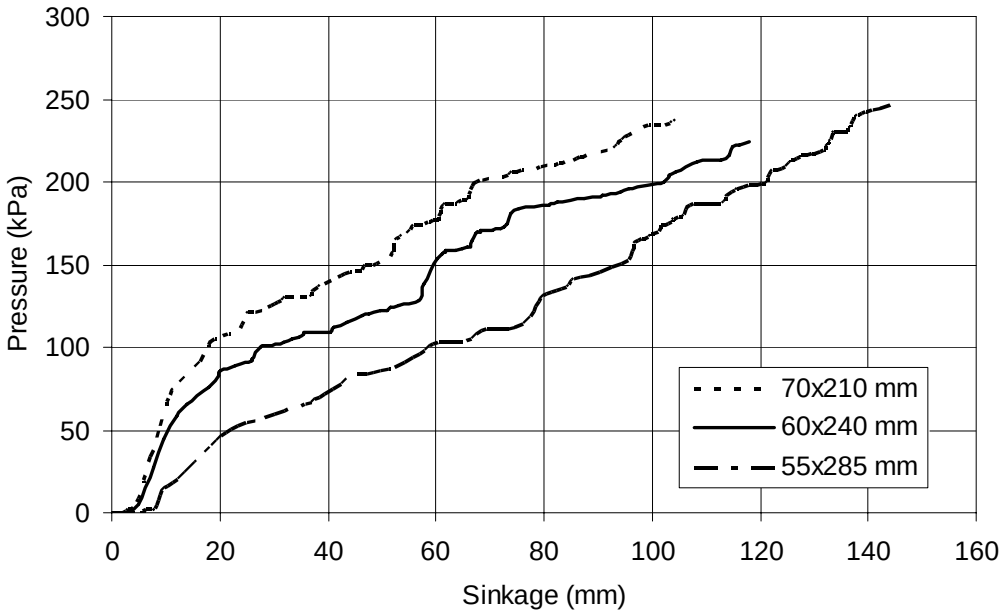

Figure 6.2. Contact pressure-sinkage curves for the sandy loam soil with soil water content 13.3% (dry basis).

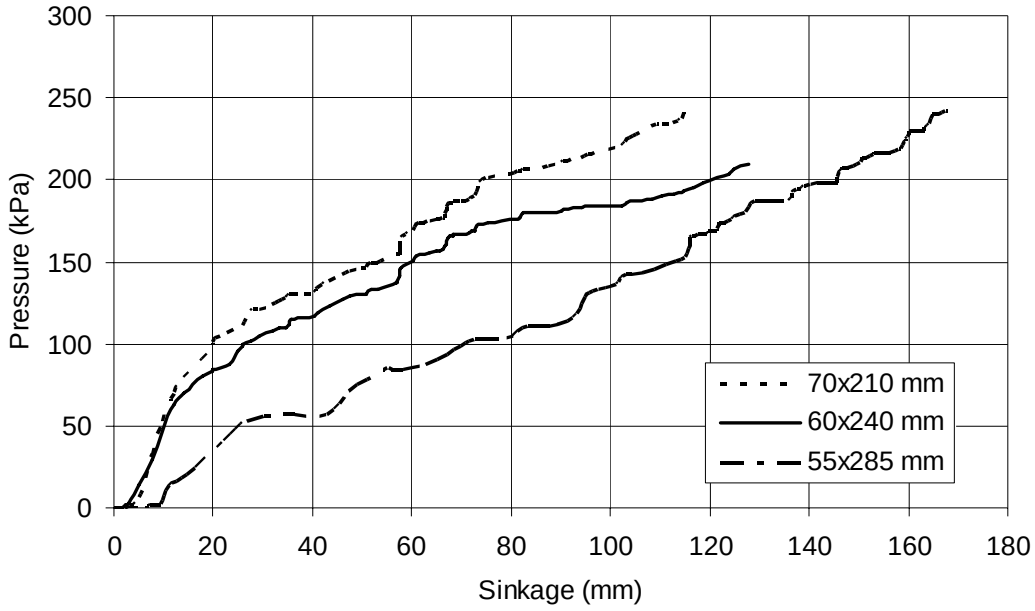

Figure 6.3. Contact pressure-sinkage curves for the sandy loam soil with soil water content 21% (dry bassis).

Table 6.2. Sinkage parameters obtained from pressure-sinkage tests.

Soil water content (dry basis, %)	k_c, (kN/m^{n+1})	k_ϕ, (kN/m^{n+2})	n
7.8	37.9	1520	0.91
13.3	56.6	1630	0.89
21	54.1	1890	0.93

To simulate the unloading and reloading of the contact load exerted by the track, repetitive pressure-sinkage tests were also carried out in the field. The repetitive loading tests were performed following the same procedure as for the conventional sinkage tests. The sinkage plate penetrated into the soil up to a specified depth and then the load was slowly reduced to zero. The plate was reloaded to obtain the original depth for the sinkage tests. The curves for the applied vertical load vs vertical sinkage are shown in Figure 6.4.

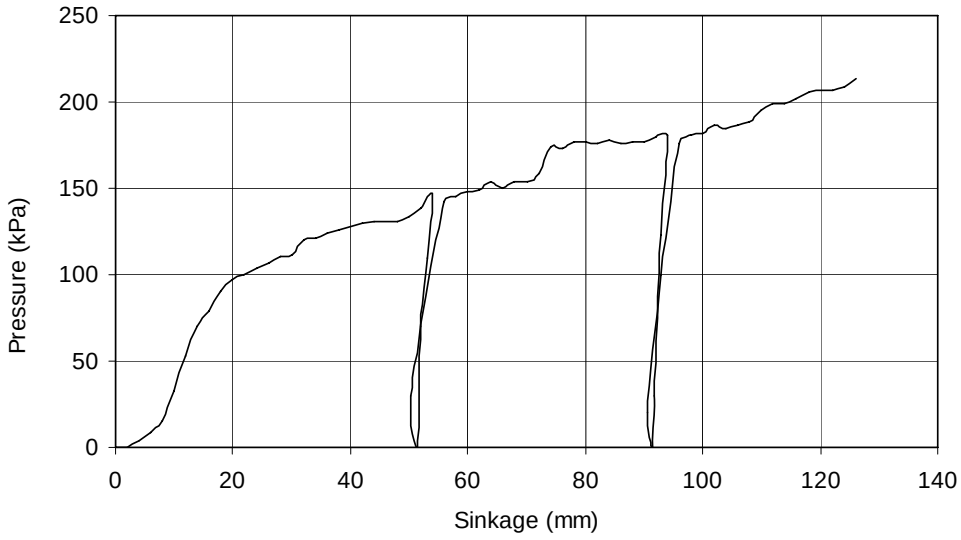

Figure 6.4. The loading/reloading curves for a sinkage tests (Sinkage plate: 60mmx240mm. Soil type: sandy loam. Soil water content=21%).

To apply the characterization for traction modelling, the related parameters, as suggested by Wong (pp. 38-44, 1989; pp. 115-125, 1993) could be used.

6.2.2 Soil-rubber frictional and soil shear characterization

To simulate the shape of the ground track contact area, the rectangular steel shear plates were used to determine the soil shear characteristics.

The investigation was initially carried out to measure soil parameters using a steel shear grouser and soil-rubber frictional characteristics by testing a track element removed from the prototype integral track assembly. The test results indicated that the shape of the soil shear stress-displacement curves and the values of the frictional characteristics for the rubber to soil interface were notably different from those obtained by the soil-soil shear caused by steel grousers (Figure 6.5 and Figure 6.6). It was shown that under the soil conditions tested, the shear curves obtained with the steel shear grouser exhibited the characteristics that the shear stress initially increased rapidly and reached a maximum value of shear stress at a particular shear displacement, and then decreased and approached a constant residual value for further shear displacement (Figure 6.5). This phenomenon can well be expressed by the equation (2.5) as reviewed in Chapter 2. The internal soil shear characteristics obtained from the field tests are shown in Table 6.3.

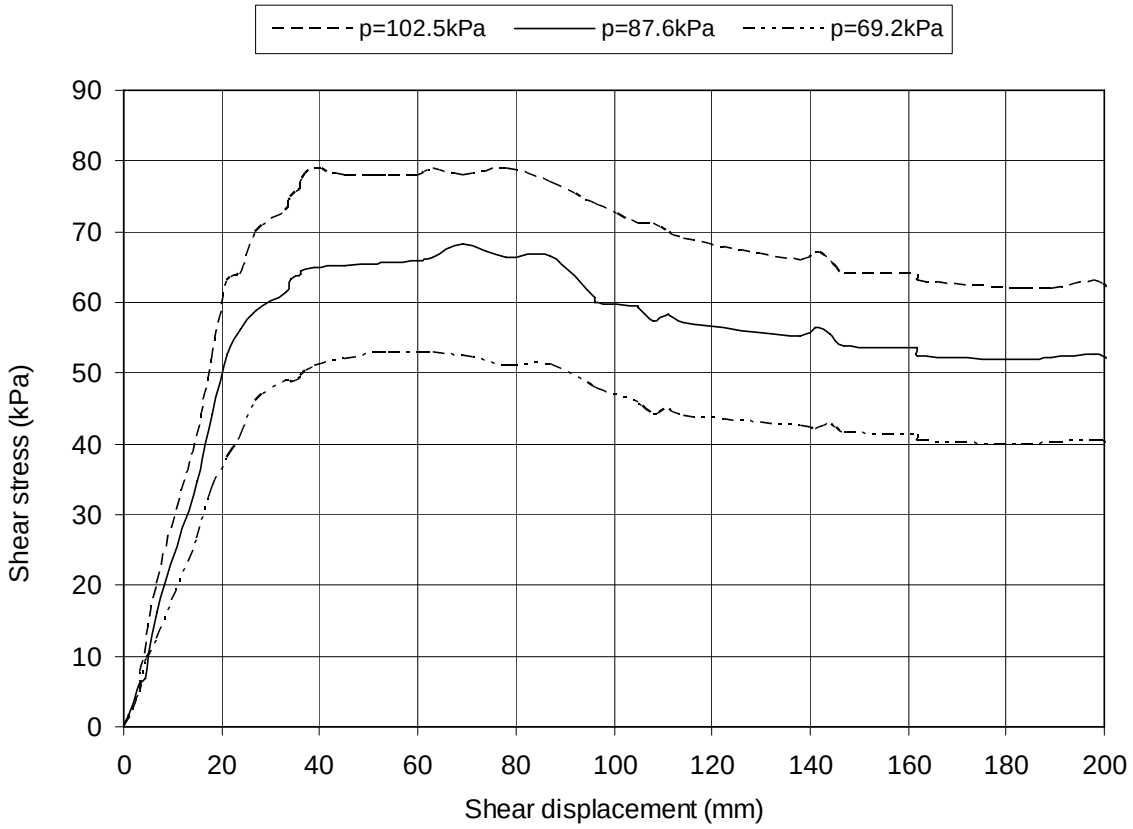

Figure 6.5. Shear curves for a soil shear test using a steel shear grouser (Soil type: sandy loam. Soil water content=7.8%).

Table 6.3. Internal soil shear characteristics from the tests.

Field No	Soil water content dry basis, (%)	Cohesion c, (kPa)	Soil internal friction angle ϕ, (deg)	Shear displacement K_ω at maximum shear stress, (m)
1	7.8	3.13	38.5	0.029
2	13.3	3.65	37	0.035
3	21	2.79	30	0.031

On the other hand, the friction-shear curves obtained with the rubber track element exhibited the characteristic that the friction-shear stress initially increased rapidly with an increase in corresponding displacement, and approached a constant value with a further increase in displacement (Figure 6.6 through Figure 6.8). This can better be fitted by an equation similar to equation (2.6) as proposed by Janosi and Hanamoto (1963). However, the contact surface of the prototype track with rubber surface was smooth without grousers penetrating into soil. It was, therefore, more reasonable that the rationale might be explained that the tangential thrust was mainly due to the friction between the rubber and the terrain surfaces, rather than the internal friction of the soil. The rubber-soil adhesion also replaced the soil-soil cohesion for conventional soil shear characterization. Consequently, the test results for traction modelling using a track element with a smooth rubber surface was better related to the actual situation than the steel shear grousers.

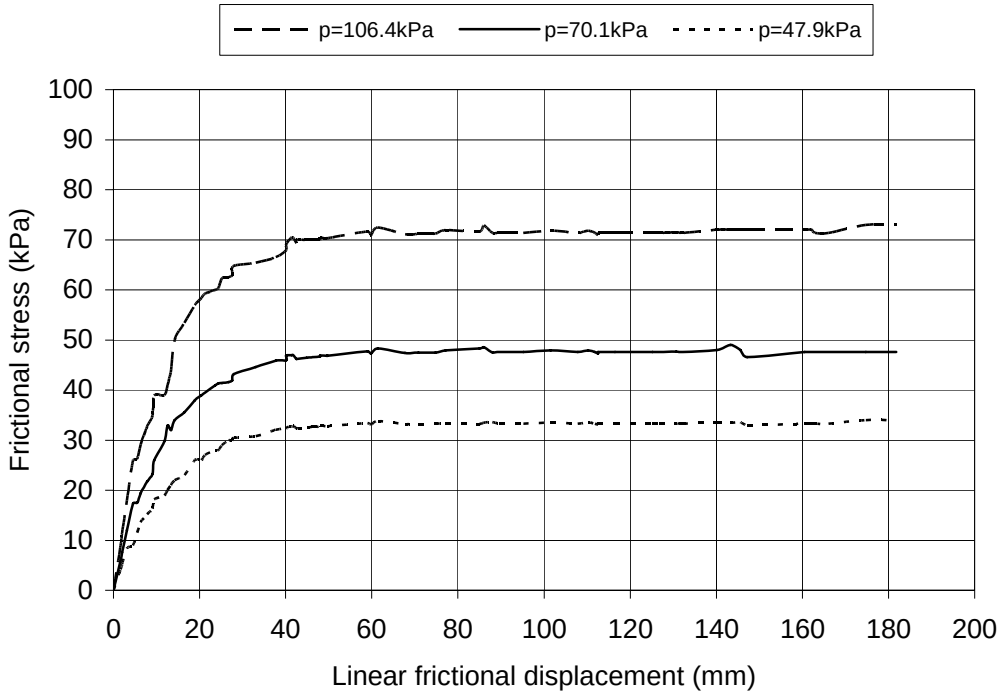

Figure 6.6. Friction curves for rubber-soil friction test (Soil type: sandy loam. Soil water content=7.8%).

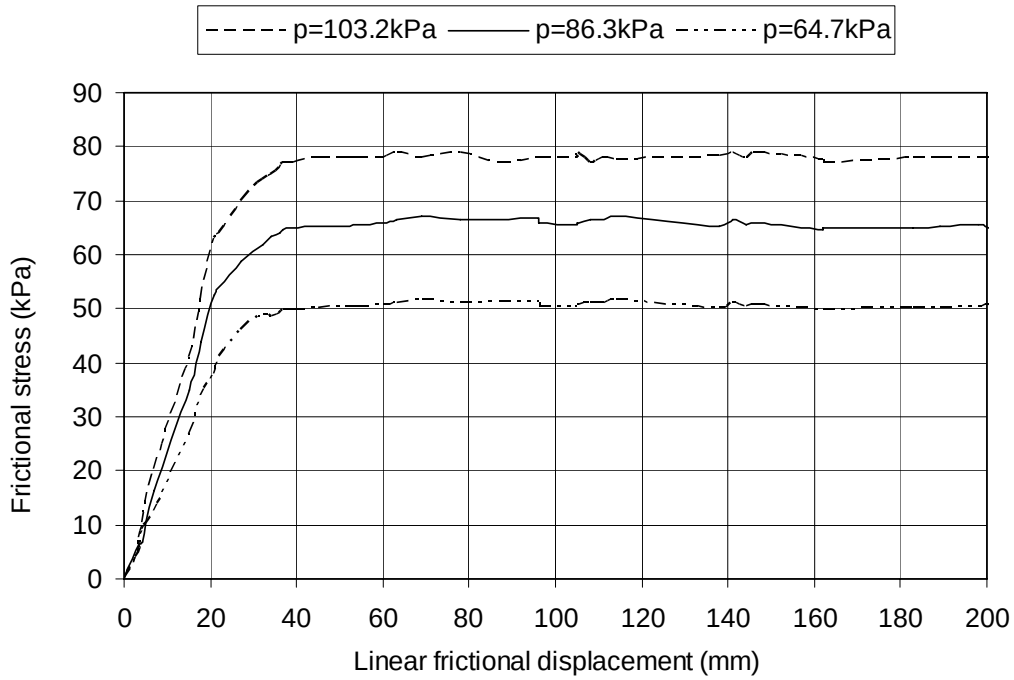

Figure 6.7. Friction curves for rubber-soil friction test (Soil type: sandy loam. Soil water content=13.3%).

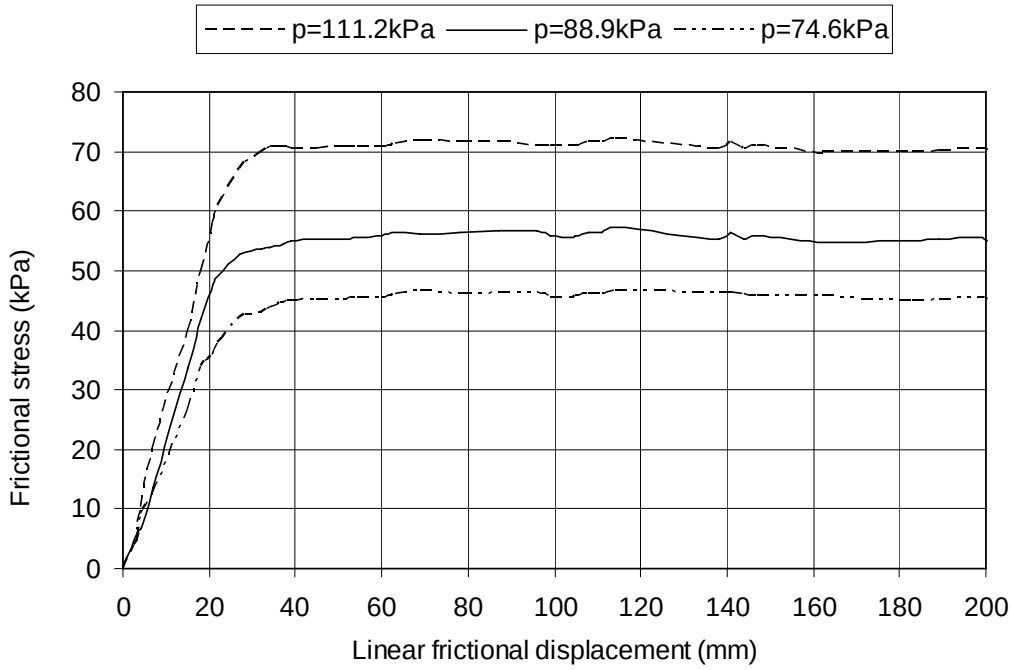

Figure 6.8. Friction curves for rubber-soil friction test (Soil type: sandy loam. Soil water content=21%).

For in situ test field measurements, ten frictional tests were conducted for each soil condition. The test results were then chosen to be analyzed by applying equation (4.2). The final results are shown in Table 6.4.

Table 6.4. Soil-rubber frictional characteristics from the tests.

Field No	Soil water content, dry basis (%)	Rubber-terrain adhesion c_a, (kPa)	Angle of rubber-terrain friction δ, (degree)	Frictional deformation modulus K, (mm)
1	7.8	1.89	33	28.5
2	13.3	2.96	36	28.8
3	21	2.49	32	27.8

The results as shown in Table 6.14 proved that the rubber-soil adhesion was much smaller than the soil-soil cohesion, whilst the angle of rubber-soil friction was very similar to the angle of soil internal friction. This tendency corresponds with data as reported by Neal (1966).

6.3 DRAWBAR PULL TESTS AND DATA COLLECTION

Full scale drawbar pull tests were conducted in the field to verify the traction models. During the drawbar pull tests, the parameters related to the distribution of the contact pressure and tangential stress per track element were also measured by the extended octagonal ring transducers. All the drawbar pull tests were conducted at relatively low speed ranges.

At the commencement of each test run, the tested tractor with the track and the loading tractor or tractors behind were properly leveled in both lateral and longitudinal directions to ensure the correct recording of the drawbar pull. The tow bar for the drawbar load was adjusted to be parallel to the ground surface. All the

instrumentation was also finally checked or calibrated if necessary for correct function. The sampling frequency for recording the data was set at 60 samples per second, based on the previous field experience and the comprehensive consideration for system response and the real time accuracy of data recording. This resulted in ten recorded samples per second for each signal channel.

Before the data was recorded, the travel speeds of the tested crawler and the loading tractor or tractors behind were steadily adjusted whilst the parameters to be measured were observed by computer monitoring in the tractor cab. As soon as the observed values of the speeds or slip and the drawbar load reached desired values, data recording was triggered for all channels. Each test run was carried out applying the same procedure.

The recording time for each test run lasted ten seconds. The test for each set of the slip and the drawbar pull values was carried out until at least six seconds of smooth and steady readings were obtained and was then repeated three times. These readings recorded for six seconds were accepted as effective readings recorded and used for further processing and final analysis. The whole test was repeated three times.

CHAPTER VII

RESULTS, ANALYSIS AND MODEL VALIDATION

7.1 INTRODUCTION

Several theoretical models, as described in Chapter 4, were considered and field experiments undertaken (Chapters 5 and 6). In this Chapter, the results of the theoretical modelling and the field experiments will be discussed and the models validated. The findings will be analyzed.

7.2 THE DISTRIBUTION OF CONTACT PRESSURE

The analysis by several researchers (Wills, 1963; Wong, 1993) proved that the contact pressure distribution affects the development of tractive effort. For both wheels and tracks the prediction of the contact pressure distribution is of vital importance in analytical traction modelling.

By applying the equations and procedures as discussed in Chapter 4, the distribution of the ground contact pressure can be predicted.

The sinkage of any point at the contact surface was determined by the assumed configuration of the track deformation as shown in Figure 4.2 (p 4-8) for the idealized distribution and Figure 4.4 (p 4-13) for the flexible deformation. By using the Bekker's sinkage equation [equation (2.1), p 2-5], the sinkage was calculated by equations (7.2) and (7.3) on page 4-14 for front and rear wheels respectively in the flexible model. Then the equation (2.1) was used to calculate the pressure at any point from sinkage and the related soil sinkage parameters. Therefore the distribution of the contact pressure below the track was predicted.

For hard surface, because it was impossible to measure and apply the relationship of sinkage and contact pressure, the distribution of contact pressure and also the distribution of tangential friction stress were not predicted.

The comparison between the measured contact pressure distribution and the predicted values, based on the flexible track model, will be discussed.

7.2.1 The contact pressure distribution and frictional stress on a hard surface

For the calculation of the actual rolling radius of the track, a test run on a concrete surface without drawbar load was undertaken. During this test, the contact pressure and the horizontal force on the track element were measured. Figure 7.1 shows the curves for the measured contact pressure distribution as well as the frictional stress.

From the figure, it is clear that the contact pressure distribution for a hard surface varies considerably over the longitudinal span of the track. However, the measured results also proved that the contact pressure distribution for the prototype track differs from the load distribution pattern for the case of wheel tractors. The section of the track only in contact with the road surface carries part of the vertical load. In this regard, the prototype track changes the pattern of contact pressure distribution by reducing the peak values of the pressure below both the front and the rear ends of the track.

By summation of the horizontal force components for each track element at zero drawbar pull, the total rolling resistance for one track was obtained as 8.0 kN. Therefore, the total rolling resistance on concrete road, when the tractor was self-propelled, was 16.1 kN for two tracks. On the other hand, with the free rolling tractor in neutral was pulled by another tractor, the pulling force was measured as 9.5 kN. Therefore the motion resistance on concrete surface was accepted as 12.8 kN which was the average of the above two rolling resistance values.

Based on the measured curves of the contact pressure distribution as shown in Figure 7.1, it is seen that the expected soil entry effect for a soft terrain surface did not occur in the case of driving on the hard surface. It was expected that the peak values of the contact pressure would have occurred below the centres of the front and the rear axles. However, the peak value of the contact pressure for the front axle was slightly behind the axle centre of the front wheels, probably due to lack of the entry effect.

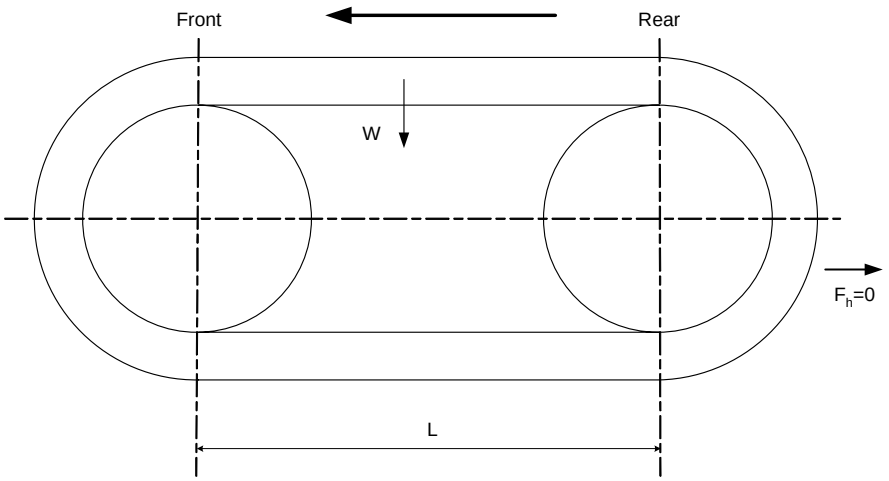

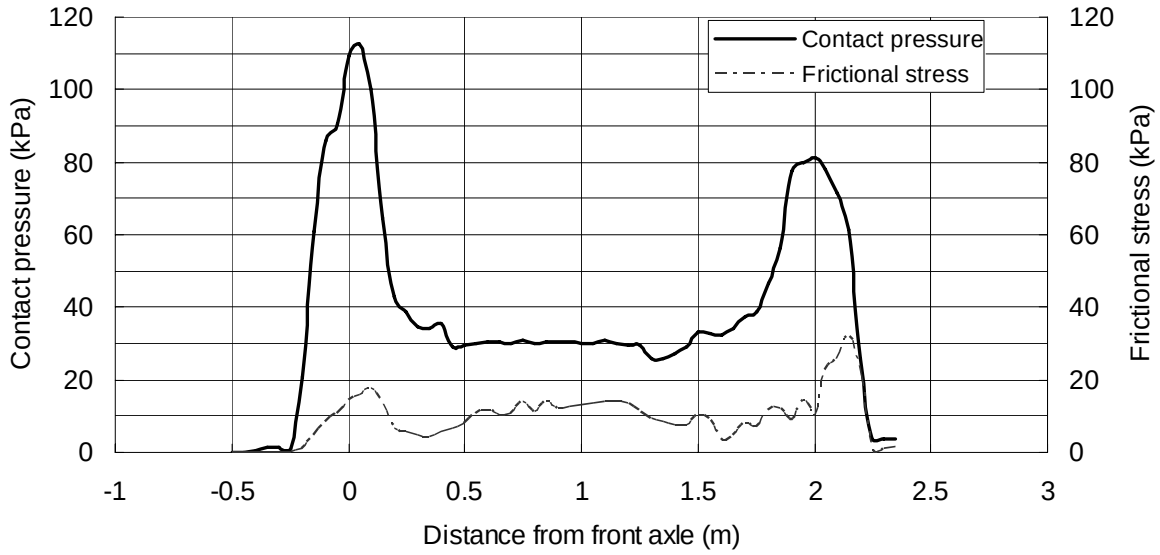

Figure 7.1. The measured distribution of contact pressure and frictional stress on concrete surface (drawbar pull=0).

7.2.2 The effect of the ground wheels on the pressure distribution and frictional stress for a hard surface

The measured contact pressure distribution and frictional stress on a concrete surface, with the centre wheels pushed down onto the track and thus road, is shown in Figure 7.2.

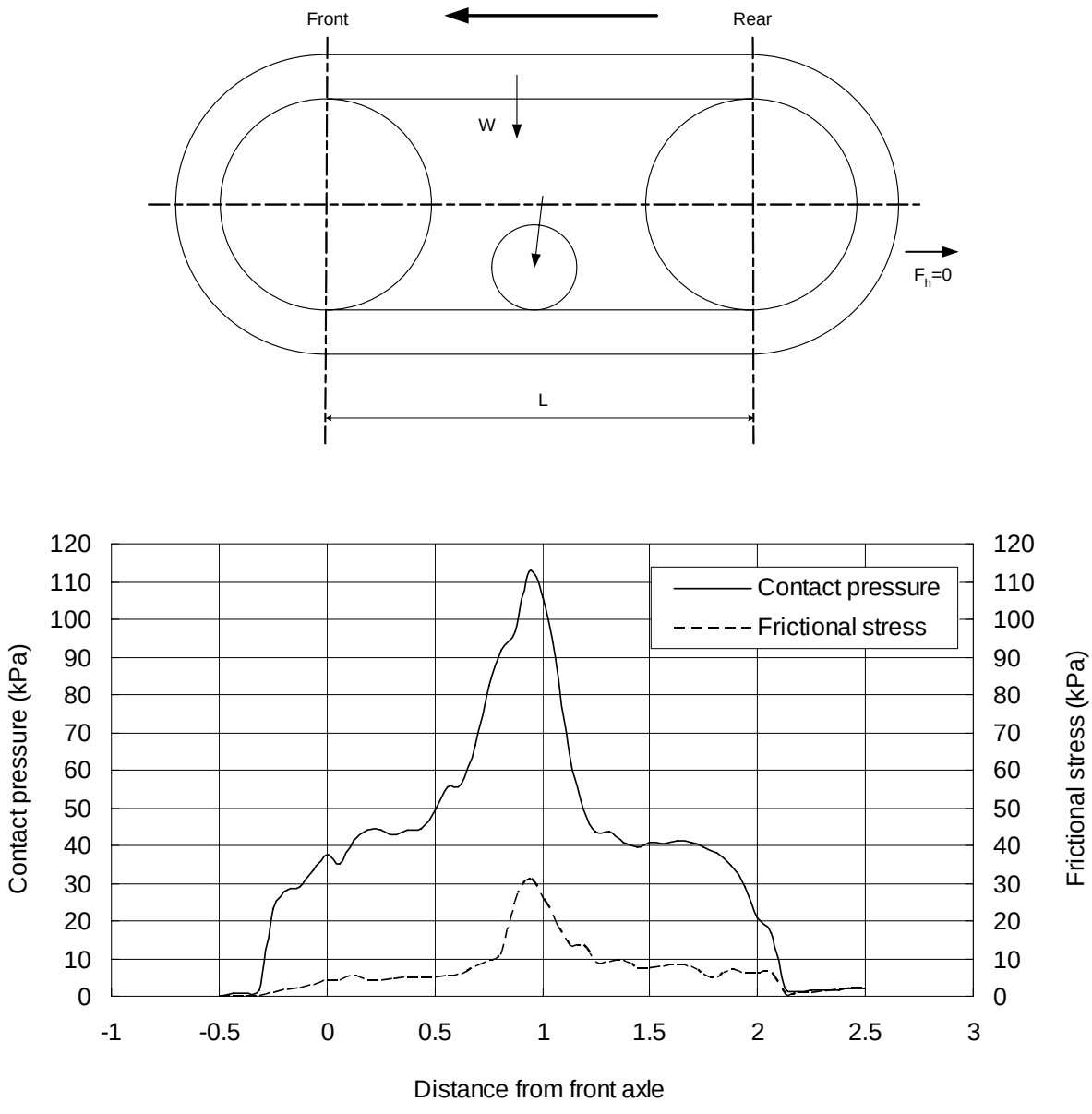

Figure 7.2. The measured contact pressure distribution and frictional stress on a concrete surface when the ground wheels in the middle of the track were pushed down (drawbar pull = 0).

As described in the previous Chapters, the originally planned function of the centre ground wheels were to reduce steering resistance, the skidding effect and soil surface damage which occurred for the traditional steel track design when the tractor was steered. It proved that the middle wheels carried a large portion of the vertical load and a high peak value of contact pressure appeared directly below the loading point of the middle wheels.

For the load wheels forced down, the rolling resistance for the tractor was measured as 15.9 kN, based on the summation of the horizontal force components. It therefore depicted a slightly reduced value when compared to the case when the middle wheels were not used.

During the field test, the operator tried to control the load on the middle wheels within a moderate range in order to obtain a more uniform contact pressure distribution. However, with the manual control, it was rather difficult to keep the pressure at a desired level.

A hydraulic close loop control system could be considered for future improved pressure control. The hydraulic pressure could be used as feedback signal.

7.2.3 The contact pressure distribution and frictional stress on a soft surface with zero drawbar pull

The established model could be used to predict the contact pressure distribution on soft terrain surface after the relevant soil characteristics based on the bevameter technique were obtained. Figure 7.3 shows the predicted distribution of the contact pressure and frictional stress as well as the measured contact pressure and frictional stress.

Equations (4.19) and (4.20) on page 4-14 were applied to calculate the sinkage for front and rear wheels respectively. Then the contact pressure at any point below the

track was calculated by the pressure-sinkage relationship as expressed by equation (2.1) (p 2-5) after the sinkage of any point at the contact surface was determined by the assumed profile configuration of the track deformation as shown in Figure 4.4 (p 4-13). The distribution of the contact pressure below the track was therefore predicted.

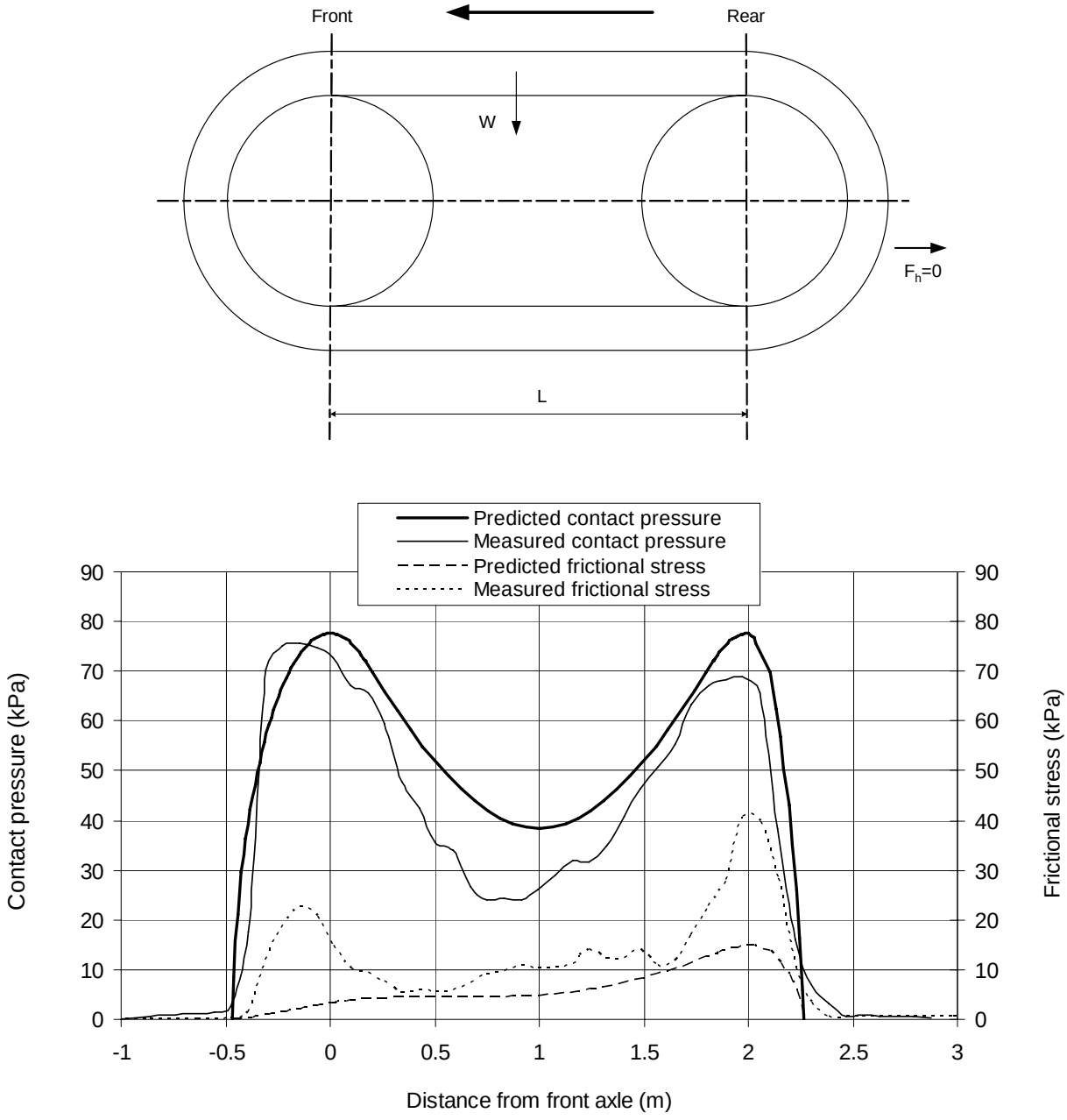

Figure 7.3. The measured and predicted contact pressure distribution and frictional stress on a soft soil surface (drawbar pull = 0, sandy loam soil, soil water content 7.8%).

The tangential stress at any point at the contact surface was calculated by equation (4.2) (p 4-4) after the soil frictional parameters were obtained and the contact pressure determined. The distribution of the tangential stress was predicted.

Based on the measured data the peak value of the contact pressure for the front axle was larger than the value for the rear axle, due to the fact that the centre of gravity of the tractor was longitudinally located in front of the track centre point. When the drawbar pull was zero, the resultant vertical force to support the tractor weight was also located in the same vertical plane running through the centre of gravity. However, for modelling, it was assumed that the front and the rear axles carried equal vertical load before the weight transfer reaches a specified transient level. Based on the model, the peak values of the contact pressure on the front and the rear wheels were therefore predicted as being equal.

The rolling resistance in this case, was measured as 22.8 kN by summing the horizontal force components on the individual track elements. According to the model, the predicted motion resistance based on sinkage was calculated as 9.5 kN which was much lower than the measured value. The contribution probably by internal friction and hysteresis losses was therefore higher than the losses caused by soil compaction and sinkage.

7.2.4 The effect of the ground wheels on the contact pressure distribution and frictional stress for a soft surface

When the ground wheels on the middle of the track were forced down for a soft terrain surface, the measured values of contact pressure distribution and frictional stress is shown in Figure 7.4. The result shows that the contact pressure distribution was more uniform than for a hard terrain surface (Figure 7.2), which proves a possible application for the ground wheels. However, beneath the ground wheels, the contact pressure was still very concentrated, probably due to the fact that the diameter of the ground wheels were relatively small when compared to that of the

drive and the tension wheels. The results, as shown in Figure 7.3 were collected for the tractor with zero drawbar pull.

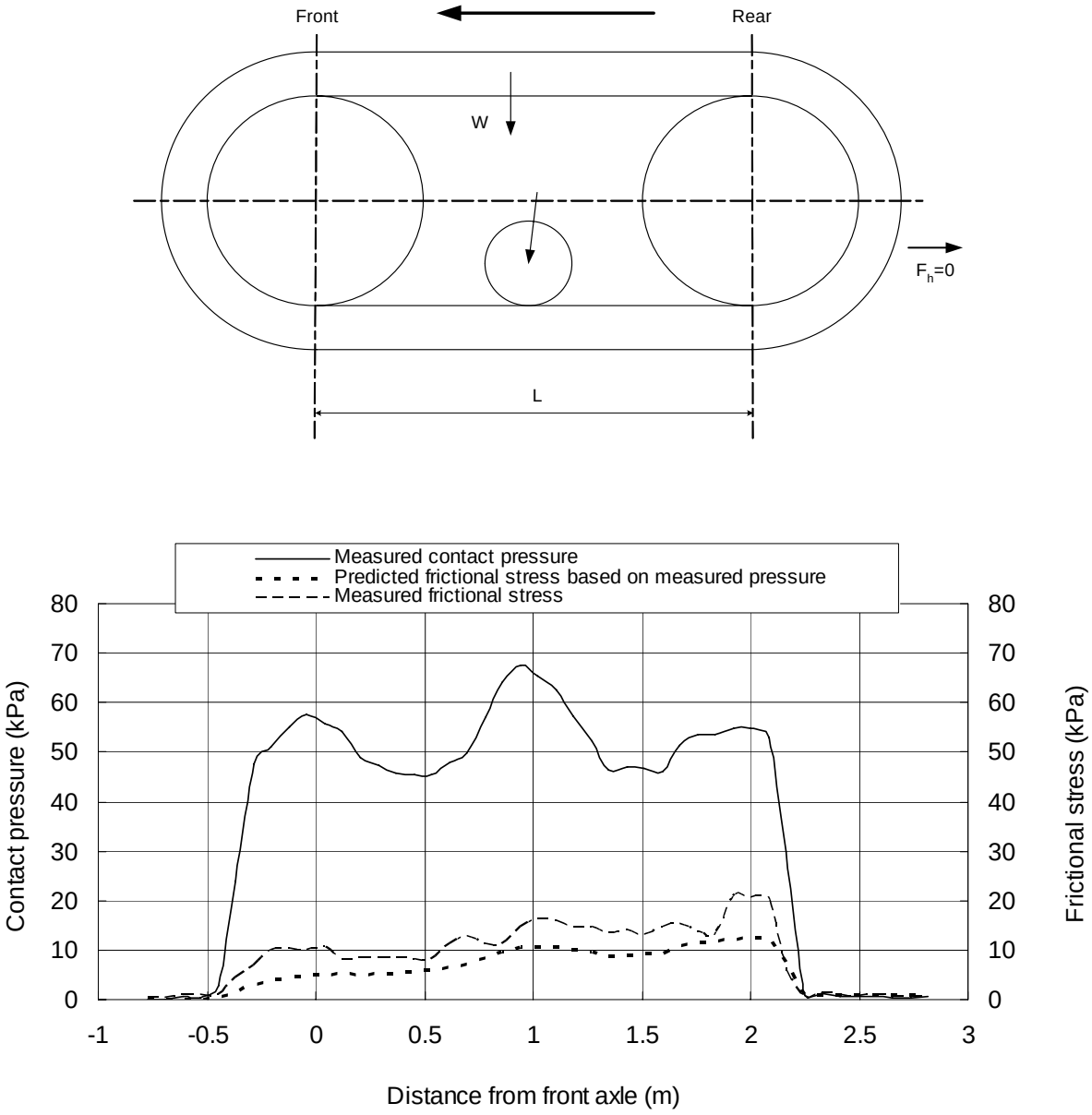

Figure 7.4. The measured contact pressure distribution and frictional stress on soft soil surface when the ground wheels in the middle of the track were pushed down (drawbar pull = 0, sandy loam soil, soil water content 7.8%).

The values for the frictional stresses are very small and mainly represent the thrust to overcome the rolling resistance on the soft terrain surface. However, it was possible to either lift or fully load the centre wheels. However, it again was difficult to achieve a uniform contact pressure below the track during tests by keeping the centre wheel load at a steady level.

Unfortunately, the flexible track model was established to be applicable only under normal operational conditions when the centre ground wheels were lifted. Therefore the predicted contact pressure distribution was not available in this case.

By summation of the measured horizontal force components, a motion resistance of 24.8 kN was obtained which was comparable to the value of 22.8 kN when the centre wheels were not utilized.

7.2.5 The influence of the soil water content and the drawbar pull on the contact pressure distribution

As described in the previous two Chapters, the contact pressure at each point underneath the track was directly related to sinkage, as influenced by the three contact pressure-sinkage parameters, i.e. k_c, k_ϕ, and n obtained from the pressure-sinkage tests. However, the soil water content had an influence on the pressure-sinkage parameters. Typical results from both modelling and experimental measurement of contact pressure and frictional stresses are shown in Figures 7.5 to 7.7. The value of the predicted frictional stresses was calculated by equation (4.2) (p 4-4) based on the predicted contact pressure and the relative slip for the specific point below the track elements. As the slip from front to the rear increased proportionally to the contact distance from the front contact point of the track, the predicted frictional stress and thus friction force on the track element increased at the position closer to the rear.

As shown in the Figures, the predicted contact pressure distribution for soil water content values of 7.8% and 13.3% are very similar in pattern and in peak values.

However, the pressure distribution values for a soil water content of 21% differs from the other two in terms of higher maximum peak contact pressure values (98 kPa vs 78kPa).

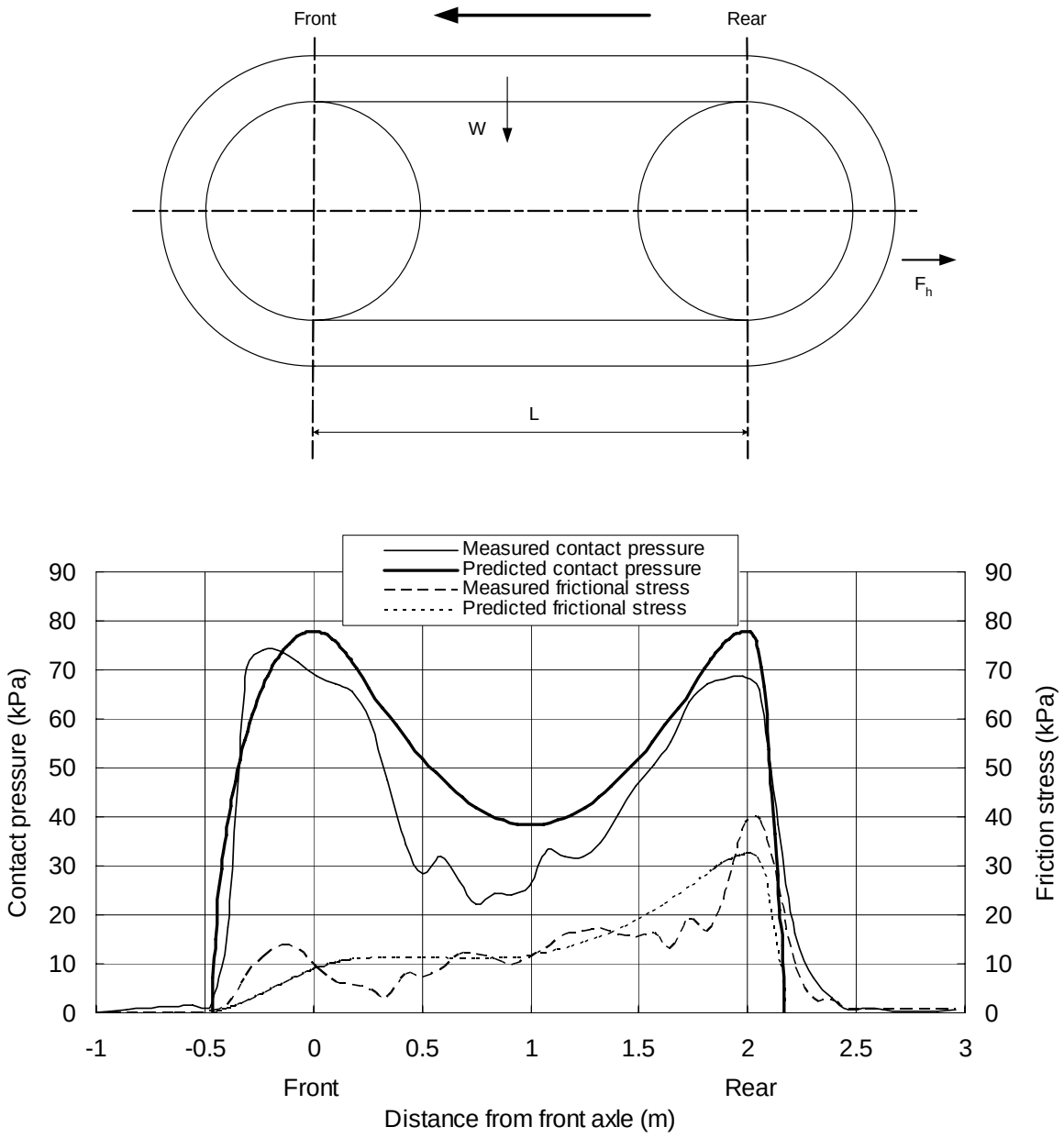

Figure 7.5. The contact pressure and frictional stress distribution for a soil water content of 7.8% (slip=7.2%, drawbar pull=38.7kN, sandy loam soil).

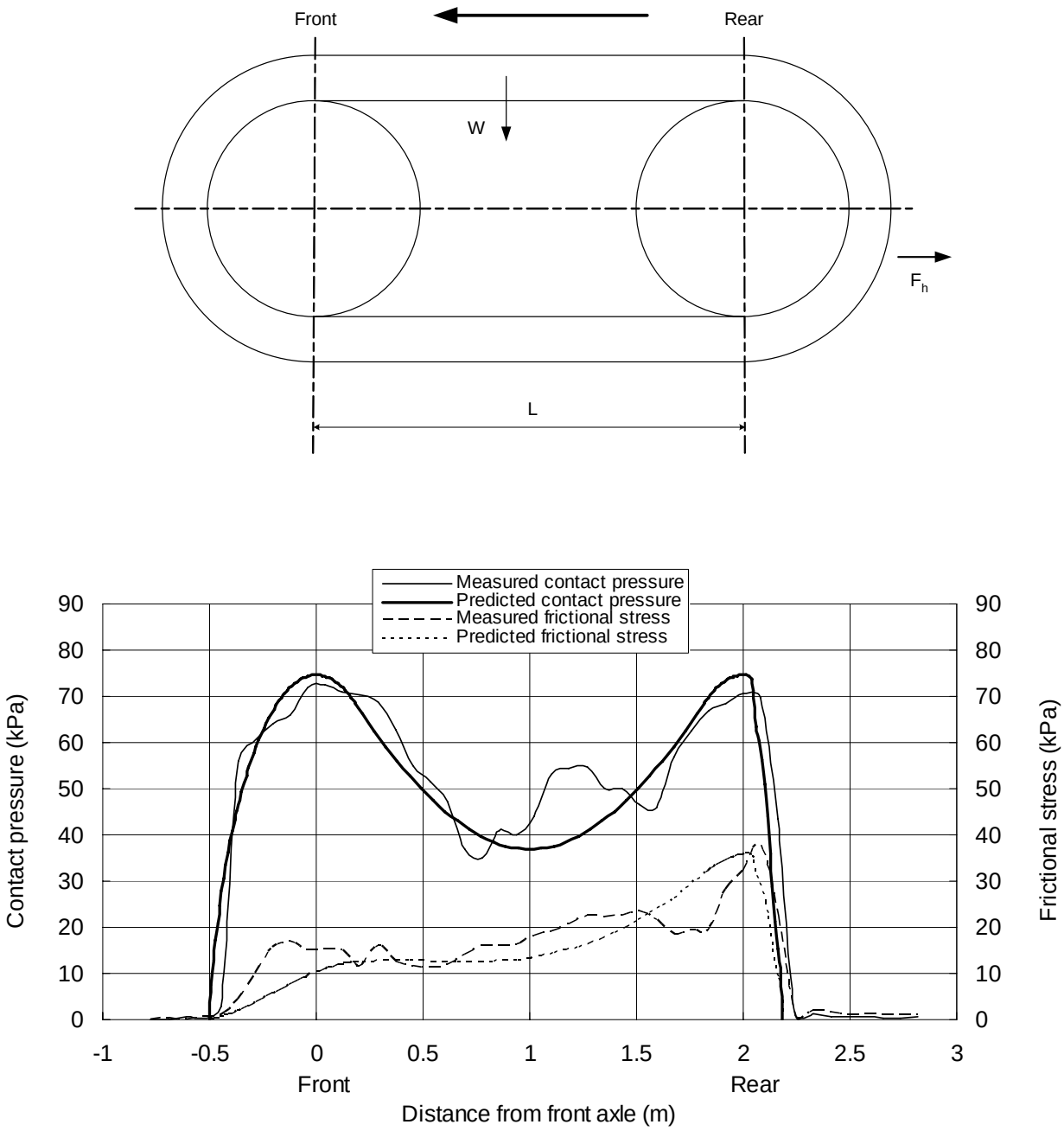

Figure 7.6. The contact pressure and frictional stress distribution for soil water content of 13.3% (slip=7.4%, drawbar pull=41.1kN, sandy loam soil).

As the total tractor mass remained the same during the test, the re-distribution of the contact pressure resulted from weight transfer was caused by different values of drawbar pull. The total vertical load, on the other hand, was kept unchanged. Under these conditions, the predicted and measured contact pressure distribution for a soil

water content value of 21% was less uniform than for the other two soil water content values in terms of the ratios of the minimum contact pressure at the centre of the track to the peak values at both the front and rear wheels.

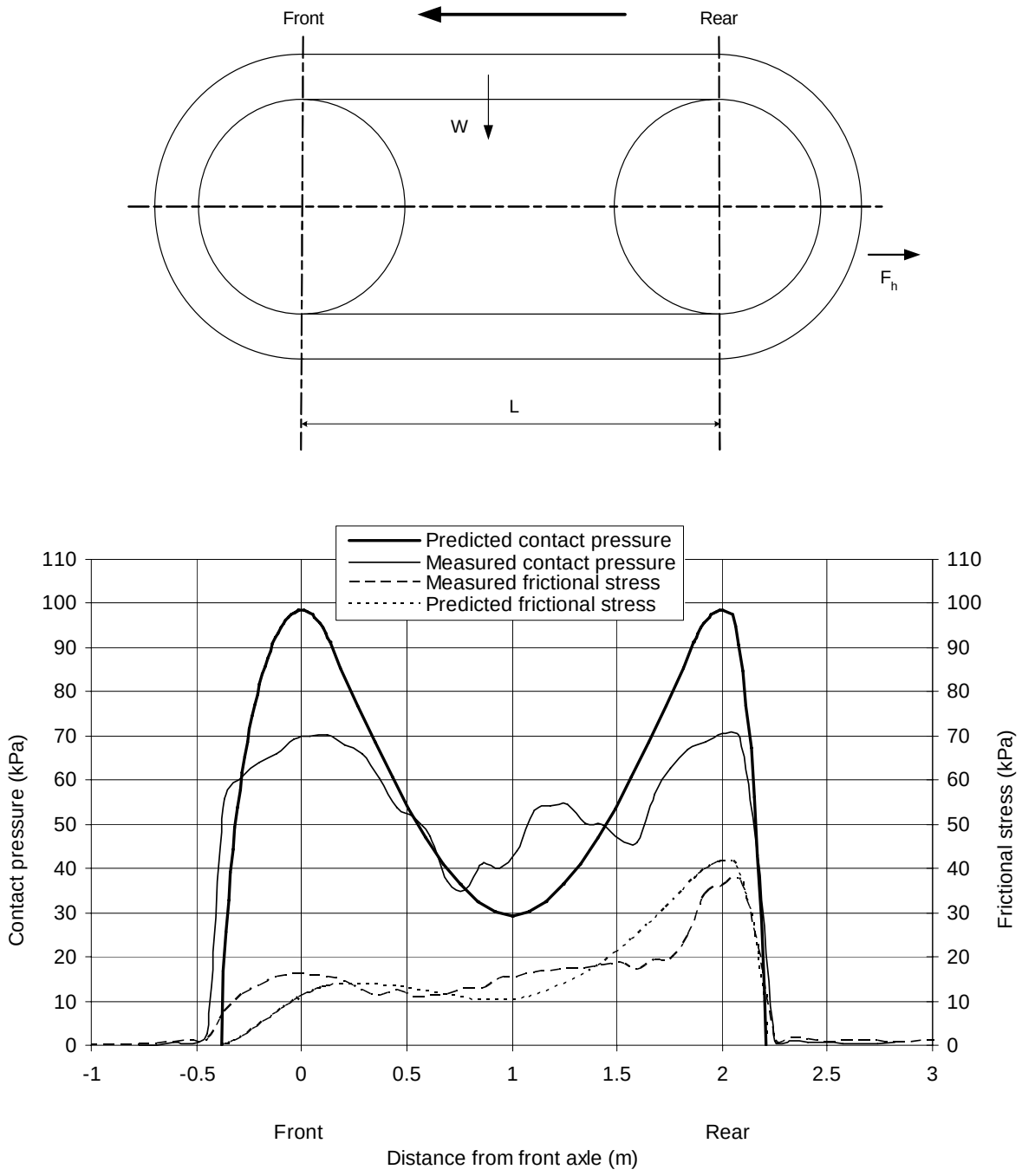

Figure 7.7. The contact pressure and frictional stress distribution for soil water content of 21% (slip=10.4%, drawbar pull=34.9kN, sandy loam soil).

The trend for the curves based on the predicted results in all cases corresponds well with the measured results.

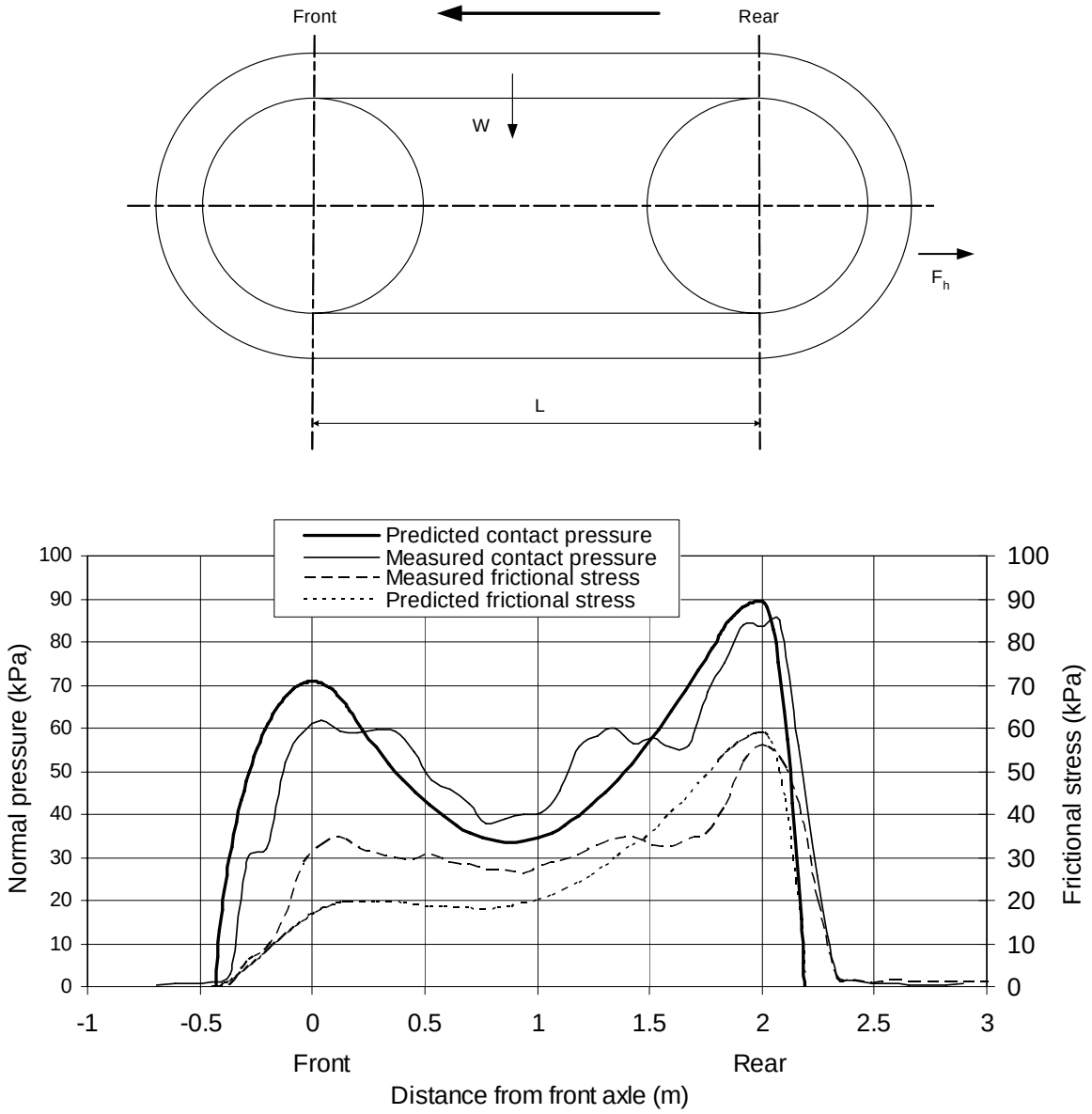

Figure 7.8. The contact pressure and frictional stress distribution for soil water content of 13.3% (slip=12.0%, drawbar pull=57.6kN, sandy loam soil).

Based on the flexible track model, for a drawbar pull of less than a specified value, i.e. 53 kN, the front and the rear wheels had the same contact pressure, thus sinkage values were also similar to the ones as shown in Figure 7.5 through 7.7. When the

drawbar pull was larger than 53 kN, the rear wheels would carry a larger vertical load and thus more sinkage would occur, caused by weight transfer (Figure 7.8). This would be followed by a change in chassis tilt angle.

From Figures 7.5 to 7.8, it can be seen that the flexible track model predicts the contact pressure distribution well for the soil water contents of 7.8% and 13.3%. However, larger differences occur between the maximum and the minimum peak values for the predicted and measured values for a soil water content of 21% (Figure 7.8). The predicted values are still in close correspondence to the measured values for all cases.

It happened during the tests that the soil was very wet for the condition with soil water content 21%. The extreme soil condition possibly caused an extra error for the prediction. The sinkage values for the front and rear wheels of the track were considerably larger than for other soil conditions as observed. The predictions are probably more accurate for soil conditions with low to moderate soil water content values.

7.3 THE RELATIONSHIPS OF TRACTION COEFFICIENT AND TOTAL SLIP

Based on the equations as shown in Chapter 4, the relationship of traction coefficient and slip are shown in Figures 7.9 to 7.10. For comparison purposes, the results for other simplified prediction models are also included in the figures.

In the Figures 7.9 to 7.11, the tractive effort for a specific level of slip was calculated by equations (4.11) (p 4-10) for the idealized distribution model and (4.23) (p 4-16) for the flexible track model when the tangential displacement was related to the slip. The motion resistance was calculated by equation (4.12) (p 4-10) for the idealized distribution model and equations (4.30) (p 4-18) and (4.31) (p 4-19) for the flexible

track model. The coefficients of traction were calculated on the base as defined by equation (4.34) (p 4-22) in Chapter 4.

For the traction coefficients, in all three cases as can be seen from the figures, the results for the uniform distribution model are all over-predicted whilst the results for the flexible model are closer to the measured values. The difference between the predicted and the measured results are probably due to the internal track friction losses. The difference between the coefficients based on the measured torque and rolling radius and the summation of measured tangential stresses also shows a minor influence of some factors which need to be further investigated. Generally speaking, better predicted results were obtained with the flexible model than the uniform contact pressure model.

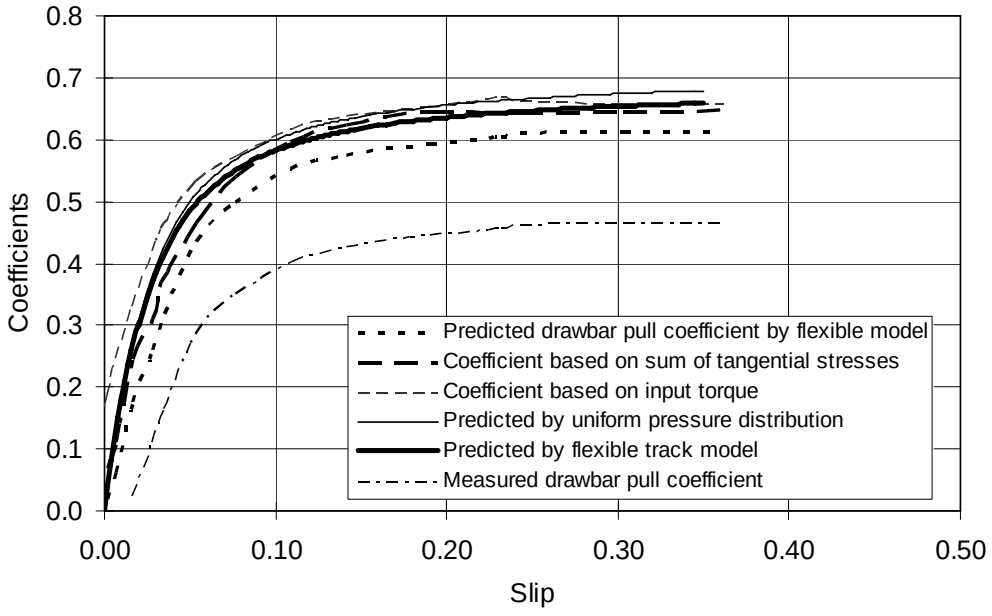

Figure 7.9. The relationship of traction coefficients and drawbar coefficient versus slip for a soil water content of 7.8% (sandy loam soil).

For the drawbar pull coefficient, a large difference exists between the measured drawbar results and the predicted results when the motion resistance is taken into account. It is proved that the internal resistance for such a track is much higher than

the value predicted by conventional modelling methods and needs to be specially investigated.

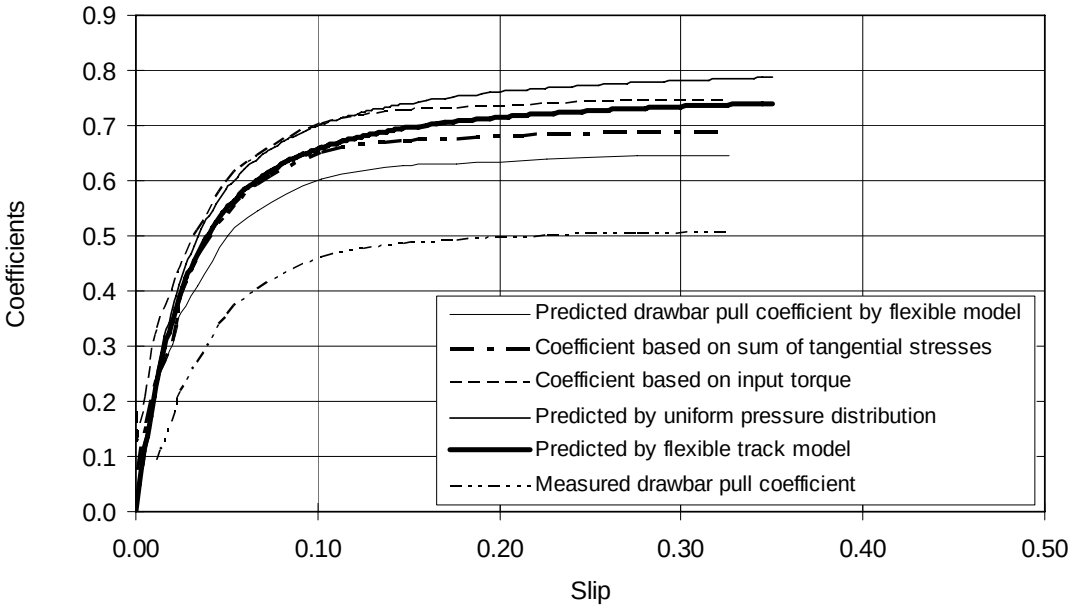

Figure 7.10. The relationship of traction coefficient and drawbar coefficient versus slip for a soil water content of 13.3% (sandy loam soil).

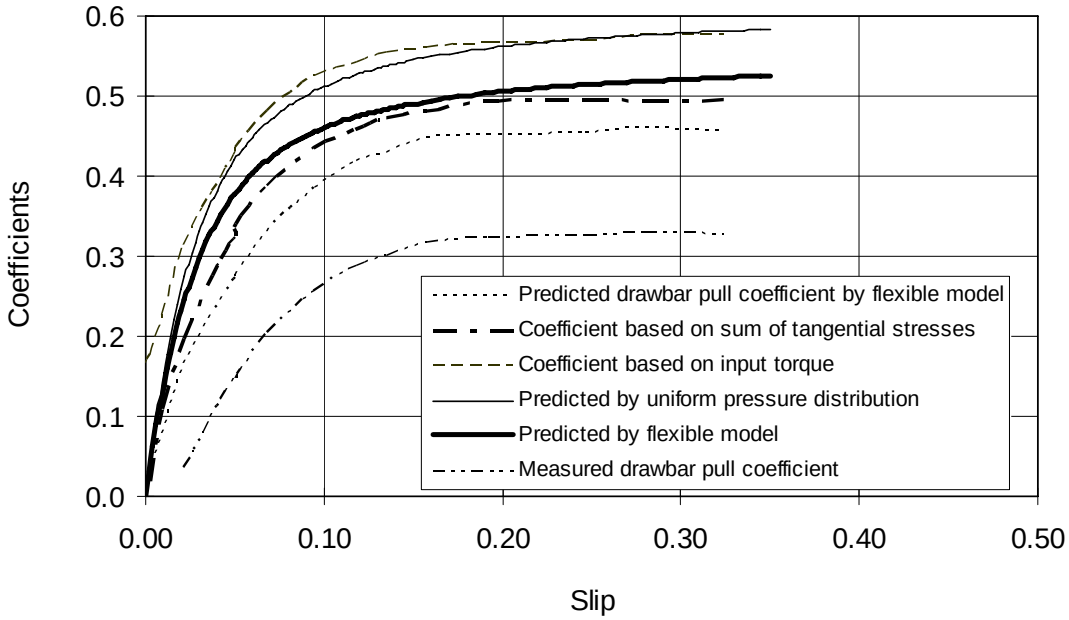

Figure 7.11. The relationship of traction coefficient and drawbar coefficient versus slip for a soil water content of 21% (Sandy loam soil).

It is noticeable that under all three values of soil water content, the predicted results for the model based on the constant contact pressure distribution is closer to the measured results based on the shaft torque, whilst the predicted results for the flexible track model is much closer to the results measured on the base of the summation of tangential stresses.

The results for drawbar pull tests are shown in Appendix A.

From the Figures 7.9 to 7.11, it can be seen that the traction performance is the best for the soil water content of 13.3% whilst it is worst for the 21% soil water content. It is indicated that the soil water content plays an important role influencing the traction performance for the soil with all other conditions unchanged.

For three different soil water content values, the drawbar performance characteristics have different maxima. However, the curves generally exhibit an increase in the traction coefficient with the slip and then approached a constant maximum value for a further increase in slip. This is in accordance with the measured frictional characteristics between the rubber track element and soil.

7.4 THE TRACTIVE EFFICIENCY

As discussed in Chapter 5, the arrangement of strain gauges on the side shaft and the velocity sensors enabled the researcher not only to measure the speeds and to calculate the slip, but also to measure the input torque to the track. It is hence possible to calculate the tractive efficiency η by applying the following equation:

$$\eta = \frac{F_h \times V}{2T\omega} \tag{7.1}$$

where

F_h = drawbar pull, (N).

V = travel speed, (m/s).

T = torque measured on one side shaft, (Nm).

ω = the angular velocity of the shaft, (rad/s).

The tractive efficiencies obtained from the measured test results are shown in Figure 7.12 for all three values of soil water content. For comparison reasons, the predicted tractive efficiencies based on the measured travel speeds are also shown in the figure.

The values of the maximum tractive efficiency obtained under three soil conditions are shown in Table 7.1. The tractive efficiency of the experimental track for low drawbar pull is very low as can be seen from the figure. This is different from the conventional wheeled tractors with a high tractive efficiency for low drawbar pull values. The tendency was probably caused by much higher internal track losses even at low values of drawbar pull.

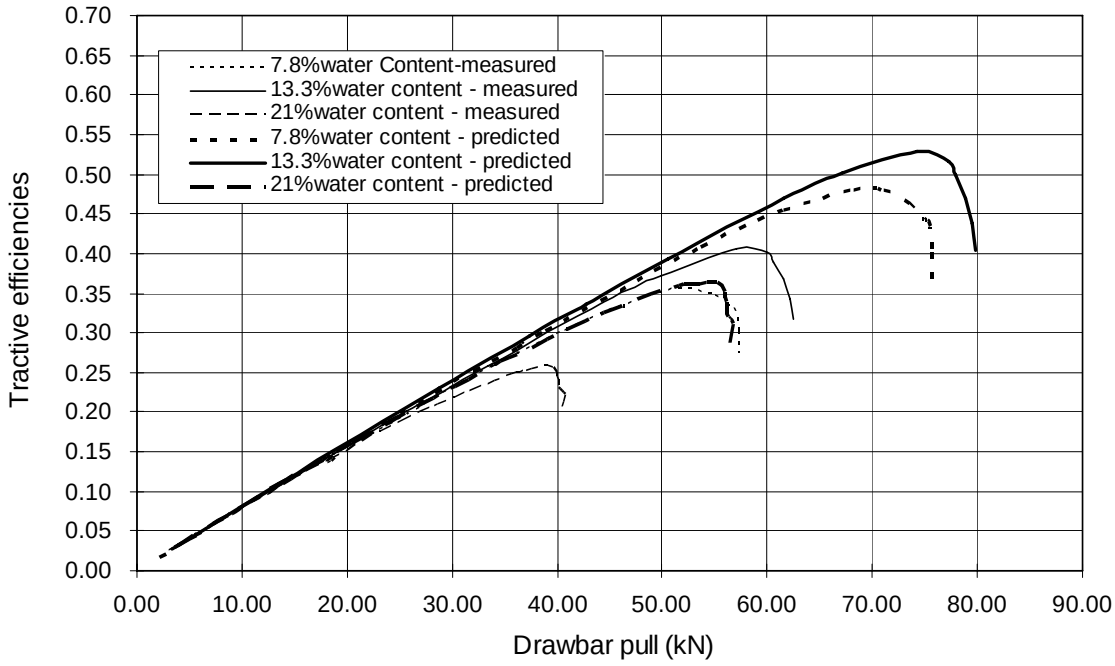

Figure 7.12. Tractive efficiencies from the experimental tests.

Table 7.1. The maximum tractive efficiency.

Soil water content (dry base, %)	7.8	13.3	21
Measured maximum tractive efficiency (%)	35.6	41.8	26.2
Predicted maximum tractive efficiency (%)	48.1	52.8	36.3

7.5 ANALYSIS OF THE FACTORS AFFECTING THE TRACTIVE PERFORMANCE

7.5.1 Soil water content

Under moderate values of soil water content, the tractive performance is the best as shown in the figures and the table. This is probably due to the fact that for a specific soil water content, the combined effect of the rubber-soil friction and adhesion reaches an optimum value when compared to other conditions when the soil is either too dry or too wet. The predicted and the measured results also corresponded well.

7.5.2 Track tension

Track tension is also a very important factor for the frictional drive traction system as it is for a conventional flat belt drive system, especially at high values of drawbar pull. In the preliminary tests, when the track tension was not set to a sufficiently high value, the track did not depict the walking beam effect and excessive slip occurred between the track and the drive wheels at relatively low drawbar pull values. After the track tension was corrected, the friction loss was reduced and the drawbar pull increased.

7.5.3 Motion resistance and internal friction losses

The measured and predicted values of the motion resistances for three soil conditions at different soil water content values are shown in Table 7.2. As can be seen, the predicted and the measured motion resistance values depict large differences probably caused by the internal frictional losses and the friction between the track elements.

Table 7.2. Measured and predicted motion resistances.

Soil type	Soil water content, %, dry basis	Predicted external motion resistance, kN	Measured motion resistance, kN
1	7.8	9.5	22.8
2	13.3	11.7	21.6
3	21	12.6	23.2
4	0, concrete surface	-	12.8

The attention must be drawn to the fact that the measured motion resistance was based on the input torque to the drive shaft and the predicted value by summation of the horizontal force components below the track when the drawbar pull was zero. It is proved that the internal resistance for all conditions was considerably higher than expected.

CHAPTER VIII

SUMMARY, CONCLUSIONS AND RECOMMENDATIONS

8.1 SUMMARY

From the literature and the validation of the field tests and modelling undertaken in this research, it was possible to develop an analytical model to predict the drawbar performance for the prototype track based on the principles pioneered by Bekker and other researchers. The proposed flexible track model was able to predict the contact pressure distribution for a soft soil surface and therefore, also the frictional stress and thrust force contributed by each track element.

Further more, the measurement and instrumentation system that was developed was able to record the required soil parameters for the development of the analytical model. Particularly, the rubber-soil friction was characterized by using a standard track element and steel sinkage test plates.

Two force transducers were specially designed and built based on the theory of the extended octagonal ring, to successfully measure the distribution of the contact pressure and the friction-shear stress and thus the frictional force per track element.

A series of full-scale drawbar pull tests were conducted in the fields and the relationships of traction and drawbar performance with total slippage under various soil conditions were obtained.

The computerized data acquisition system was used to record all the in situ test results for the soil characterization and the full-scale drawbar tests.

Through the modelling and the measurement, some design features of the prototype traction system and the soil parameters were evaluated for their influence on the

tractive performance. These factors such as the frictional drive principle, the track tension, the centre ground wheels and the soil water content played important roles for the development of traction performance.

8.2 CONCLUSIONS

Based on the results from the field experiments and the performance prediction of the analytical traction model, the following detailed conclusions were drawn:

1. The sinkage tests and the shear and frictional tests could be performed by the instrumented test device. Related soil characteristics were obtained by applying the processing procedure as required by the bevameter technique.

2. The contact pressure as recorded for all terrain conditions still displayed typical peak values under the different wheels and the envisaged beam effect did not materialize for the prototype track.

3. Wear and friction between steel track elements might be the major reason causing the track to loose its initial bridging beam effect, resulting in an increase in contact pressure under the driving and tension wheels.

4. As peak contact pressure still occurred, it proved that for the present it is not justifiable to accept a uniform contact pressure distribution for the track as envisaged by the inventor, thus omitting road wheels.

5. The track motion resistance was recorded as unacceptably high under all test conditions, although the resistance on a concrete surface was considerably lower than on soft surfaces. This appeared to be due to internal energy loss in the track unit.

6. For the two models tested for predicting drawbar pull, i.e. a constant contact pressure model, changing to trapezoidal and a flexible track model, with typically undeformable truck wheels at the front and rear end and a circular

deflecting track section in between, the former proofed to be more idealized and the later more practical.

7. For the deformable track model, reasonable agreement between the measured and predicted values of contact pressure and traction force were observed for individual traction elements.

8. The traction and drawbar pull coefficients of the prototype track, based on measurements, were not as good as expected from modelling. In the criteria for drawbar pull performance, the measured values were rather unacceptably low when compared to results as reported in the other literature. This could only be attributed to substantial internal energy losses for the tracks.

9. The tractive efficiency was also unacceptably low, apparently caused by high internal friction between adjacent track elements and frictional slip between the track and the driving wheels.

10. The soil water content influenced the soil characteristics and thus also the traction performance of the tracks.

11. The research undertaken identified and confirmed a model to be used to predict contact pressure and tangential stresses for a single track element.

12. By applying two octagonal ring transducers and other necessary test apparatus and instrumentation, it was possible to measure the contact pressure and tangential force on a single track element with minimal interference which was confirmed by the predicted values.

13. Based on the proposed theoretical analysis, the tractive performance for different possible contact pressure values could be predicted.

8.3 RECOMMENDATIONS

For possible future research, the following are recommendations, based on the results from this study:

1. As the tractive performance of the tractor was not ideal as expected, it is suggested that the complete operating principle of the walking beam concept be reanalyzed and the source of the high internal losses be identified and corrected.

2. The principle of an articulated beam track, with optimum traction characteristics, was hampered by wear on the contact surfaces between adjacent track elements. However, advantages offered by the tractor drive train and steering system and the replacement of individual track elements when damaged, justifies the development and testing of some effective means to minimize friction and wear between track elements and sustain track tension and the bridging effect.

3. Alternatively other available rubber covered steel tracks, with a positive drive system, could be tested and combined with the novel steering and automatic differential lock system.

4. The flexible track model, with the specific configuration of the contact profile, was still not a universal model. To be applicable to new types of or modified future tracks, the contact profile at the interface of the track and the terrain surface may need to be observed and re-shaped.

5. Additional loading rollers or road wheels between the front and rear tension and driving wheels could be added to achieve a more uniform distribution of ground contact pressure under the tracks.

6. Based on the theoretical analysis, an optimum contact pressure distribution can be proposed.

7. A modified track system based on the theoretical analysis is to be built and tested and a modified model for tractive performance be tested.

LIST OF REFERENCES

ASAE, 1988. ASAE Standard S313.2. American Society of Agricultural Engineers, St. Joseph, MI.

Barnard, J. H., 1989. United States Patent No. 4,882,947 dated November 28, 1989. Track-laying device.

Bekker, M. G., 1956. Theory of Land Locomotion. University of Michigan Press, Ann Arbor, MI.

Bekker, M. G., 1960. Off-the-road Locomotion. University of Michigan Press, Ann Arbor, MI.

Bekker M. G., 1969. Introduction to Terrain-vehicle Systems. University of Michigan Press, Ann Arbor, MI.

Caterpillar Inc., 1995. In pursuit of the ideal tractor – development of the rubber belt tractor (ASAE distinguished lecture series, tractor design No. 20). Chicago, Illinois.

Chi, L., Tessier, S., McKyes, E. and Laguë, C., 1993. Modelling mechanical behavior of agricultural soils. Transaction of the ASAE, 36 (6), pp. 1563-1570.

Chi, L., Kushwaha, R. L. and Shen, J., 1993. An elasto-plastic constitutive model for agricultural cohesive soil. Canadian Agricultural Engineering, 35 (4), pp. 245-251.

Culshaw, D., 1988. Rubber tracks for traction. Journal of Terramechanics, 25 (1), pp. 69-80.

Dudzinksi, P. and Ketting, M., 1996. New hybrid friction/positive drive for rubber belt running gear. Proceedings of the 12th International Conference of the ISTVS, Beijing, China.

du Plessis, H.L.M., 1996. The Bi-Pole traction system-construction and performance. Proceedings of the 12th International Conference of the ISTVS, Beijing, China.

du Plessis, H. L. M. and Yu, T., 1999. The tractive performance of a prototype track based on rubber/soil friction and shear. Proceedings of the 13th International Conference of the ISTVS, pp. 217-224. München, Germany.

Dwyer, M. J., Okello, J. A. and Scarlet, A. J., 1993. Theoretical and experimental investigation of rubber tracks for agriculture. Journal of Terramechanics, 30 (4), pp. 285-298.

Evans, W. C. and Gove, D. S., 1986. Rubber belt track in agriculture. ASAE Paper No.86-1061. St. Joseph, MI 49085-9659.

Esch, J. H., Bashford, L. L., Von Bargen, K. and Ekström, R. E., 1990. Tractive performance comparisons between a rubber belt track and a four-wheel drive tractor. Transactions of the ASAE, 36 (4), pp. 1563-1570.

Freitag, D. R., 1965. A dimensional analysis of the performance of pneumatic tires on soft soils. Technical report No. 3-688, U.S. Army Engineers Waterways Experiment Station, Vicksburg, Mississippi.

Girma, G., 1989. Multicomponent dynamometer for measurement of forces on plough bodies. Journal of Agricultural Engineering Research, 42 (2), pp. 85-96.

Godwin, R. J., 1975. An extended octagonal ring transducer for use in tillage studies. Journal of Agricultural Engineering Research, 20 (4), pp. 347-352.

Green, W. G., 1955. Theory of Machines. Blackie & Son Limited, London, pp. 674-685.

Holm, C., Hefer, G. J. and Hintze, D., 1987. The influence of shape and size of a penetration body on the pressure-sinkage relationship. Proceedings of the 9th International Conference of the ISTVS. Barcelona, Spain.

Janosi, Z., Hanamoto, B., 1961. The analytical determination of drawbar pull as a function of slip, for tracked vehicles in deformable soils. Proceedings of the 1st Int. Conference Mech. Soil-Vehicle Systems. Turin, Italy.

Karafiath, L. L. and Nowatzki, E. A., 1978. Soil mechanics for off-road vehicle engineering. Trans Tech Publications, Clausthal, Germany.

Koolen, A. J. and Kuipers, H., 1983. Agricultural Soil Mechanics. Springer-Verlag, New York.

Lowen, E. G. and Cook, N. H., 1956. Metal cutting measurement and their interaction. Experimental Stress Analysis, 13 (2), pp. 57-62.

McKyes, E. and Fan, T., 1985. Multiplate penetration tests to determine soil stiffness moduli. Journal of Terramechanics, 22 (3), pp. 157-162.

McKyes, E., 1989. Agricultural Engineering Soil Mechanics (Developments in Agricultural Engineering 10). Elsevier Science Publishers B.V., Amsterdam.

Neal, M.S., 1966. Friction and adhesion between soil and rubber. Journal of Agricultural Engineering Research, 11 (2), pp. 108-112.

O'Dogherty, M. J., 1975. A dynamometer to measure the forces on a sugar beet. Journal of Agricultural Engineering Research, 20 (4), pp. 339-345.

O'Dogherty, M. J., 1996. The design of octagonal ring dynamometer. Journal of Agricultural Engineering Research, 63 (1), pp. 9-18.

Okello, J. A., 1991. A Review of soil strength measurement techniques for prediction of terrain vehicle performance. Journal of Agricultural Engineering Research, 50 (2), pp. 129-155.

Okello, J. A., 1994. Prediction and experimental validation of the field tractive performance of a rubber track unit. Journal of Agricultural Engineering Research, 59 (2), pp. 163-171.

Okello, J. A., Dwyer, M. J. and Cottrell, F. B., 1994. The tractive performance of rubber tracks and a tractor driving wheel tyre as influenced by design parameters. Journal of Agricultural Engineering Research, 59 (1), pp. 33-43.

Okello, J. A., Watany, M. and Crolla, D. A., 1998. A theoretical and experimental investigation of rubber track performance models. Journal of Agricultural Engineering Research, 69 (1), pp. 15-24.

Reece, A. R., 1965-1966. Principles of soil-vehicle mechanics. Proc. Instn. Mech. Engrs., 180, Part 2A(2), pp. 45-67.

Rula, A. A. and Nuttall, C. J., 1971. An analysis of ground mobility models (ANAMOB). Technical Report M-71-4, U.S. Army Engineer Waterways Experiment Station, Vicksburg, Mississippi.

Sela, A. D. and Ehrlich, I. R., 1972. Load support capability of flat plates of various shapes in soil. Journal of Terramechanics, 8 (3), pp. 39-70.

Shen, J. and Kushwaha, R. L., 1998. Soil-machine interactions: a finite element perspective. Marcel Dekker, New York.

Taylor, J. H. and Burt, E. C., 1973. Track and tire performance in agricultural soil. Transaction of the ASAE, Vol. 18 (1), pp. 3-7.

Terzaghi, K., 1966. Theoretical Soil Mechanics. John Wiley & Sons, New York.

Thakur, T. C. and Godwin, R. J., 1988. Design of extended octagonal ring dynamometer for rotary tillage studies. Agricultural Mechanization in Asia, Africa and Latin America, 19 (3), pp. 23-28.

Turnage, G. W., 1972. Performance of soils under tire loads; Application of test results to tire selection for off-road vehicles. Technical report No. 3-666, Report 8, U.S. Army Engineers Waterways Experiment Station, Vicksburg, Mississippi.

Turnage, G. W., 1978. A synopsis of tire design and operational considerations aimed at increasing in-soil tire drawbar performance. Proceedings of the 6th International Conference of the ISTVS, Vol. II, pp. 757-810.

Upadhyaya, S. K., Wulfsohn, D. and Mehlschau, J., 1993. An instrumented device to obtain traction related parameters. Journal of Terramechanics, 30 (1), pp. 1-20.

Upadayaya, S. K. and Wulfsohn, D., 1993. Traction prediction using soil parameters obtained with an instrumented analog device. Journal of Terramechanics, 30 (2), pp. 85-100.

Wills, B. M. D., 1963. The measurement of soil shear strength and deformation moduli and a comparison of the actual and theoretical performance of a family of rigid tracks. Journal of Agricultural Engineering Research, 8 (2), pp. 115-131.

Wismer, R. D. and Luth, H. J., 1973. Off-road traction prediction for wheeled vehicles. Journal of Terramechanics, 10 (2), pp. 49-61.

Wong, J. Y. and Reece, A. R., 1967. Prediction of rigid wheel performance based on the analysis of soil-wheel stresses – Part II. Performance of towed rigid wheels. Journal of Terramechanics, 4 (2), pp. 7-25.

Wong, J. Y., 1980. Data processing methodology in the characterization of the mechanical properties of terrain. Journal of Terramechanics, 17 (1), pp. 13-41.

Wong, J. Y., 1989. Terramechanics and off-road vehicles. Elsevier Science Publishers, B.V., Amsterdam.

Wong, J. Y., 1993. Theory of ground vehicles, 2nd Edition. John Wiley & Sons, Inc., New York.

Yong, R. N., Fattah, E. A. and Skiadas, N., 1984. Vehicle Traction Mechanics (Developments in Agricultural Engineering 3). Elsevier Science Publishers B.V., Amsterdam.

Youssef, A. F. A. and Ali, G. A., 1982. Determination of soil parameters using plate test. Journal of Terramechanics, 19 (2), pp. 129-148.

Yu, T., 1996. Measurement of soil characteristics for traction modelling under African conditions. Proceedings of the 12th International Conference of the ISTVS, Beijing, China.

Yu, T. and du Plessis, H. L. M., 1996. Extended octagonal ring transducers to measure vertical and tangential forces between a track element of the bi-pole traction system and the terrain. Agricultural Engineering in South Africa, 28 (1), pp. 32-40.

Yu, T. and du Plessis, H. L. M., 1997. Pressure distribution and frictional-shear stress under a prototype crawler track. Agricultural Engineering in South Africa, 29 (1), pp. 79-87.

APPENDIX A

DRAWBAR PULL TEST RESULTS

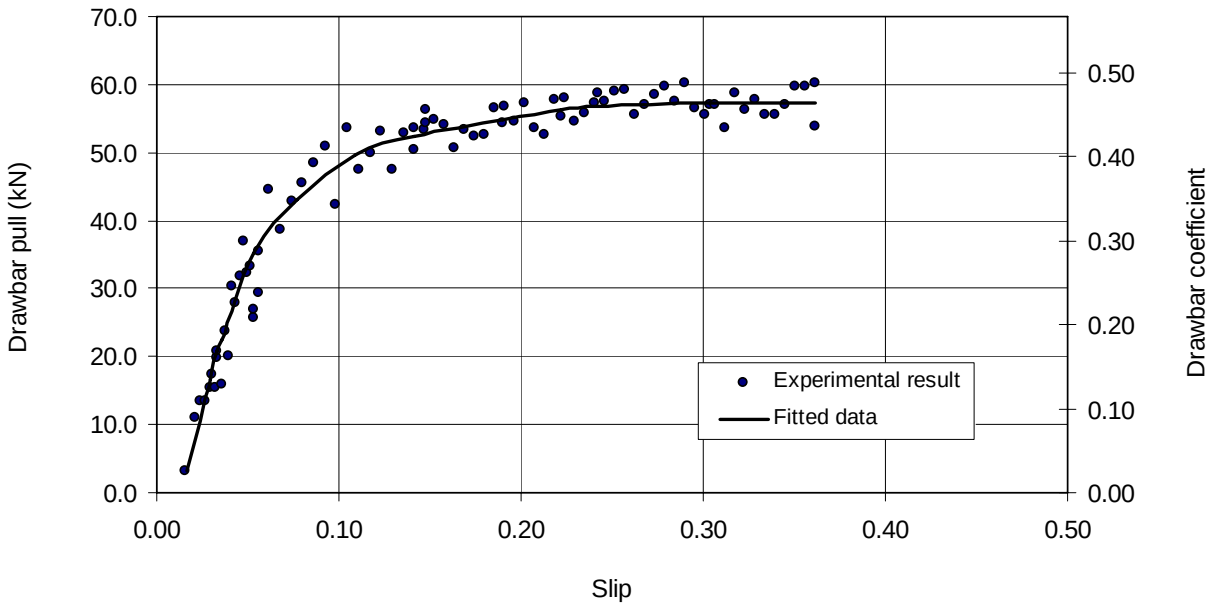

Figure A1. Drawbar pull test results for soil water content 7.8% (dry basis), sandy loam soil.

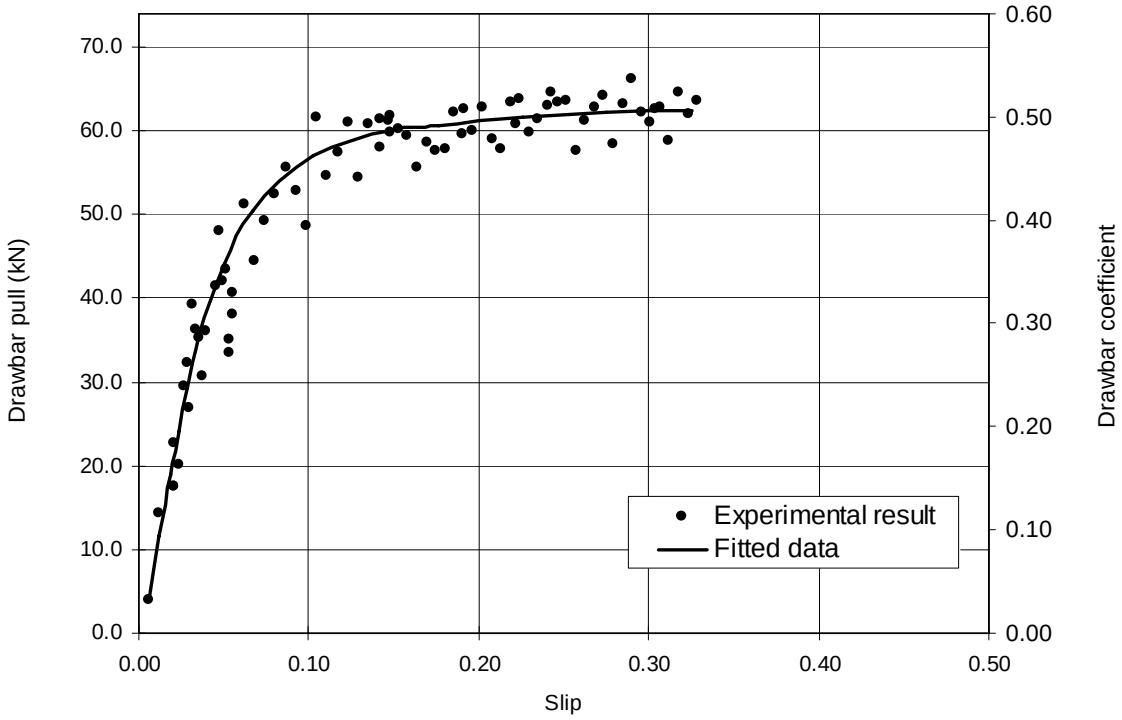

Figure A2. Drawbar pull test results for soil water content 13.3% (dry basis), sandy loam soil.

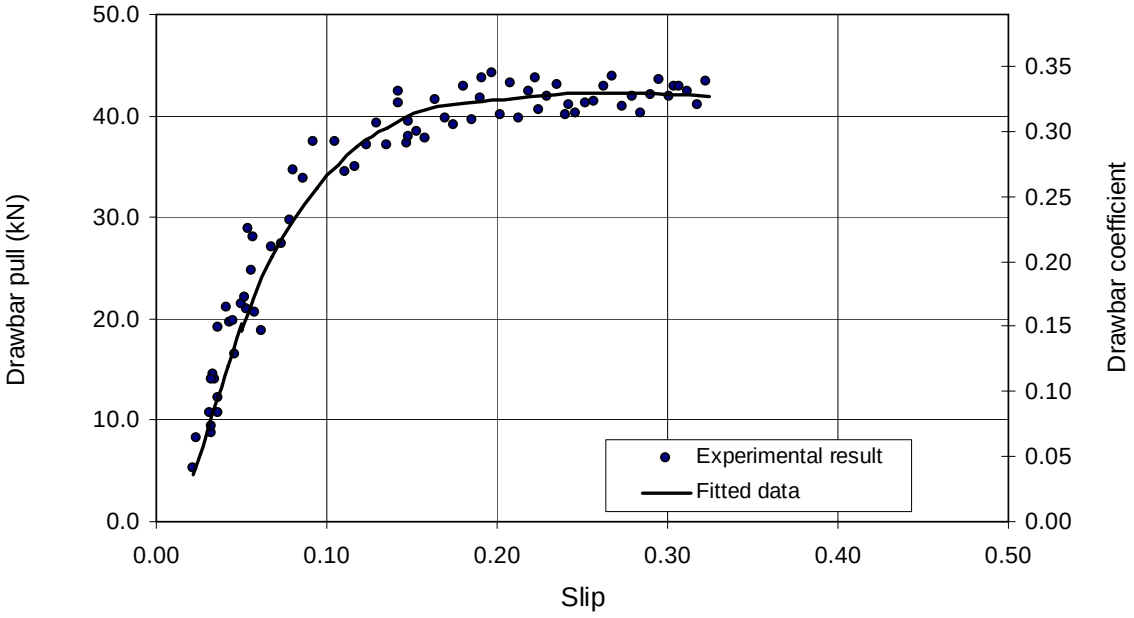

Figure A3. Drawbar pull test results for soil water content 21% (dry basis), sandy loam soil.